Dynamics of Spiral and Scroll Waves: An Experimental and Numerical Study

A Dissertation Submitted to the
Indian Institute of Technology Guwahati
as Partial Fulfillment for the Degree of

Doctor of Philosophy in Chemistry

submitted by

Nirmali Prabha Das

Supervisor: **Dr. Sumana Dutta**

Department of Chemistry
Indian Institute of Technology Guwahati
Guwahati-781039, Assam, India

May 2016

Dynamics of Spiral and Scroll Waves: An Experimental and Numerical Study

Nirmali Prabha Das

DEDICATED TO MY FAMILY

DECLARATION

I hereby declare that the matter embodied in this thesis entitled **"Dynamics of Spiral and Scroll Waves: An Experimental and Numerical Study"** is a result of investigations carried out by me in the Department of Chemistry, Indian Institute of Technology Guwahati, India under the supervision of Dr. Sumana Dutta.

In keeping with the general practice of reporting scientific observations, due acknowledgements have been made wherever the work described is based on the findings of other investigators.

Nirmali Prabha Das

भारतीय प्रौद्योगिकी संस्थान गुवाहाटी
INDIAN INSTITUTE OF TECHNOLOGY GUWAHATI
Dr. Sumana Dutta
Associate Professor
Department of Chemistry
Ph: + 91 361 258 2332
Fax: + 91 361 258 2349
E-mail: sumana@iitg.ernet.in

To whom it may concern

This is to certify that the thesis entitled **"Dynamics of Spiral and Scroll Waves: An Experimental and Numerical Study"** submitted by **Nirmali Prabha Das (Roll No. 11612239)** for the award of PhD degree to IIT Guwahati, is absolutely based on her own research work and that neither this thesis nor any part of it has been submitted for any degree/diploma or any academic award anywhere before.

31 May 2016
IIT Guwahati

(**Dr. Sumana Dutta**)
PhD Supervisor

ACKNOWLEDGEMENTS

First and foremost, I would like to start by thanking God for all the blessings that He has bestowed upon me. My thesis would not have been complete without the constant support from my family, co-workers, my well wishers and friends. I am grateful to have the most supportive and loving people around me and therefore would like to give my heartfelt thanks to the people mentioned here and others whose name I might have forgotten to mention.

I will never be able to thank enough my supervisor Dr. Sumana Dutta for her inspiration, assistance and guidance throughout my PhD career. Thank you for introducing me to this field of science, without you I would never have known the existence of this field. Thank you for offering me the opportunity to work within your group. It was an honor to be one of the members of the group. Thank you for being so kind and so supportive in every aspect. I am also thankful for giving me the scientific ideas which could be transformed into reality.

I would like to extend my special gratitude to the members of my doctoral committee: Dr. Chandan Jana, Prof. Manabendra Ray, and Dr. Achalkumar for their help, advice and suggestions and for being a member of my committee. It also gives me immense pleasure to offer my sincere thanks to all other staff of the department.

I will never be able to repay my parents, Maa and Papa for their endless love, encouragement, help, guidance and prayers that they have bestowed upon me. You have always been there for me in both my happiest and difficult moments. I would like to take this opportunity to especially thank my sister, Bornali Das for her constant support no matter what situation I was in, and also thank my brother Abhigyanjyoti Das and my sweet sister Chandramika Das for their endless love and respect.

I would like to thank IIT Guwahati and Department of Chemistry for financial support and all the facilities that were made available to me. I would also like to thank my MSc supervisor Prof. Diganta Kumar Das along with other faculties of the Department of Chemistry, Gauhati University, for their help, guidance and encouragement during the stay in the University and for still helping me to this day. I also want to acknowledge Dr. Jitumoni Rajbongshi for inspiring me to study Chemistry without whom I would not have been a student in Chemistry. I must thank my lab mate Dhriti for her help and support in difficult times. Thank you Dhriti for being such a good friend and a wonderful co-worker. I would also like to thank my friends Bedika, Bhanita, Gargi, Mahmuda, Priya, Richa, Sabera, Samir, Manas, Ganesh, Ujjal and my class mates for their friendship and moral support. I would also like to take this opportunity to thank my friends Aieshri, Bhaswati, Madhulika, Mingyaophy, Parimita, Payel, Poly, Santwana and Solan for always being there with me.

Lastly, but not the least of course, I would like to thank all others who are associated with me or my work directly or indirectly.

Abstract

This thesis entitled, "*Dynamics of Spiral and Scroll Waves: An Experimental and Numerical Study*" deals with understanding the dynamics of two dimensional (2D) and three dimensional (3D) waves. In recent decades, the dynamics of cardiac arrhythmias has become a paramount interest for research. It has been proven that cardiac arrest results from self-organization of electrical waves in the heart. The waves arise from the irregular pumping of blood, resulting in uncoordinated heartbeats. These waves can also anchor to small obstacles (i.e. ischemic or scar tissues, collagen fibers, or coronary vessels) and are likely to rotate around the unexcitable obstacles, generating stationary electrical signals. Scroll waves of reentrant activity and their interactions pose a serious threat to cardiac health. This thesis outlines the results of experimental and theoretical study of the two dimensional (2D) spiral and three dimensional (3D) scroll waves carried out in a reaction diffusion system. The research has been primarily focused on 3D waves and its behavior in heterogeneous medium.

The Belousov-Zhabotinsky (BZ) reaction is one of the most widely studied reaction diffusion system in which different kinds of waves can be generated. It sustains similar wave forms as in the cardiac tissue. Oscillations occur from red to blue in a homogeneously stirred reaction solution. On the other hand, in an unstirred BZ system, propagating waves of different shapes are found. Travelling waves are seen in a unstirred solution of BZ reaction and in a thicker medium of about 2 mm, two dimensional wave forms such as target and spiral patterns can be generated. Three dimensional scroll waves can be produced when the height is atleast 4 mm.

Two and three dimensional waves observed in the BZ reaction can also be stabilized using pinning obstacles. We have mainly focussed on the pinning of three dimensional scroll waves. The stabilization of the filaments may occur on attaching to

heterogeneities with toroidal, spherical, cylindrical shape or other variations. This kind of stability changes the shape of the scroll ring and enhances its lifetime to a great extent. Sometimes, filament expansion or breakage occurs depending on the size and shape of the heterogeneity. For pinning purposes, unexcitable obstacles of any shape made from plexiglass or polymer can be used. We used spherical glass beads to perform our pinning experiments. This method of stabilization highly elongates the life span of a scroll wave. For pinning, beads of different sizes can also be used. The strength of pinning also depends on the size and shape of the obstacles.

Application of temperature gradient across a chemical mixture leads to diffusion current of the constituent components and as a result a concentration gradient is built up. This phenomenon is known as Soret effect or Ludwig-Soret effect or thermodiffusion or thermal diffusion. It has been named after Swiss scientist Charles Soret. We take the BZ reaction, where the components undergoing chemical reaction are ionic in nature. The migration and transport of these constituent ions are affected by thermal gradient. The interaction between this diffusion and reacting components brings about spatiotemporal instability. Thermal gradient is employed to study unpinning process. By unpinning, we mean destabilization of the scroll wave pinned to an obstacle, by application of temperature gradient across the reaction system.

The study of electric field on chemical systems has been a subject of interest for decades. Due to its resemblance to the electrical cardioversion in treatments of cardiac condition, scientists have been trying to study its effect on reaction diffusion systems. Electric field can induce spatial inhomogeneities, such as wave breakage and instability in spiral and scroll waves. For theoretical studies, electric field effect can be explained on the basis of Nernst-Planck equation.

Plan of the thesis

Chapter 1 is a brief introduction to the field of Nonlinear Dynamics, its discovery, an up to date review on this field along with a brief introduction to the present thesis. The chapter elucidates self-organizing patterns and the methods involved in studying such formation. It gives a brief introduction on oscillating chemical reactions and the

concept of far from equilibrium thermodynamics.

Chapter 2 of the thesis describes the details of the experimental and theoretical methods. It also elucidates the various models used in our study. The chapter explains in detail the mechanism involved in BZ reaction and also elucidates the theoretical models in brief. It also gives a gist of the dynamics of the waves formed in one, two and three dimensions.

Chapter 3 illustrates the detailed study of the effects of reactant concentrations on the dynamics of spiral waves in the Belousov-Zhabotinsky reaction. For the first time, investigations were performed over a parameter space where methodical studies on spiral waves were not reported earlier. We have studied the dynamics of spiral waves in a thin layer of the BZ system varying the concentrations of sulphuric acid, sodium bromate and malonic acid. The main purpose is to compare the experimental results with that of numerical predictions. The period and wavelength decreases with increase in concentrations of sulphuric acid and sodium bromate, whereas the velocity increases. In contrast, there was no significant change with change in concentration of malonic acid. The core of the spiral becomes smaller with increase in concentration of sulphuric acid and sodium bromate, and it traces hypocycloid curves.

Chapter 4 elaborates pinning and unpinning of three dimensional scroll vortices around heterogeneities. Scroll waves can attach themselves to unexcitable obstacles, and this sometimes highly elongates their life span. Hence, the unpinning and annihilation of these vortices have attracted much attention in recent decades. In this work, we study the influence of a thermal gradient on scroll waves pinned to inert obstacles in the Belousov-Zhabotinsky reaction. Under a temperature gradient, scroll rings were seen to unpin from these obstacles, thus strikingly reducing their lifetimes. These results were also reproduced by numerical simulations using the Barkley model.

Chapter 5 discusses the study of the effect of external gradients and their varying orientation on the scroll waves. In this study, we have tried to control the position of a scroll wave by different kinds of field gradients like thermal and electric and

compared their strength. In the presence of a single field (electric field or thermal gradient), the scroll aligns perpendicular and moves towards anode or hot end of the field or gradient, whereas in the presence of electric field and thermal gradient aligned perpendicular with respect to one another, the scroll moves in a diagonal direction between the anode and hot end. Though the effects of the two gradients on scroll waves are similar, it takes longer for the thermal gradient to act as compared to the electric field gradient. Again stronger the field, lesser is the time taken for the scroll to move from its initial position. This will give us new insights into the behavior of these scroll waves and may pave the way for their control in the heart and other biological systems.

Chapter 6 explains the interaction of two scroll waves in experiments with the Belousov-Zhabotinsky reaction. We show that depending on their mutual orientation, two scroll rings can push each other away and rupture on touching the system boundary, or they can reconnect to form a single, large ring. Reconnection only occurs when the filaments lie within one core length of each other. The reconnected filament has extended lifetimes, which could have serious implications in systems where they occur. The experimental results are explained on the basis of a simple numerical model.

Table of Contents

Chapter 1

Self Organizing patterns

1.1 Background

This chapter serves as an introduction to the field of nonlinear dynamics (NLD) regarding the work presented in this thesis. The field of nonlinear dynamics pervades systems across biochemistry [1], biology [2], chemistry [3], engineering [4], evolution [5], physics [6] and their various sub disciplines. It is necessary to understand the fundamentals of nonlinear dynamics in order to interpret underlying properties of these systems.

1.1.1 Pattern

The study of pattern formation and transition in non-equilibrium, non-linear systems has been a subject of particular interest during the last few decades. The natural world abounds in eye-catching patterns, examples of which include synchronization of a school of fish, coordinated movements of a flock of birds, the coiling of a grape tendril, the undulating ripples of sand dunes, the network of army-ant trails, the synchronized flashing of fireflies at night, etc [7].

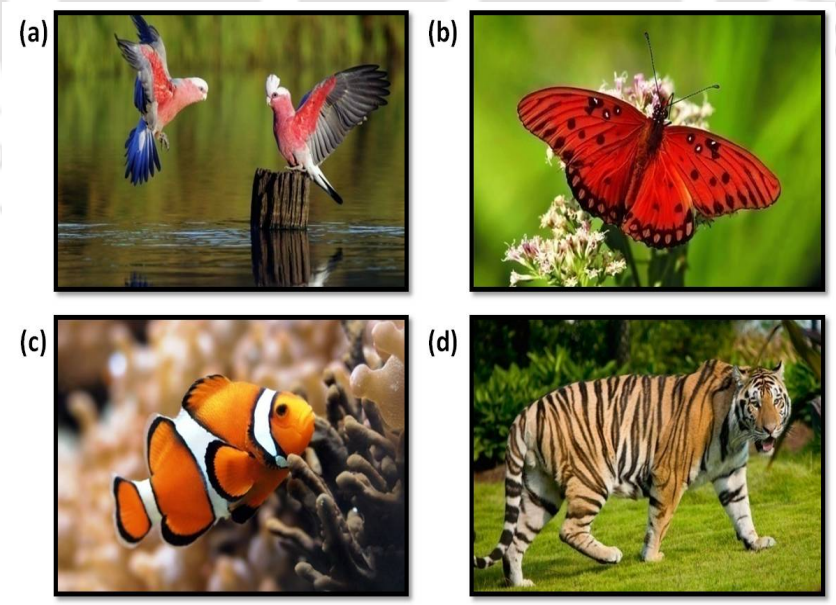

FIG. 1.1: Patterns formed on skin of a) birds, b) butterfly, c) fish and d) animal [8, 9, 10, 11].

Patterns are also seen on a butterfly's wing, skins and coats of animals, birds, fishes

and many more natural systems [12, 13]. Though these wonderful creations delight the imagination, they also challenge our understanding.

Shapes and forms that seem to repeat under any magnification are known as fractals. This applies, for example, to the branching of lightning, rivers, trees, chambered nautilus, cauliflowers, coastlines, clouds, tessellations, snowflakes, blood vessels and bronchi [14].

Figure 1.1 shows some static patterns observed in the biological world. These types of patterns evolve with time but develop so slowly that they appear static to the human eye.

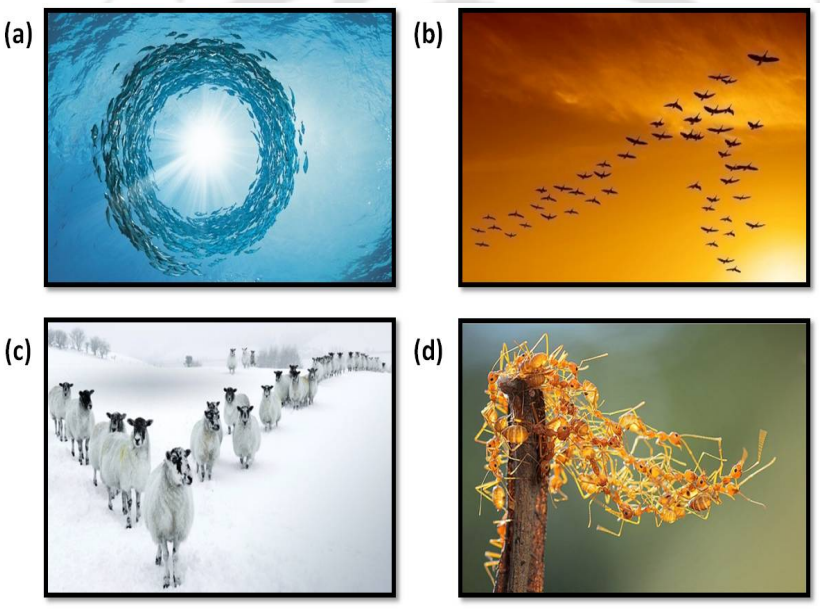

FIG. 1.2: Self organizing patterns in a) a school of fish, b) a flock of birds, c) herd of sheep and, d) Army ant trails [15, 16, 17, 18].

In Fig. 1.2, we can see examples of another type of self organization that are more of a dynamic nature. One of the fundamental questions in developmental biology is how the vast range of patterns and structures we observe in nature emerge despite being subject to numerous sources of noise or disturbances. The mechanism by which biological systems maintain robustness, is still a mystery and the subject is not fully understood yet. Postulating possible theoretical models for such biological systems are of utter difficulty and complicacy. The models are very sensitive to slight variations in the set of initial and boundary conditions. Alan Turing was one of the

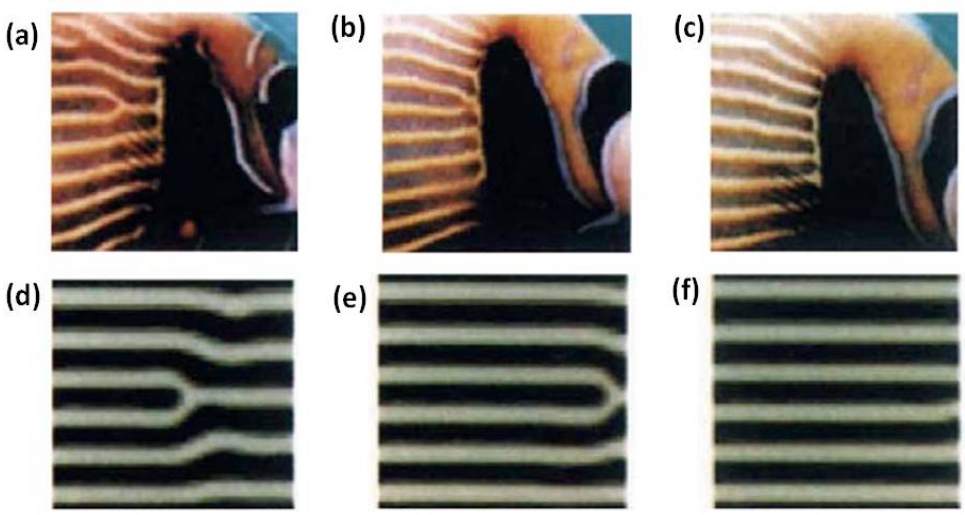

FIG. 1.3: (a), (b), (c) Striped patterns seen in Pomocanthus imperator along with computer simulation results (d), (e), (f) [19].

first scientists to study the formation of such types of pattern. In 1952, he published a paper "The Chemical Basis of Morphogenesis" in the journal Theoretical Biology and put forth a mathematical model for spatial pattern formation which is widely studied till this day [20]. The model makes use of the coupling between chemical reaction and diffusion and is able to generate spatial patterns under appropriate conditions. It comprises of a system of partial differential equations which he termed as reaction-diffusion (RD) model. Since then, many studies have been conducted to bring forward the mechanisms behind the formation of such beautiful patterns [21]. Figure 1.3 shows such an example. Figures 1.3 a, b, and c are snapshots of the pomocanthus fish at different ages and d, e, and f are solutions of a mathematical RD model [19]. These types of mathematical models (RD) can be used to predict the structure and formation of various kinds of patterns formed in nature. However, it requires thorough understanding and knowledge of the system to develop such kinds of models and reproduce exact results.

1.1.2 Self-Organization

The patterns we talked about are normally termed as self-organizing patterns, since they organize themselves without the help of any external parameter. In self-organizing

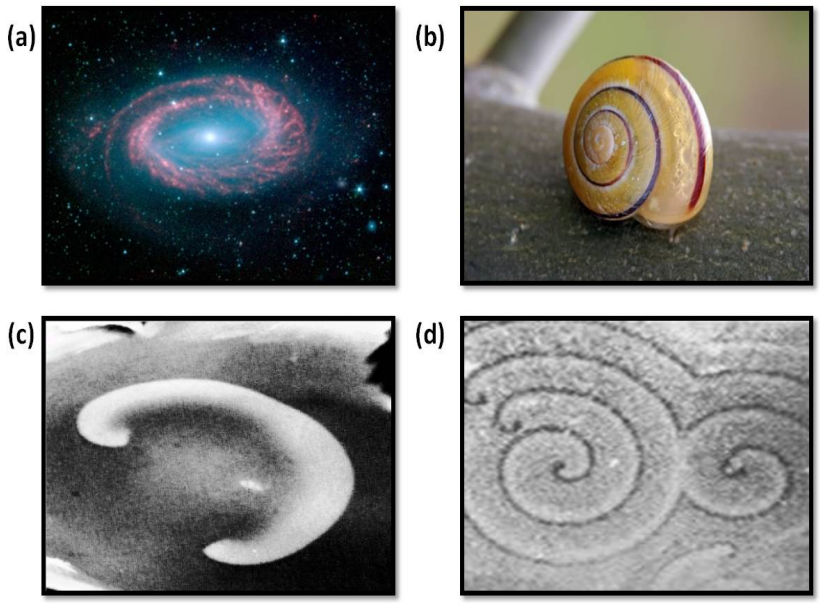

FIG. 1.4: Spiral formation in a) galaxy, b) snail shell, c) neuronal tissue and, d) amoeba [22, 23, 24, 25].

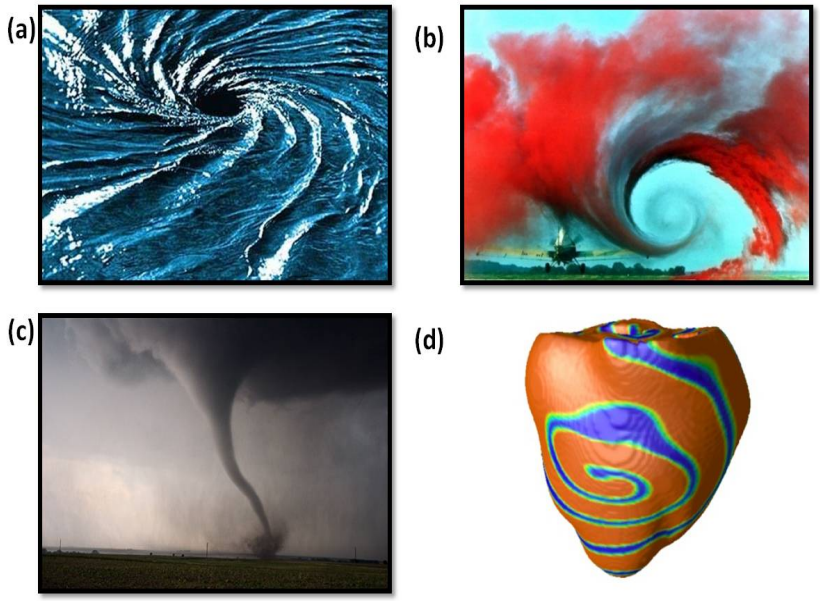

FIG. 1.5: Three dimensional scrolls observed in a) water vortex, b) cloud vortex from airplane, c) tornado and, d) heart [26, 27, 28, 29].

systems, a pattern at the global level emerges solely from interactions among lower-level components. Remarkably, even very complex structures result from the iteration of surprisingly simple behaviors performed by individuals relying only on local information. This character is demonstrated by different physical, biological and chemical processes. In addition to those patterns exemplified earlier, spirals are among the most

widely occurring patterns in nature that have captured the attention of researchers in the last few decades. The three dimensional counterparts of spirals, known as scroll waves, are relatively understudied.

Examples of such systems are abundant in nature and include chicken retina [30], slime mold Dictyostelium discoideum cultures (amoeba) [31], frog oocytes [32], cerebral cortex [33], cardiac tissue [34], the Belousov-Zhabotinsky (BZ) reaction [35], the Briggs-Rauscher reaction [36], and the oxidation of CO on Pt surfaces [37] [Fig. 1.4 and 1.5]. These systems show a common property in spontaneously giving rise to spirals. Hence, they offer one of the most exciting topics of study.

1.1.3 Reaction-Diffusion systems

A "reaction diffusion" (RD) system comprises of two processes, chemical reaction, which transforms the constituents into each other and diffusion which transports the constituents in space. The central idea behind the theory is that, novel shapes and gradients may arise in a homogeneously distributed system, having one species "locally activated" and the other capable of "long-range inhibition" [38]. Let us consider a two variable system,

$$\frac{du}{dt} = f(u,v) \tag{1.1}$$

$$\frac{dv}{dt} = g(u,v) \tag{1.2}$$

where the activator and the inhibitor species is represented by u and v respectively. The above system has only time dependency. However, in spatially extended systems, the diffusion of various chemical species x_i also counts, which is given by Fick's second law [39]:

$$\frac{\partial x_i}{\partial t} = D_i \nabla^2 x_i \tag{1.3}$$

where D_i denotes the diffusion coefficient for the ith species. We therefore get a system of partial differential equations of concentrations related to both time and space.

$$\frac{\partial u}{\partial t} = f(u,v) + D_u \frac{\partial^2 u}{\partial x^2} \tag{1.4}$$

$$\frac{\partial v}{\partial t} = g(u,v) + D_v \frac{\partial^2 v}{\partial x^2} \tag{1.5}$$

These sets of equations are termed as "Reaction-Diffusion" (RD) systems. Here the pattern formation depends on the coupling between the two equations, and the diffusion of chemical species u and v. D_u and D_v are diffusion coefficients for u and v respectively.

The Belousov-Zhabotinsky reaction is also a kind of reaction diffusion system which shows wave propagation and spatio-temporal pattern formation. In experiments, an unstirred and convection free BZ system can give rise to one, two and three dimensional wave patterns. 1D travelling waves, 2D target patterns (concentric rings), 2D spiral waves, and 3D scroll waves (three-dimensional spiral waves) can be generated depending on the concentration and dimension (thickness) of the medium. The system radiates excitation waves periodically and is also known as excitable medium [2, 13, 40].

The Oregonator model [41, 42] is a reaction diffusion equation based prototype of the BZ system. Additionally, there are more RD models proposed for the study of pattern formation in excitable media. Two of these models are the Barkley model [43] and the FitzHugh-Nagumo (FHN) model [44].

1.1.4 Oscillations and the second law of thermodynamics

The BZ system demonstrates an interesting phenomenon of oscillating chemical reaction. This reaction is one the most classical example of an oscillatory system developed in history. In a stirred solution of BZ, bulk oscillations are observed from orange to blue and again back to orange. This keeps repeating in cycles [45].

Figure 1.6 shows an example of bulk oscillation occurring in a beaker. Oscillating chemical reactions have always been considered a controversy because of the notion that it does not obey the second law of thermodynamics. It is due to the term "oscillating" linked to models used in classical mechanics. In such models, like in a

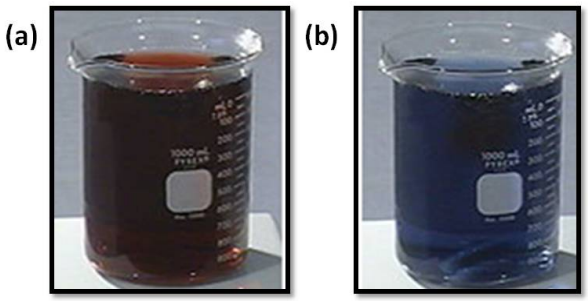

FIG. 1.6: Oscillation in BZ reaction. (a) Reduced state and (b) oxidized state [46].

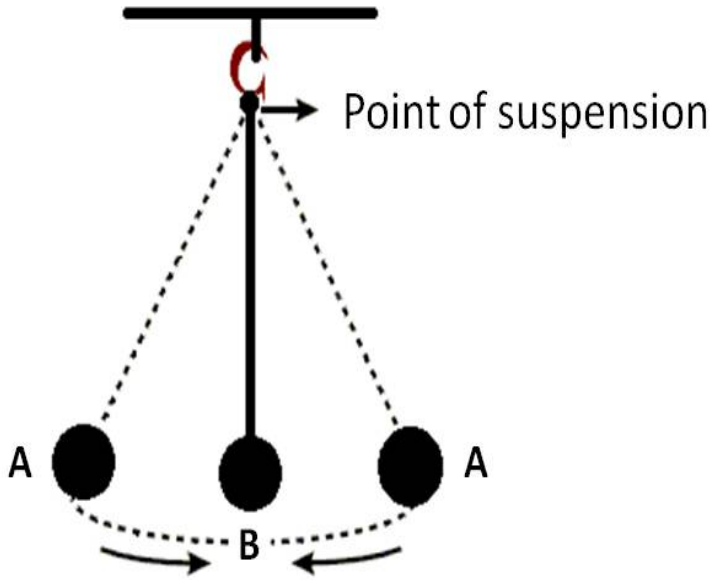

FIG. 1.7: Oscillation in classical model (pendulum) [47].

pendulum, a mass oscillates around the equilibrium position as shown in the Fig. 1.7.

The second law of thermodynamics states that a chemical reaction must come to a thermodynamic equilibrium, but once the equilibrium is established, there cannot be periodic oscillations around the equilibrium. But as seen in the case of BZ reaction, oscillations occur as though the reaction never reaches equilibrium. An oscillating chemical reaction is a complex process which consists of several elementary steps. These steps involve many intermediates which are produced and consumed in the chemical reaction, but they are not formed as the final product. The oscillating chemical reaction moves towards a thermodynamic equilibrium with its reactant, and product concentrations decreasing and increasing respectively. Moreover, some of the intermediates produced during the reaction can undergo oscillations in concentrations.

Thus an oscillatory chemical reaction obeys the second law of thermodynamics and ultimately it approaches equilibrium [40]. In case of BZ reaction, the ferroin oscillates between oxidized Fe^{3+} and reduced Fe^{2+} [48]. The oscillations observed are actually happening far from equilibrium.

1.1.5 Far from equilibrium phenomenon

The term "oscillation" in chemical reaction was not approved completely until the phenomenon of "far from equilibrium" was explained. The term was coined by Belgian chemist Ilya Prigogine in the 1970s. This phenomenon was first used to explain the Benard cell formation. In Benard cell, spontaneous formation of hexagonal convection cells is observed in viscous medium, such as silicon oil, when it is placed on a hot plate and heated. According to Prigogine, far from equilibrium states of systems are those subjected to flows of matter or energy, but the system can lose its stability and evolve into one of the many states available in this non-linear system. In 1977, Prigogine got "Nobel Prize" for his work in thermodynamics, particularly in reference to his work "far from equilibrium theory" [49].

1.2 Research Motivation

Phenomena like oscillations, chemical patterns and self-organization have become a subject of great interest in recent years among the world chemistry community. Apart from these chemical systems, similar patterns are observed in biology and its sub disciplines which can have a direct effect on health and life expectancy [50].

Wave propagation in myocardium

The heart is a specialized muscular organ whose primary function is to circulate blood throughout the body. It contracts and expands rhythmically to pump blood to the body. It has four chambers: two upper chambers (right and left atrium) and two lower chambers (right and left ventricles). The atria are smaller and thinner than the ventricles. The atria act as a blood receiving chamber, therefore the direction of the

flow of blood is from the atria to ventricles.

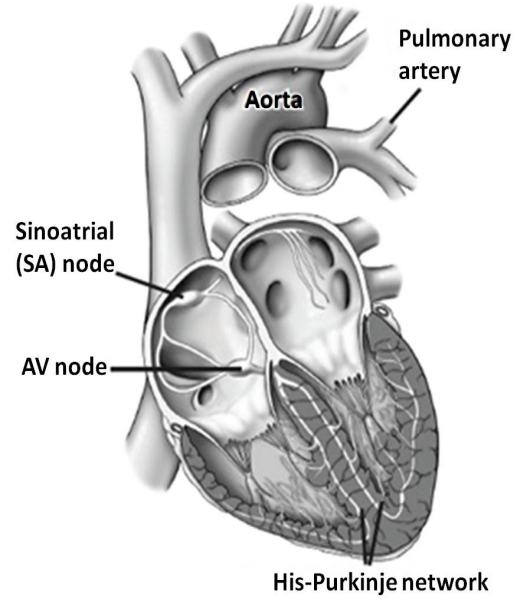

FIG. 1.8: Schematic diagram of a heart showing the location of the cardiomyocytes with electrical activity [51].

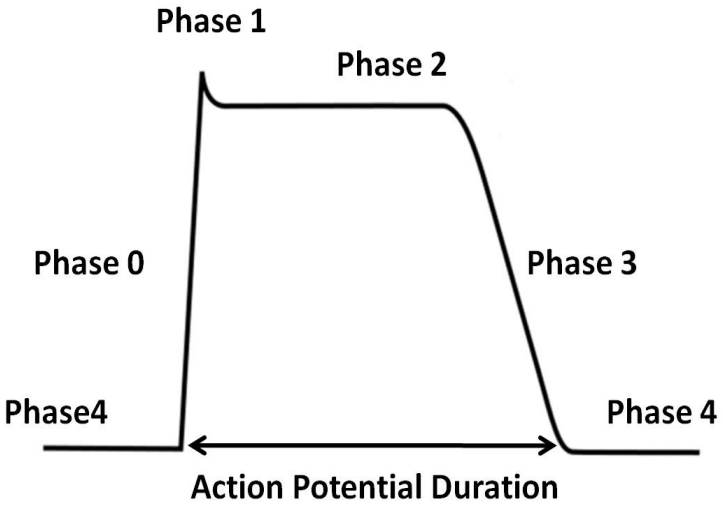

FIG. 1.9: Cardiomyocyte action potential[52].

Cardiac muscle, which has interconnected cells called cardiomyocytes and connective tissue have the ability to generate electrical activity spontaneously. These cells form the sinoatrial node, the atrioventricular node and the His-Purkinje system [Fig. 1.8]. This electrical activity causes a change in the cell's electrical potential, which is termed as cardiac potential [Fig. 1.9]. Phase 4 represents the resting state where the

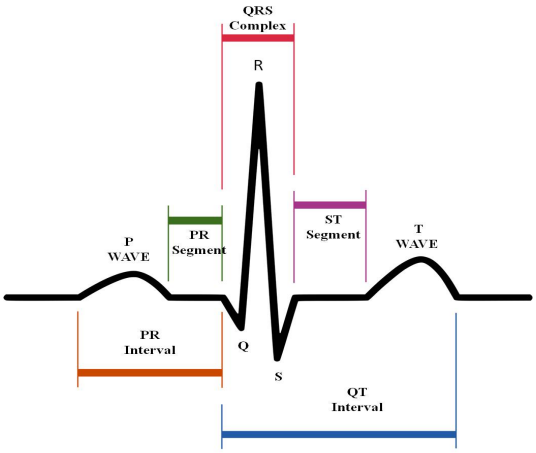

FIG. 1.10: Schematic diagram of normal sinus rhythm[53].

sodium and potassium channels are closed. Phase 0 represents the threshold state, where a stimulus opens the sodium channels. This causes the influx of sodium ions into the cell. Phase 1 corresponds to the depolarization state. In this state, the sodium ion channels become inactive, but there is an outflow of potassium ions and an inward flow of calcium ions. In Phase 2, there is still inflow of calcium ions. Phase 3 shows the repolarization of the cells. The sodium channels are closed, but there is still an outflow of potassium ions and the calcium channels become inactive. In Phase 4, they come back to the resting potential [54, 55].

The electrical activity that is produced in the heart is associated with wave formation which can be measured by electrocardiography and the result can be seen on an electrocardiogram (ECG). An ECG of a normal heart is shown in Fig. 1.10. The P wave is associated with the excitation of atria, QRS is associated with the excitation of the ventricles, and T is associated with the relaxation of the ventricles [56]. An ECG can help detect malfunction of the heart system. One can consider the cardiac rhythm to be normal when: (a) the electrical impulse begins in the sinoatrial node and the rate of beat is within the normal range(60 - 100 bpm), (b) the electrical impulse is sent to the ventricles through the atrioventricular node in unidirection, (c) the ventricular contraction is normal.

Arrhythmia is an abnormally irregular heart rhythm. There are three types of cardiac arrhythmias: 1) supraventricular arrhythmias (atrial tachycardia, atrial flutter, and atrial fibrillation), 2) ventricular arrhythmias (ventricular tachycardia and ventricular

fibrillation) and 3) bradyarrhythmias.

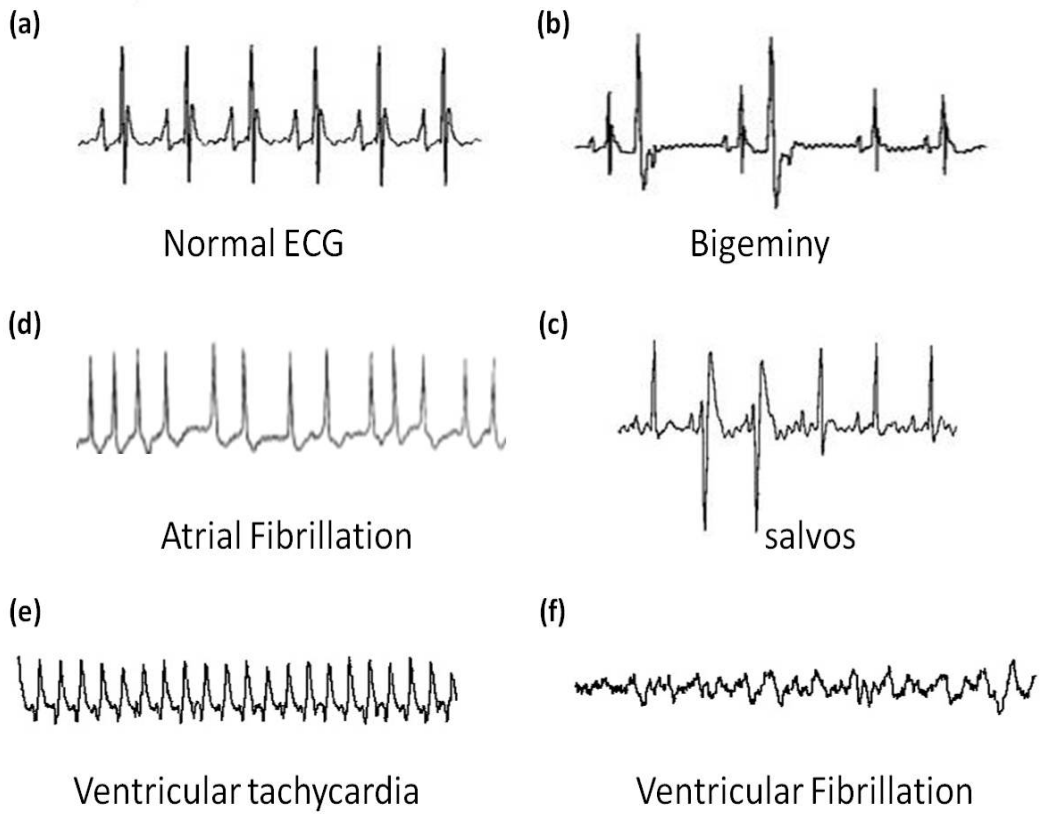

FIG. 1.11: ECG of (a) normal and (b, c, d, e, f) abnormal heartbeats [57].

Fig. 1.11 shows some ECG's of the heart that have been recorded for irregular beats. We can see in Fig. 1.11 (a) that there is continuity in the rhythm in the case of a normal ECG. But this pattern is no longer followed when the rhythm of the heart becomes abnormal [Fig. 1.11 (b, c, d, e, f)].

Atrial and ventricular fibrillation are the two most important among the abnormal rhythms. Atrial fibrillation is the most common heart disease, whereas ventricular fibrillation is the most life threatening. It can cause death when not cured within two minutes. Atrial fibrillation is characterized by rapid, irregular activation of the upper two chambers of the heart, the atria's. Although not as life threatening as fibrillation it can be a major cause for a stroke Fig. 1.11 (d) [58].

Spiral or scroll waves of electrical activity are among the mechanisms believed to be responsible for the rapid, unsynchronized contraction of the ventricles and thereby reduces the heart's ability to pump blood. It has been found in recent studies that during tachycardia, a single wave can rotate forming a spiral. This results in rapid

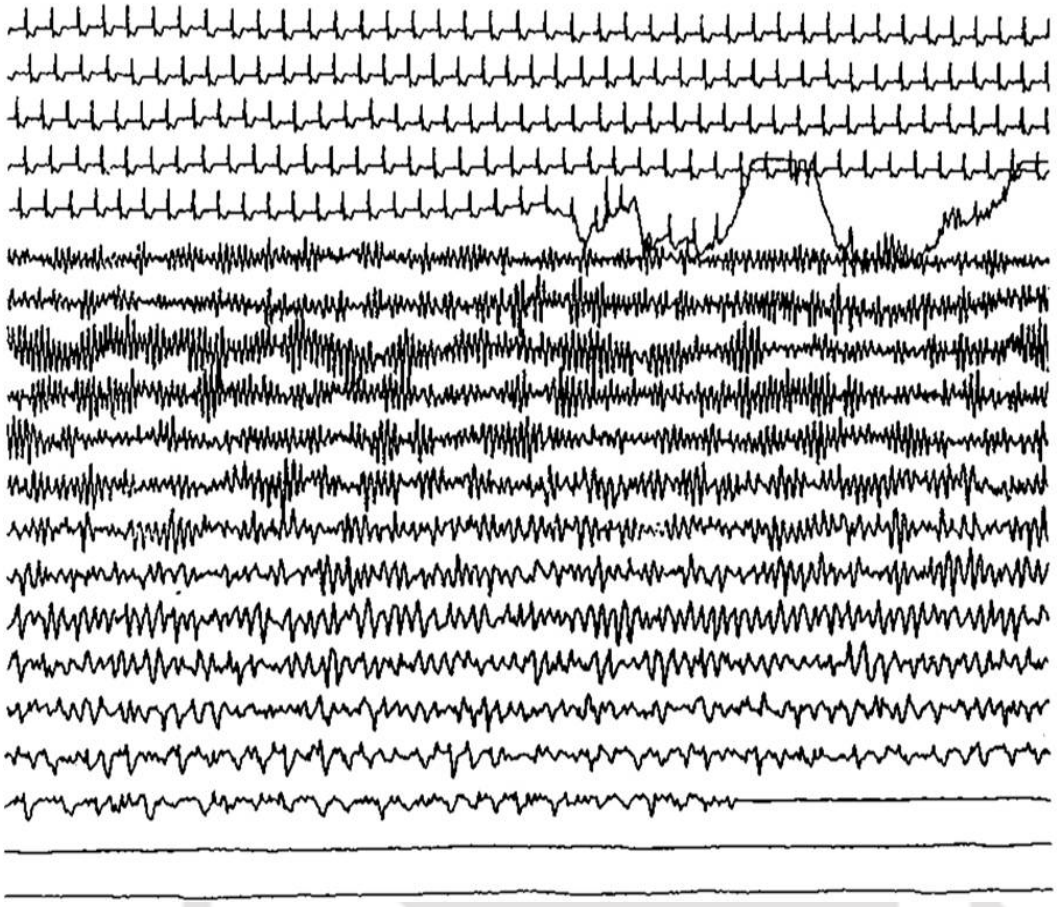

FIG. 1.12: ECG obtained from a Holter monitoring device on a patient [59].

heartbeats and utter complexity. Whreas during fibrillation, a single spiral wave splits into multiple waves. The detailed mechanism is still unclear. Ventricular tachycardia [Fig. 1.11 (e)] is a rhythm characterized by wide, weird QRS complexes and frequent ventricular premature contractions. It can degenerate rapidly to ventricular fibrillation and result in sudden death. The rotation period of spiral waves in heart tissue is shorter than the period of normal heart's wave. Consequently the spiral has higher frequency which overtakes the frequency generated by the heart's natural pacemaker, the Sinoatrial (SA) node. Ventricular fibrillation has a chaotic electrical wave passage. The heart cannot pump blood in this condition. The ECG during ventricular fibrillation does not show distinctive QRS complexes as shown in the Fig. 1.11 (f). The detailed process involved in the spiral wave breakup is believed to be one of the major mechanism by which tachycardia evolves into fibrillation. But this fact is still poorly understood [60, 61, 62].

Figure 1.12 shows a portion of a 24-h ECG recording from a patient who died from

sudden cardiac arrest. The lines shown in the figure are separated by one minute. The patient initially had normal sinus rhythm as shown in the top four and half-lines. After this, the heart beat of the patient was no longer normal and culminated in ventricular fibrillation, which continued, resulting in death and electrical quiescence [59]. The control of these scroll waves is thus very vital to the understanding and probable cure of such conditions in the human body. For over a hundred years, physicians and scientists have come together to understand the electrical activity of the cardiac muscle [63]. Jalife et al. carried out the application of high frequency electric pulse to generate ventricular fibrillation in an isolated rabbit heart [64]. Davidenko et al. used thin slices of sheep and dog epicardial muscle to initiate spiral wave activity [65]. These experiments could observe only the surface of the heart and was restricted from accessing the electrical activity inside. Hence, understanding of the bulk phenomena still remains a challenge. In light of these events, theoretical biologists and physicists have developed a bunch of mathematical models of excitable media in order to better understand this highly complex system. These models tried to reproduce the experimental observations. Some electrical activity of the heart can be explained with the help of these models [66]. Fenton and Cherry have illustrated and discussed numerous models and summarized their properties which can be used to study the various wave phenomena arising in cardiac cells [67]. Numerical simulations of such models provide information about the dynamics of electrical wave propagation in the heart muscle. Results of these simulations are very much sensitive to initial conditions. Hence, though the results are able to explain experimental fact, it is not dependable while making new predictions. Therefore, there is a need for an experimental model which can be probed and studied in every possible way to understand better the activity of the electrical waves in the heart. The excitable Belousov-Zhabotinsky (BZ) reaction is a system which exhibits self oscillating patterns mainly spirals and scroll waves just like the heart. Though the heart has many contrasting features as compared to the BZ system: the heart is inhomogeneous, discontinuous and anisotropic, whereas the BZ system is homogeneous and continuous. Wave velocity is also different in the two mediums. But the innate similarity between the two systems, like their excitability,

ensures that they propagate through a medium and have a refractory phase or a rest period. Also the property that the waves in both the systems annihilate upon collision makes the BZ system a good laboratory model to study complicated wave behaviors in cardiac tissues and other related systems [55]. In the BZ system, we also get action potential kind of curve, similar to as seen in the heart. Similar mathematical models can also be applied to study the wave formation in both the systems [54].

The heart is a heterogeneous excitable medium having highly structured arrangements of cardiomyocytes and fibroblasts, blood vessels and extracellular matrix. Blood vessels are made up of epithelial cells which have no electrical connections with the cardiomyocytes and therefore can act as heterogeneities and obstacles in the cardiac electrical system. This heterogeneity induces the formation of the scroll waves within the excitable cardiac muscles [65]. These newly generated waves have much higher frequencies and so are detrimental to cardiac health. These scroll waves can further attach themselves to the inert, heterogeneous obstacles by a process called pinning, which highly elongate their lifetimes [64]. Thus a better understanding of the process of pinning and possible methods of unpinning of scroll waves from obstacles is highly desirable. Recent studies with the BZ system has shown that scroll waves in the BZ medium also get pinned to geometrically regular inert obstacles [68]. So this process of pinning can be further studied using the BZ systems, and the possibility of unpinning of the waves could be explored. In earlier studies, it was shown that the excitability of reaction diffusion systems can be influenced by various external and internal perturbations like noise, electromagnetic fields, thermal and concentration gradients [69, 70, 71, 72, 73]. Whether such external or internal perturbations can be employed to control the scroll waves and also to unpin the stable filaments that are attached to unreactive obstacles, is a question worth exploring. Quantitative studies of mathematical models have revealed that an advective field can unpin vortices that are pinned to inert obstacles [74]. Current methods of defibrillation of the heart employ a strong electric field, that at often times have lasting effects on the cardiac muscles. This may result in tissue damage and be a cause of further arrhythmias [66]. So, we are in search of milder techniques to control scroll waves and bring about

their unpinning. In our studies, we use the BZ system for generating spiral and scroll waves and studying their dynamics. We try to reproduce various phenomena seen in the heart and study them closely. We also try to control the wave forms using external field gradients.

Bibliography

[1] M. A. Aon, S. Cortassa, and D. Lloyd, Cell Biol. Int. **24**, 581 (2000). Chaotic dynamics and fractal space in biochemistry: Simplicity underlies complexity.

[2] J. Walleczek, *Self-Organized biological dynamics and nonlinear control: Towards understanding complexity, chaos and emergent function in living systems* (Cambridge University Press, 2006).

[3] I. R. Epstein, and K. Showalter, J. Phys. Chem. **100**, 13132 (1996). Nonlinear chemical dynamics: Oscillations, patterns and chaos.

[4] J. Jerrelind, and A. Stensson, Chaos Soliton. Fract. **11**, 2413 (2000). Nonlinear dynamics of parts in engineering systems.

[5] D. M. Green, Trends Ecol. Evol. **10**, 333 (1991). Chaos, fractals and nonlinear dynamics in evolution and phylogeny.

[6] A. E. Motter, Nat. Phys. **6**, 164 (2010). Nonlinear dynamics: Spontaneous synchrony breaking.

[7] S. Camazine, J-L. Deneubourg, N. R. Franks, J. Sneyd, G. Theraulaz, and E. Bonabeau, *Self-Organization in Biological Systems* (Princeton University Press, 2001).

[8] https://plus.google.com/communities/104408123011331897357/stream/08104c5b-f634-4948-80af-cf6575cada1a

[9] http://www.clickertraining.com/the-butterfly-project

[10] http://dreamatico.com/fish.html

[11] http://dreamatico.com/data_images/tiger/tiger-5.jpg

[12] P. Ball, *The self-made tapestry: Pattern formation in nature* (Oxford University Press, 1999).

[13] M. Cross, and H. Greenside, *Pattern formation and dynamics in non-equilibrium systems* (Cambridge University Press, 2009).

[14] P. Meakin, *Fractals, scaling and growth far from equilibrium* (Cambridge University Press, 1998).

[15] http://www.simontuckett.com/_Portfolio/PortPages_Hi/Il_FishSchool.html

[16] https://www.pinterest.com/pin/265853184224238351/

[17] http://www.istockphoto.com/photo/winter-sheep-v-formation-gm182432041-11692727

[18] https://www.pinterest.com/pin/66639269455958350/

[19] P. K. Maini, T. E. Woolley, R. E. Baker, E. A. Gaffney, and S. S. Lee, Interface Focus **2**, 487 (2012). Turing's model for biological pattern formation and the robustness problem.

[20] A. M. Turing, Phil. Trans. R. Soc. Lond. B **237**, 37 (1952). The chemical basis of morphogenesis.

[21] T. Leppanen, M. Karttunen, R. A. Barrio, and K. Kaski, Braz. J. Phys. **34**, 368 (2004). Turing systems as models of complex pattern formation.

[22] http://www.spotlight-online.de/news/technology/nasa-images-that-are-out-of-this-world

[23] http://www.imgmob.net/snail-shells.html

[24] M. A. Dahlem, and S. C. Müller, Ann. Phys. **13** 442 (2004). Reaction-diffusion waves in neuronal tissue and the window of cortical excitability.

[25] http://www.strukturbildung.ovgu.de/Forschung/Bildergalerie.html

[26] http://www.meditation24-7.com/page32/page41/page41.html

[27] https://en.wikipedia.org/wiki/Wingtipvortices/media/File:Airplanevortexedit.jpg

[28] http://tornado-facts.com/

[29] http://www.psc.edu/science/2003/fenton/

[30] N. A. Gorelova, and J. Bures, J Neurobiol. **14**, 353 (1983). Spiral waves of spreading depression in the isolated chicken retina.

[31] S. C. Müller, T. Mair, and O. Steinbock, Biophys. Chem. **72**, 37 (1998). Travelling waves in yeast extract and in cultures of Dictyostelium discoideum.

[32] J. Lechleiter, S. Girard, E. Peralta, and D. Clapham, Science **252**, 123 (1991). Spiral calcium wave propagation and annihilation in Xenopus laevis Oocytes.

[33] X. Huang, W. Troy, Q. Yang, H. Ma, C. Laing, S. Schiff, and J. Y. Wu, J. Neurosci. **44**, 9897 (2004). Spiral waves in disinhibited mammalian neocortex.

[34] N. Wessel, J. Kurths, W. Ditto, and R. Bauernschmitt, Chaos **17**, 015101 (2007). Introduction: Cardiovascular physics.

[35] A. T. Winfree, Science **175**, 634 (1972). Spiral waves of chemical activity.

[36] Zs. Nagy-Ungvarai, S. C. Müller, and B. Hess, Chem. Phys. Lett. **156**, 433 (1989). Spatial patterns in the Briggs-Rauscher reaction.

[37] G. Ertl, Angew. Chem. Int. Ed. **47**, 3524 (2008). Reactions at Surfaces: From atoms to complexity.

[38] B. A. Grzybowski, *Chemistry in motion* (John Wiley & Sons Ltd, 2009).

[39] D. S. Jones, M. Plank, and B. D. Sleeman, *Differential equations and mathematical biology* (Second edition, CRC Press Uk, 2009).

[40] I. R. Epstein, and J. A. Pojman, *An introduction to nonlinear chemical dynamics, oscillations, waves, patterns and chaos* (Oxford University Press, 1998).

[41] R. J. Field, and R. M. Noyes, J. Chem. Phys. **60**, 1877 (1974). Oscillations in chemical systems. Iv. Limit cycle behavior in a model of a real chemical reaction,

[42] I. Schebesch, and H. Engel, Phy. Rev. E **60**, 6429 (1999). Interacting spiral waves in the Oregonator model of the light-sensitive Belousov-Zhabotinskii reaction.

[43] D. Barkley, M. Kness, and L. S. Tuckerman, Phy. Rev. A **42**, 2489 (1990). Simple-wave dynamics in a simple model of excitable media: The transition from simple to compound rotation.

[44] E. M. Izhikevich, and R. FitzHugh, Scholarpedia **1**, 1349 (2006). FitzHugh-Nagumo Model.

[45] A. M. Zhabotinsky, Scholarpedia **2**, 1435 (2007). Belousov-Zhabotinsky reaction.

[46] http://www.syngenta.com/country/uk/en/about/learning-zone/KS345/chemistry/Pages/BZ-Clock.aspx.

[47] http://www.opsrules.com/supply-chain-optimization-blog/bid/228425/Is-Your-Inventory-on-a-Pendulum.

[48] G. Dupuis, and N. Berland, http://www.faidherbe.org/site/cours/dupuis/oscil.htm (2004). Oscillating reactions - Chemical waves.

[49] J. Ross, *Thermodynamics and fluctuations far from equilibrium* (Springer Belin Heidelberg, New York, 2008).

[50] N. Sperelakis, Y. Kurachi, A. Terzic, and M. V. Cohen, *Heart physiology and patholphysiology* (fourth edition, Academic Press, 1984).

[51] Cleveland Clinic. Pacemaker implant. http://my.clevelandclinic.org/heart/services/tests/procedures/pacemaker.aspx, April (2010).

[52] https://en.wikipedia.org/wiki. Cardiac-action-potential.

[53] S. S. Ryan, Atrial fibrillation, resourses for patients, a-fib.com (2002).

[54] www.sjmedgroup.org

[55] J. Jalife, M. Delmar, J. Anumonwo, O. Berenfeld, and J. Kalifa, *Basic cardiac electrophysiology for the clinician* (Wiley-Blackwell, Oxford, UK, second edition, 2009).

[56] P. Kuklik, L. Szumowski, P. Sanders, and J. J. Zebrowski, Comput. Biol. Med. **40**, 775 (2010). Spiral wave breakup in excitable media with an inhomogeneity of conduction anisotropy.

[57] http://ajpheart.physiology.org/content/ajpheart/287/3/H1286/F1.large.jpg.

[58] www.the virtualheart.org.

[59] P. S. Chen, A. Garfinkel, J. N. Weiss, and H. S. Karagueuzian, Chaos **8**, 127 (1998). Computerized mapping of fibrillation in normal ventricular myocardium.

[60] D. Allexandre, and N. F. Otani, Phys. Rev. E **70**, 061903 (2004). Preventing alternans-induced spiral wave breakup in cardiac tissue: An ion-channel-based approach.

[61] R. A. Gray, and J. Jalife, Chaos **8**, 65 (1998). Ventricular fibrillation and atrial fibrillation are two different beasts.

[62] A. V. Panfilov, Chaos **8**, 57 (1998). Spiral breakup as a model of ventricular fibrillation.

[63] I. R. Efimov, M. W. Kroll, and P. J. Tchou, *Cardiac Bioelectric Therapy: Mechanisms and Practical Implications* (Springer, New York, 2008).

[64] J. Jalife, R. A. Gray, G. E. Morley, and J. M. Davidenko, Chaos **8**, 79 (1998). Self-organization and the dynamical nature of ventricular fibrillation.

[65] J. M. Davidenko, A. V. Pertsov, R. Salomonsz, W. Baxter, and J. Jalife, Nature **355**, 349 (1992). Stationary and drifting spiral waves of excitation in isolated cardiac muscle.

[66] F. X. Witkowski, L. J. Leon, P. A. Penkoske, W. R. Giles, M. L. Spano, W. L. Ditto, and A. T. Winfree, Nature **392**, 78 (1998). Spatiotemporal evolution of ventricular fibrillation.

[67] E. M. Cherry, and F. H. Fenton, Scholarpedia **3**, 1868 (2008). Models of cardiac cell.

[68] Z. A. Jiménez, B. Marts, and O. Steinbock, Phys. Rev. Lett. **102**, 244101 (2009). Pinned scroll rings in an excitable system.

[69] S. Dutta, S. S. Riaz, and D. S. Ray, Phys. Rev. E **71**, 036216 (2005). Noise-induced instability: An approach based on higher-order moments.

[70] H. Sevčíková, M. Marek, and S. C. Müller, Science **257**, 951 (1992). The reversal and splitting of waves in an excitable medium caused by an electric field.

[71] S. Dutta, and D. S. Ray, Phys. Rev. E **75**, 066206 (2007). Thermodiffusion induced instabilities in reactive systems.

[72] S. Dutta, and O. Steinbock, Phys. Rev. E **83**, 056213 (2011). Spiral defect drift in the wave fields of multiple excitation patterns.

[73] P. Sadeghi, and H. H. Rotermund, Chaos **21**, 013125 (2011). Gradient induced spiral drift in heterogeneous excitable media.

[74] D. Pazó, L. Kramer, A. Pumir, S. Kanani, I. Efimov, and V. Krinsky, Phys. Rev. Lett. **93**, 168303 (2004). Pinning force in active media.

Chapter 2

Experimental Methods, Models and Tools

2.1 Mathematical Models (Biological Oscillators)

There are numerous mathematical models of the cardiac system by which the wave formation in the heart can be studied. Examples include "Lou-Rudy Model" [1], "Aliev-Panfilov model" [2], "the Hodgkin-Huxley (H-H) Formalism" [3] and "FitzHugh-Nagumo (FHN) model".

2.1.1 FitzHugh-Nagumo model

FitzHugh and Nagumo constructed a two dimensional form of Hodgkin-Huxley model that explains the initiation and propagation of action potentials in the squid giant axon. It has been reduced to H-H model for better and easy fundamental understanding. The FHN model is described below [4]:

$$\frac{dV}{dt} = V - \frac{V^3}{3} - v + I \tag{2.1}$$

$$\frac{dv}{dt} = 0.08(V + 0.7 - 0.8v) \tag{2.2}$$

where V, v and I are the membrane potential, the recovery variable and the magnitude of stimulus current respectively. This model can also be used to describe important phenomena in various biological and biochemical processes.

2.1.2 Lou-Rudy model

In 1991, Luo and Rudy presented a model of the Mammalian Ventricular Myocyte. It describes the action potential in guinea pig ventricular cells which can be described as below [5]:

$$C\frac{dV}{dt} = -\sum_i I_i + \frac{1}{\rho_x S_v}\frac{\partial^2 V}{\partial x^2} + \frac{1}{\rho_y S_v}\frac{\partial^2 V}{\partial y^2} \tag{2.3}$$

where C is the capacitance, V is the membrane potential, I_i are the various ionic currents, ρ is the resistivity due to the gap junctions, S_v is the surface to volume ratio of the cell.

These models are widely used to study wave formation in cardiac tissue. As discussed before, numerical simulations are very much sensitive to initial conditions and not

totally reliable while making new predictions. Therefore, there is always a demand for an experimental model. However, there are some laboratory models that have been in use for quite some time to study the spatio-temporal pattern formation and some of these models also mimic wave formation in the heart.

2.2 Chemical Models

Some examples of reactions that give rise to chemical patterns are Briggs-Rauscher [6, 7] and Belousov-Zhabotinsky reactions [8], the catalytic oxidation of CO on Pt [9], the Liesegang rings [10], the chlorite-iodide-malonic acid (CIMA) and chlorine dioxide-iodide-malonic acid (CDIMA) reactions [11].

2.2.1 Catalytic oxidation of CO on Pt

The catalytic oxidation of CO on Pt is an oscillating reaction, where spatio-temporal concentration structures like target patterns and spirals are observed. The mechanism of catalytic CO oxidation on surfaces of the platinum consists of the following steps [12]:

$$CO(g)+^* \rightleftharpoons CO_{ad} \tag{2.4}$$
$$O_2(g)+2^* \rightarrow 2O_{ad} \tag{2.5}$$
$$CO_{ad}+O_{ad} \rightarrow CO_2(g)+2^* \tag{2.6}$$

where, * denotes a free adsorption site. The reactions correspond to adsorption of CO and O_2 respectively. In the third step, diffusion of a CO towards an oxygen atom occurs which is followed by the production of CO_2. CO_2 immediately leaves the surface.

2.2.2 CIMA and CDIMA reactions

The CIMA and CDIMA reactions along with the Belousov-Zhabotinsky reaction represent the most important prototype for studying spatio-temporal patterns in chemical media. CIMA and CDIMA reactions exhibit oscillatory behavior and Turing patterns. The model consists of three important steps [11]:

$$MA + I_2 \rightarrow IMA + I^- + H^+ \quad (2.7)$$
$$ClO_2 + I^- \rightarrow ClO_2^- + 0.5I_2 \quad (2.8)$$
$$ClO_2^- + 4I_4^- H^+ \rightarrow 2I_2 + Cl^- + 2H_2O \quad (2.9)$$

where, MA stands for malonic acid. Spatio-temporal Turing patterns are observed when there is a huge difference in the diffusion coefficients of activator and inhibitor.

2.2.3 The Belousov-Zhabotinsky reaction

In the early 50's, Boris Pavlovich Belousov, a soviet chemist/biophysicist was trying to find an inorganic counterpart for the Krebs cycle. As citrate ion is one of the main intermediates in the cycle, Belousov used citric acid to study the reaction along with bromate and Ce^{4+} salts. In a regular stirred reaction solution, he observed a monotonic change of color of the solution from yellow Ce^{4+} to colorless Ce^{3+}. Surprisingly, the system was oscillating between the yellow and clear state. He even noticed yellow travelling waves in an unstirred solution. Contemporary scientists found it repelling to believe his results because of the contradiction that arose regarding the well-established thermodynamic laws. The concept of "far from equilibrium" was unknown then. Anatol Zhabotinsky developed Belousov's recipe a decade later by replacing citric acid with malonic acid. He was successful in mimicking the same oscillatory behavior, giving rise to similar results as before. The cerium catalyst can be replaced with ferroin which gives a better contrast in the color change; in this case, the catalyst change back and forth between red ferroin (Fe^{2+}, reduced state) and blue ferrin (Fe^{3+}, oxidized state). This contribution from Zhabotinsky led to the establishment of propagating chemical waves. The results of experiments was later supported by Prigogine's concept of "far from equilibrium" phenomenon. The main reactants of a classical Belousov-Zhabotinsky (BZ) reaction are malonic acid, sodium bromate, sulfuric acid, and cerium (III) sulfate [13, 14].

In the unstirred BZ reaction, there is a nonlinear coupling between reactions and diffusion which gives rise to nonlinear phenomena [15]. The chemical reaction exhibits a prolonged non-equilibrium state and during this period, it shows various macroscopic

temporal oscillations and spatial pattern formation, such as target waves, spirals and scrolls. In general, the BZ reaction is a catalytic oxidation of an organic species by bromate ion in the presence of strong acid [16]. The overall reaction can be expressed as [17]:

$$2BrO_3^- + 3CH_2(COOH)_2 + 2H^+ \rightarrow 2BrCH(COOH)_2 + 3CO_2 + 4H_2O \quad (2.10)$$

The BZ reaction is one of the most widely studied oscillating chemical reaction that exhibits spatio-temporal pattern formation. Since we mostly use BZ reaction for studying chemical patterns, the mechanism is explained in details below.

The detailed mechanism of the BZ reaction was studied by Field, Korös and Noyes [24, 25] which came to be known as "FKN mechanism". The BZ reaction is divided into three processes in order to account for the oscillatory behavior of the system. The main intermediates of the BZ reaction are bromide (Br^-) and bromous acid. Bromide (Br^-) acts as the inhibitory species and bromous acid ($HBrO_2$) acts as the autocatalytic species.

Process 1 involves the reduction of BrO_3^- to Br_2 by bromide, and the bromination of malonic acid which leads to the formation of bromomalonic acid.

$$\begin{aligned} BrO_3^- + Br^- + 2H^+ &\rightarrow HBrO_2 + HOBr & (2.11)\\ HBrO_2 + Br^- + 2H^+ &\rightarrow 2HOBr & (2.12)\\ HOBr + Br^- + H^+ &\rightarrow Br_2 + H_2O & (2.13)\\ Br_2 + CH_2(COOH)_2 &\rightarrow BrCH(COOH)_2 + Br^- + H^+ & (2.14) \end{aligned}$$

$$BrO_3^- + 2Br^- + 3CH_2(COOH)_2 + 3H^+ \rightarrow 3BrCH(COOH)_2 + 3H_2O \quad (2.15)$$

This decreases the concentration of bromide to a critical level. Once this is obtained, process 2 becomes dominant.

In process 2, the autocatalytic production of $HBrO_2$ takes place. The bromous acid competes with bromide to reduce bromate which results in the oxidation of the catalyst Ce^{3+} to Ce^{4+}.

$$\begin{aligned} BrO_3^- + HBrO_2 + H^+ &\rightarrow 2.BrO_2 + H_2O & (2.16)\\ BrO_2 + Ce^{3+} + H^+ &\rightarrow HBrO_2 + Ce^{4+} & (2.17) \end{aligned}$$

$$BrO_3^- + HBrO_2 + 2Ce^{3+} + 3H^+ \rightarrow 2HBrO_2 + 2Ce^{4+} + H_2O \quad (2.18)$$

The third process involves the reduction of the catalyst and the production of Br^- ions:

$$CH_2(COOH)_2 + 6Ce^{4+} + 2H_2O \rightarrow 6Ce^{3+} + HCOOH + 2CO_2 + 6H^+ \quad (2.19)$$
$$BrCH(COOH)_2 + 4Ce^{4+} + H_2O + HOBr \rightarrow 4Ce^{3+} + 2Br^- + 3CO_2 + 6H^+ \quad (2.20)$$
$$Br_2 + HCOOH \rightarrow 2Br^- + CO_2 + 2H^+ \quad (2.21)$$

The oscillation in the BZ system can be quantitatively evidenced by following the pathways of bromide ions, its production and consumption.

2.2.4 Experimental techniques

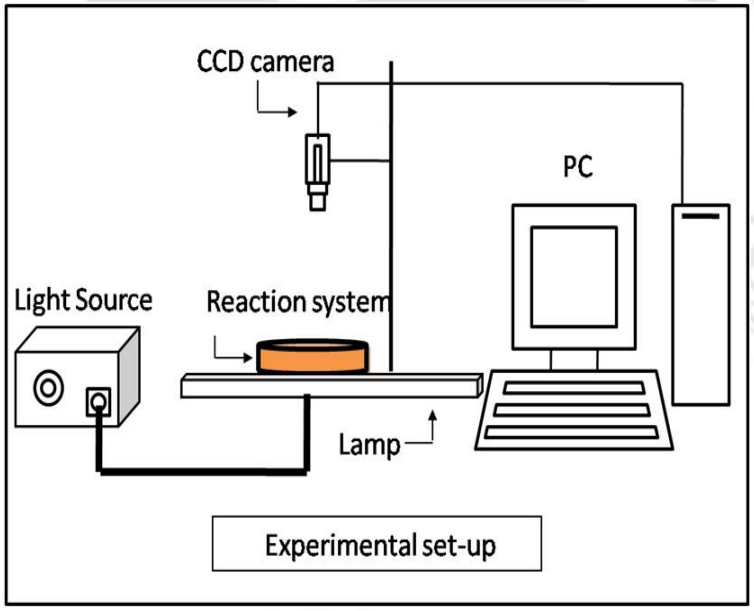

FIG. 2.1: Schematic diagram of our experimental set up.

A simple experimental set up of our experiments is shown in Fig. 2.1. We perform our experiments in a petri dish. The reaction system is monitored from above by a charge coupled device (CCD) camera (mvBlueFOX220a) through a blue filter, while it is illuminated from below with a diffused white light. The images are recorded onto a personal computer at an interval of 2 s or 10 s, and the data analyzed using MATLAB codes.

We carried out experiments using the Ferroin-catalyzed Belousov-Zhabotinsky reaction. All solutions were made in Millipore water and the experiments carried out at room temperature. In most of our experiments, the initial concentrations of the different components of the Ferroin-catalyzed BZ system were as follows: sodium bromate 0.04 M, malonic acid 0.04 M, sulphuric acid 0.2 M and ferroin indicator solution 0.08 mM. Most of the experiments were done in gel, where the reaction solution was embedded in a 0.8 % w/v agar gel matrix.

2.3 Numerical Models

2.3.1 Oregonator model

The BZ mechanism was reduced to a two variable model mechanism by Field, Korös and Noyes, which is well known as the Oregonator model [20]:

$$\begin{aligned} A+Y &\rightarrow X+P(k_1) && (2.22)\\ X+Y &\rightarrow 2P(k_2) && (2.23)\\ A+X &\rightarrow 2X+2Z(k_3) && (2.24)\\ 2X &\rightarrow A+P(k_4) && (2.25)\\ B+Z &\rightarrow \frac{1}{2}fY(k_5) && (2.26) \end{aligned}$$

where $A = [BrO_3^-]$; $B =$ malonic acid; $X = [HBrO_2]$; $P =$ HOBr; $Y = [Br^-]$; $Z = [Ce^{4+}]$; and f is an adjustable stoichiometric factor. From this simplified model, we can write the rate equations as:

$$\begin{aligned} \frac{dX}{dt} &= k_1AY - k_2XY + k_3AX - 2k_4X^2 && (2.27)\\ \frac{dY}{dt} &= -k_1AY - k_2XY + \frac{1}{2}fK_5BZ && (2.28)\\ \frac{dZ}{dt} &= 2k_3AX - k_5BZ && (2.29) \end{aligned}$$

To non-dimensionalize the rate equations, the following definitions suggested by Tyson and Fife [21] are used.

$$
\begin{aligned}
u &= \frac{2k_4}{k_3A}X, \\
v &= \frac{k_4k_5B}{(k_3A)^2}Z, \\
w &= \frac{k_2}{k_3A}Y, \\
\epsilon' &= \frac{2k_4k_5B}{k_2k_3A}, \\
\tau &= k_5t, \\
\epsilon &= \frac{k_5B}{k_3A}, \\
q &= \frac{2k_1k_4}{k_2k_3}, \\
h &= 2f
\end{aligned}
$$

and therefore the balance equations now become:

$$\epsilon\frac{du}{d\tau} = qw - uw + u - u^2 \tag{2.30}$$

$$\frac{dv}{d\tau} = u - v \tag{2.31}$$

$$\epsilon'\frac{dw}{d\tau} = -qw - uw + fv \tag{2.32}$$

The relatively small value of ϵ' compared to ϵ allows the steady-state approximation, giving rise to the following two variable Oregonator system:

$$\epsilon\frac{du}{d\tau} = u(1-u) - \frac{fv(u-q)}{q+u} \tag{2.33}$$

$$\frac{dv}{d\tau} = u - v \tag{2.34}$$

2.3.2 Barkley model

In 1991, Barkley proposed a simple mathematical model that explains the dynamics of a reaction diffusion (excitable) system. This model is not a derivation from any particular excitable system, but it is derived in such a manner that it has all the characteristics to explain an excitable system. It also shows various types of wave patterns. The two-variable system of reaction-diffusion equations are given below [22]:

$$\frac{\partial u}{\partial t} = f(u,v) \tag{2.35}$$
$$\frac{\partial v}{\partial t} = g(u,v) \tag{2.36}$$

where $f(u,v)$ and $g(u,v)$ express the local kinetics of the two variables u and v;

$$f(u,v) = \frac{1}{\epsilon}\left\{u(1-u)\left(u-\frac{v+b}{a}\right)\right\} \tag{2.37}$$
$$g(u,v) = u-v \tag{2.38}$$

u represents the activator (excitation) and v the inhibitor (recovery), where a, b, and ϵ are parameters. These local parameters can be adjusted according to the requirement of the system. These values provide the properties of the medium. In the simplest Barkley model, it is assumed that v does not diffuse. There can also be systems where v is considered to be diffusing.

2.4 Solving Differential Equations on Computer

The numerical simulation is widely used in diverse fields as a result of recent development of computer technology. Simulation techniques play a very important role in almost all the scientific and non-scientific study that we can imagine. Numerical simulation has many advantages when it comes to performing faster, better and cheaper. To discuss the details of the numerical simulation, it is necessary to understand the basic concept of simulation. Numerical simulation is the study of a mathematical representation of a physical system by a device such as a computer or can also be described as a way of understanding the dynamics of a model that imitates the behavior of the system. It designates a process by which one or more programs are performed on one or more computers, in order to accomplish a calculation in a faster and efficient way. Scientific numerical simulations are built on established theoretical models. Simulation is used to study the operation and properties of a system and to predict its evolution.

2.4.1 Euler method

The computer enables us to approximate the solutions to analytically intractable problems, and also to visualize those solutions. Let us use the vector field analysis of

$$\dot{y} = f(y) \tag{2.39}$$

Given the differential equation, subjected to initial condition $y = y_o$ at $t = t_o$, a systematic method can be formalized to approximate the solution $y(t)$. We consider a fluid flowing steadily on the y-axis, with velocity $f(y)$ at the location y. Let us consider the initial point to be y_0, with local velocity $f(y_0)$. If the fluid flows for a very short time $\Delta t = h$, it will move a distance of $f(y_0)h$, since, distance=rate $\times$ time. Hence, the new position $y(t_0 + h)$ is approximately $y_0 + f(y_0)h$. Let the new position be y_1 [23]. Therefore,

$$y(t_0 + h) \approx y_1 = y_0 + f(y_0)h \tag{2.40}$$

The velocity for the new position y_1 is $f(y_1)$. From iteration, we get

$$y_2 = y_1 + f(y_1)h \tag{2.41}$$

This gives us the general rule

$$y_{(n+1)} = y_n + f(y_n)h \tag{2.42}$$

This method is known as "Euler method", and is the simplest numerical simulation technique.

2.4.2 Runge-Kutta method

The Euler method is also known as the first order Runge-Kutta Method. The Euler method has sometimes large truncation error, and is sometimes highly unstable. In that case, we can use higher order Runge-Kutta method to solve our equations, which are described below [24].

2nd order Runge-Kutta method

The second order Runge-Kutta method is shown below:

$$\dot{y} = f(y,t), y(0) = y_0 \tag{2.43}$$
$$y_{(n+1)} = y_n + k_2 \tag{2.44}$$
$$k_1 = hf(y_n, t_n) \tag{2.45}$$
$$k_2 = hf(y_n + \frac{k_1}{2}, t_n + \frac{h}{2}) \tag{2.46}$$

4th order Runge-Kutta method

The fourth order Runge-Kutta method takes the form:

$$\dot{y} = f(y,t), y(0) = y_0 \tag{2.47}$$

$$y_{(n+1)} = y_n + \frac{k_1}{6} + \frac{k_2}{3} + \frac{k_3}{3} + \frac{k_4}{6} + o(h^5) \tag{2.48}$$

$$k_1 = hf(y_n, t_n) \tag{2.49}$$

$$k_2 = hf(y_n + \frac{k_1}{2}, t_n + \frac{h}{2}) \tag{2.50}$$

$$k_3 = hf(y_n + \frac{k_1}{2}, t_n + \frac{h}{2}) \tag{2.51}$$

$$k_4 = hf(y_n + k_3, t_n + h) \tag{2.52}$$

The above described methods are used to integrate and solve first order ordinary differential equations.

Comparison between Euler and Runge-Kutta method:

Let us consider the following equation

$$\dot{y} = y - t^2 + 1, y(0) = 0.5 \tag{2.53}$$

The exact solution is given by,

$$y = t^2 + 2t + 1 - \frac{1}{2}e^t \tag{2.54}$$

To solve this equation with Euler method and fourth order Runge-Kutta method, we will take step size $h = 0.5$.

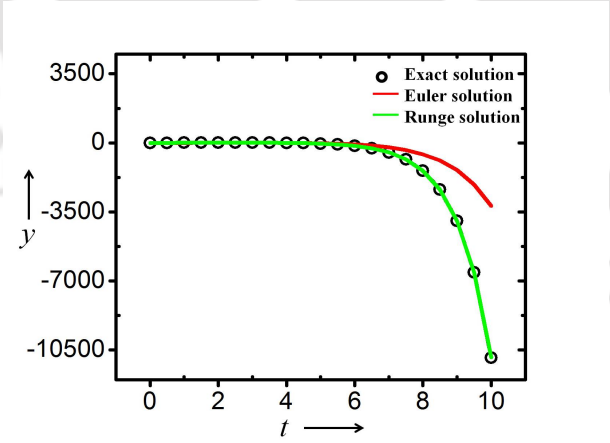

FIG. 2.2: Graph showing the comparison between Euler and fourth order Runge-Kutta method. Black circles represent the exact solutions, green curve is obtained from fourth order Runge-Kutta method and red curve from Euler method.

The plot of y vs t is shown in Fig. 2.2. It elucidates the difference between the solution of the Euler and Runge-Kutta method. From the graph, it can be said that Runge-Kutta integration gives more accurate results than Euler method.

2.5 Chemical Waves in Two and Three Dimensions:

The most widely studied wave patterns are those that occur in two dimensions.

2.5.1 Target patterns

Target patterns are initiated from a localized pacemaker and gives out expanding concentric circles with a constant period.

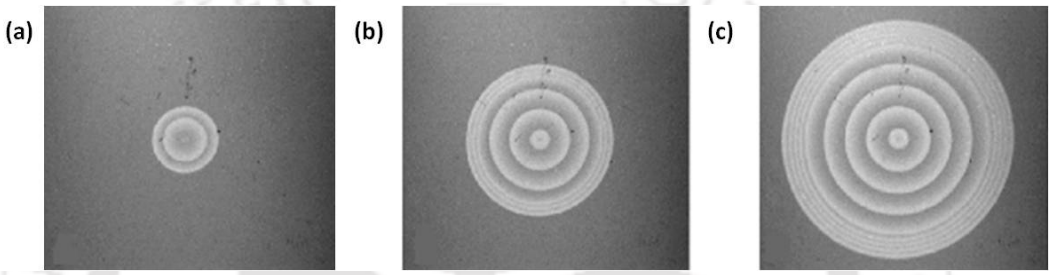

FIG. 2.3: Target patterns seen in BZ system. Snapshots (a), (b) and (c) are for three different periods [25]

.

An example of target wave is shown in Fig. 2.3 [25].

2.5.2 Spirals

Spiral waves can be obtained in a thin layer of a 2D chemical excitable medium.

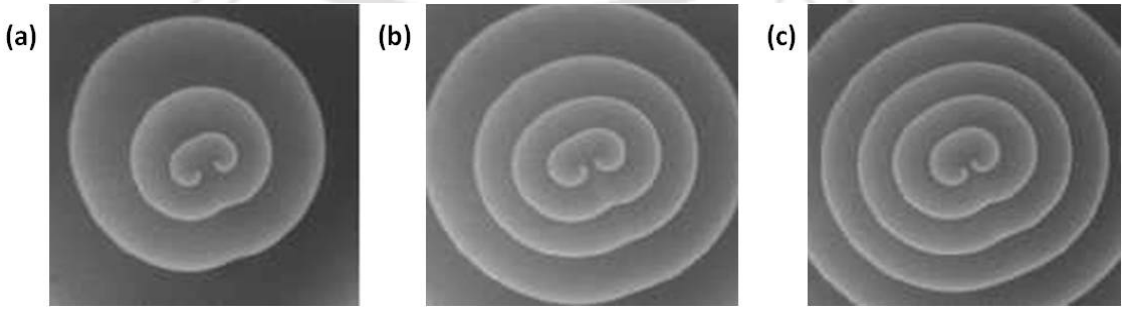

FIG. 2.4: Snapshots of counter rotating spiral wave created by disrupting a circular wave in BZ reaction.

It is created by disrupting the front of a circular propagating wave. These causes each free end to curl and form a spiral.

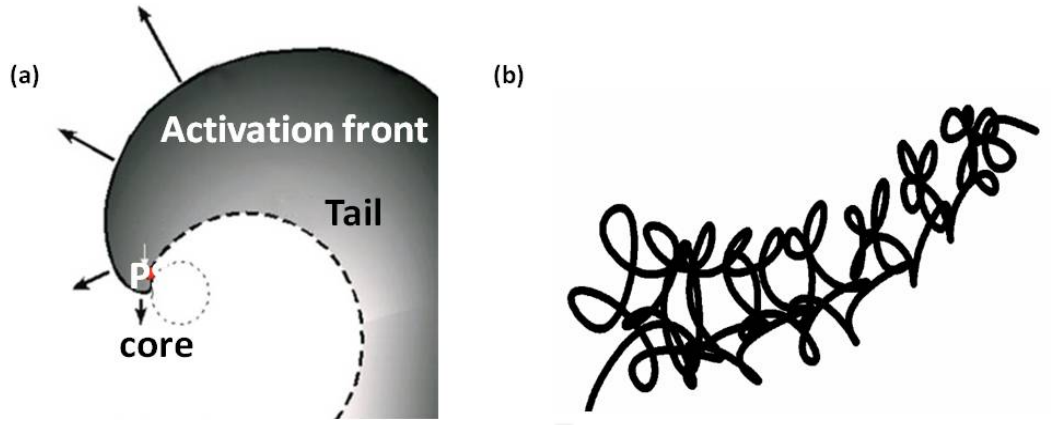

FIG. 2.5: (a) Activation front of a wave showing its curling [26], (b) An example of a trajectory traced by the tip of a spiral wave in BZ experiment.

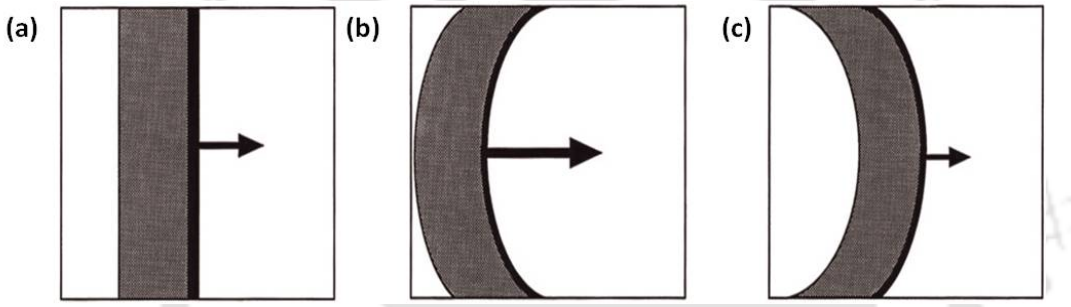

FIG. 2.6: Cartoons showing the effect of curvature on wave propagation [26, 27].

Figure 2.4 shows an example of a pair spiral waves generated in a BZ solution. The two ends of the spiral have opposite chirality and therefore are called counter-rotating spirals. The brighter areas (white part) correspond to the higher concentration zone of ferroin in the oxidized state whereas the dark areas are that of ferroin in a reduced state. The area around which the spiral rotates is called the tip or core [Fig. 2.5 (a)] [26]. The path traced by the tip of the spiral is known as its trajectory [Fig. 2.5 (b)]. The trajectory of a spiral tip may be either circular or meandering. An example of meandering trajectory is shown in Fig. 2.5 (b).

The dynamic behavior of spiral waves of reaction–diffusion systems depend strongly on the curvature of the surface. A linear relationship between the propagating velocity and the curvature of a travelling wave is given by

$$\hat{N} = \hat{c} - D\hat{K} \tag{2.55}$$

$\hat{N}$ is the normal velocity, $\hat{c}$ is the velocity of plane waves, D is the diffusion coefficient

of the autocatalytic species and $\hat{K}$ is the curvature of the waves. This equation is known as the "Eikonal equation". The effect of curvature is shown in Fig. 2.6. The propagation velocity of a plane wave [Fig. 2.6 (a)] is slower than the one with negative curvature [Fig. 2.6 (b)], but is faster than the wave with positive curvature [Fig. 2.6 (c)] [27, 28].

2.5.3 Scrolls

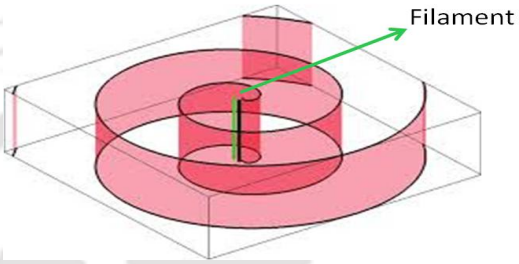

FIG. 2.7: Scroll with a straight filament (red) [29].

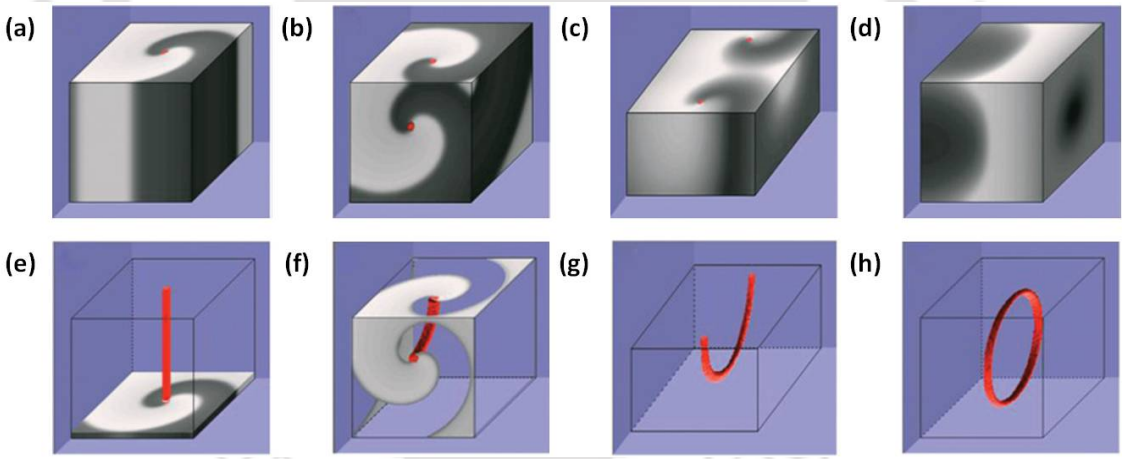

FIG. 2.8: Scroll wave with (a, e) straight filament, (b, f) curved filament (c, g) U shaped filament and (d, h) round filament [26].

Three dimensional waves are more complex than 2D patterns. However, these patterns have some basic similarities with those occurring in two dimensions. A simple scroll wave is a three dimensional entity which rotates around a one dimensional phase singularity known as filament [Fig. 2.7] [30].

A simple three dimensional scroll waves can be created by stacking a multiple of two dimensional spiral waves [Fig. 2.7]. The filament may be straight, curve, round or

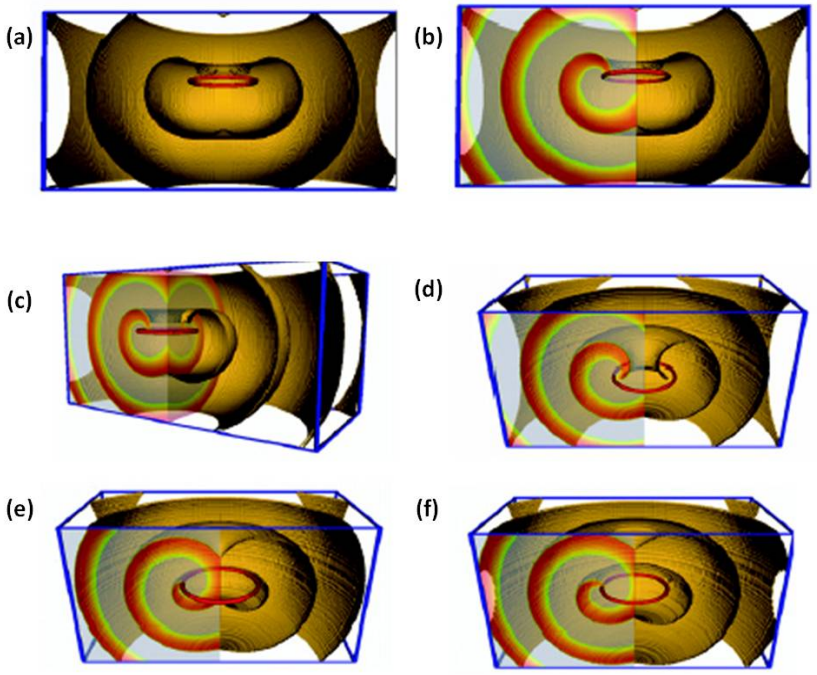

FIG. 2.9: Three dimensional view of a scroll wave with round filament taken from different angles [31].

it may take any shape [Fig. 2.8]. The filaments are either close loop or end at the system boundary.

Figure 2.9 shows a three dimensional view of a scroll with round filament (red). It is also known as scroll ring. Scroll waves rotating around filaments can also move in space and change shape. The phase of rotation may vary along the filament, the feature known as twist of scroll wave. Twist of a scroll wave and curvature of the filament are factor of its dynamics that are specifically three dimensional.

The motion of a filament can be described by the curvature flow model. This model describes the collapse or shrinkage of the filament, expansion and also the drifting of the filament. The curvature-flow model expresses the motion of the filament $\hat{s}$ in the directions of its unit normal vector $\hat{N}$ and unit binormal vector $\hat{B}$. The filament velocity is proportional to the local curvature $\hat{K}$ as follows:

$$\frac{d\hat{s}}{dt} = (\alpha\hat{N} + \beta\hat{B})\hat{K} \tag{2.56}$$

Where, α and β are the filament tension and the translational drift coefficient respectively. When $\beta = 0$, the filament does not move in the binormal direction. When α

is positive, it gives rise to positive filament tension, which means that the filament shrinks in size with time and when α is negative, it gives rise to negative filament tension, i.e., it expands [32].

2.5.4 Generating spiral wave

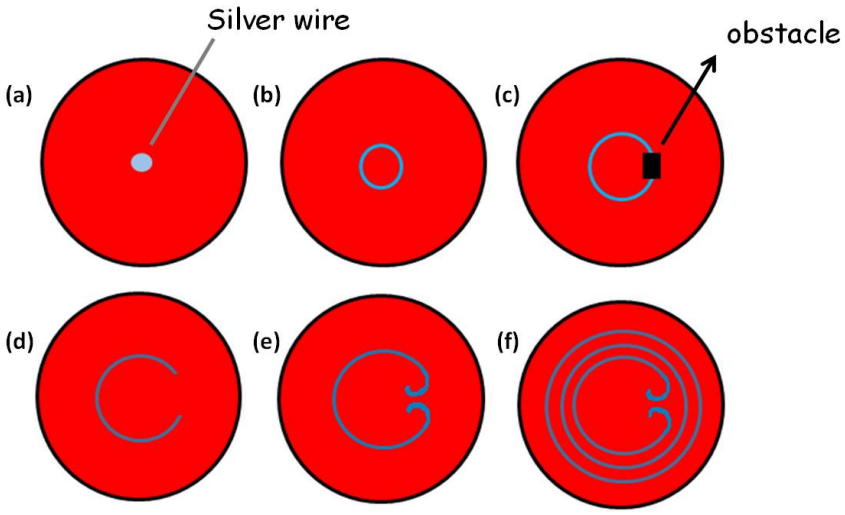

FIG. 2.10: Schematic diagram for generation of spiral waves. (a) Initiation of a wave with silver wire. (b) Circular expansion of the wave. (c) Black obstacle disrupts the wave, generating open ends (d). (e) A pair of spirals formed from the curling of the two ends. (f) A Propagating spiral wave.

Figure 2.10 shows a schematic diagram of generating a spiral wave which we employ in our laboratory. First, we generate a plane wave with the help of a silver wire [Fig. 2.10 (a)], and then we allow it to expand. After it has reached the desired dimension, we use an obstacle which is an unexcitable object that does not react with the reaction system [shown in black in Fig. 2.10 (c)] to break the wave. The two ends curl to form a pair of spiral waves [Fig. 2.10 (e)].

2.5.5 Generating free scroll ring

A scroll wave with a circular filament is known as a scroll ring. Scroll waves can be generated in a thick reaction medium. In BZ system, a scroll is generated in a two layer gel system. In the first gel layer, a wave is generated using the tip of the

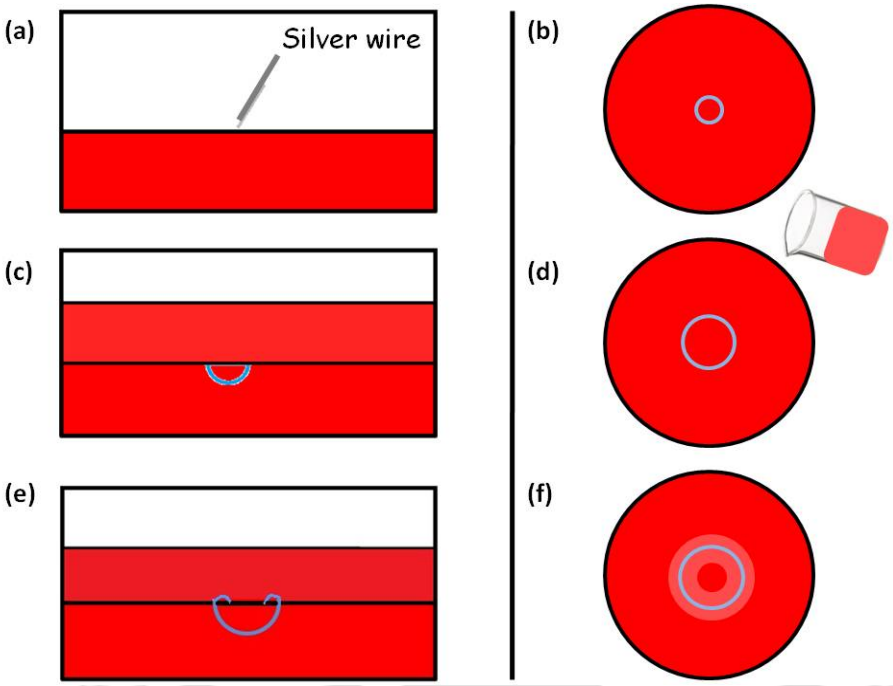

FIG. 2.11: Schematic diagram for generating scroll waves in a BZ gel solution. The left panel shows the side view and right panel demonstrate the top view of our experiment. In (a) and (b), a wave is initiated with the help of a silver wire.

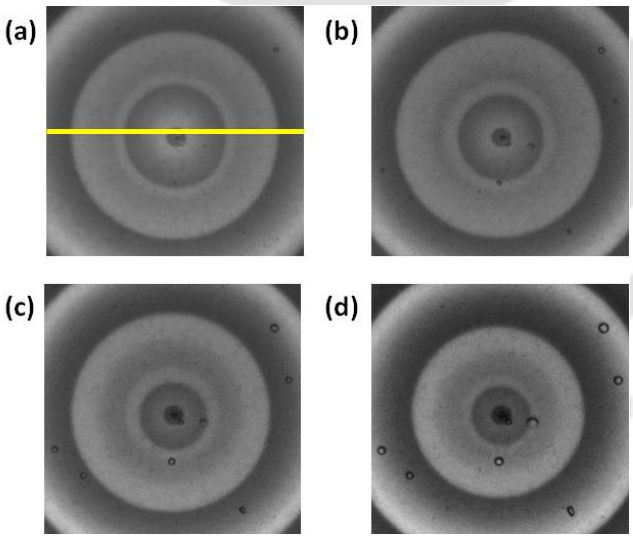

FIG. 2.12: (a, b, c, d) Snapshots of scroll wave for 525 s, 105 s, 1540 s and 2060 s, respectively. The scroll is shrinking in size with time.

silver wire which initiates a half spherical wave. When the wave reaches the desired dimension, another gel solution is poured over it at a temperature slightly above its gelling point and is allowed to gel over the first layer. The semi-spherical wave generated in the first layer now curls into the top layer forming a scroll of circular

filament.

A schematic diagram of the procedure of generating a scroll wave in a laboratory is shown in Fig. 2.11. Figure 2.11 (a, c, e) shows a lateral view and (b, d, f) shows the top view.

A scroll wave with a positive filament tension has a definite lifetime depending on its size. Such a free scroll ring in each rotation decreases in diameter until it completely collapses. In Fig. 2.12 (a, b, c, d), we can see that the scroll waves shrinks with the evolution of time.

2.5.6 Time – space plot

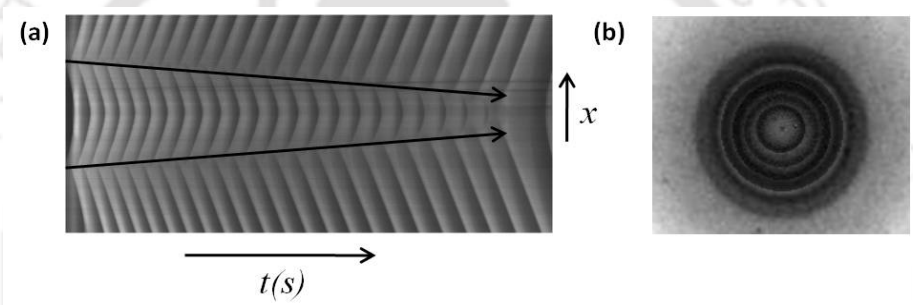

FIG. 2.13: (a) Time – space plot of a scroll ring with positive filament tension, and (b) Computationally simulated graphic of the two dimensional filament of a scroll ring in BZ reaction.

Time – space plot is one of the first and foremost methods for filament detection. Time – space plot is obtained as a time variation cross-section [yellow line in Fig. 2.12 (a)] of the two dimensional projection of the experimental system captured from above. Figure 2.13 (a) shows an example of such a plot obtained for a free scroll ring with a positive filament tension. The area where the filament lies is marked with the arrow (black). In the figure, we can notice that there is phase difference near the region of the arrow line. This is where the filament lies. As can be seen, the filament shrinks in size with time. A filament detected from computation is shown in Fig. 2.13 (b), where the shrinking is clearly shown.

Bibliography

[1] S. Cortassa, M. A. Aon, B. O'Rourke, R. Jacques, H. J. Tseng, E. Marban, and R. L. Winslow, Biophys. J. **91**, 1564 (2006). A computational model integrating electrophysiology, contraction, and mitochondrial bioenergetics in the ventricular myocyte.

[2] R. FitzHugh, Biophys. J. **1**, 445 (1961). Impulses and physiological states in theoretical models of nerve membrane.

[3] C. H. Luo, and Y. Rudy, Circ. Res. **68**, 1501 (1991). A model of the ventricular cardiac action potential, depolarization, repolarization, and their interaction.

[4] E. M. Izhikevich, and R. FitzHugh, Scholarpedia **1**, 1349 (2006). FitzHugh-Nagumo model.

[5] C. H. Luo, and Y. Rudy, Circ. Res. **74**, 1071 (1994). A dynamic model of the cardiac ventricular action potential.

[6] T. S. Briggs, and W. C. Rauscher, J. Chem. Educ. **50**, 496 (1973). An oscillating iodine clock.

[7] R. M. Noyes, and S. D. Furrow, J. Am. Chem. Soc. **104**, 45 (1982). The oscillatory briggs-rauscher reaction. III. a skeleton mechanism for oscillations.

[8] O. Benini, R. Cervellati, and P. Fetto, J. Chem. Educ. **73**, 865 (1996). The BZ reaction: experimental and model studies in the physical chemistry laboratory.

[9] R. Imbihl, and G. Ertl. Chem. Rev. **95**, 697 (1995). Oscillatory kinetics in heterogeneous catalysis.

[10] J. H. E. Cartwright, J. M. G. Ruiz, and A. I. Villacampa, Comput. Phys. Commun. **121**, 411 (1999). Pattern formation in crystal growth: Liesegang rings.

[11] A. P. Muñuzuri, M. Dolnik, A. M. Zhabotinsky, and I. R. Epstein, J. Am. Chem. Soc. **121**, 8065 (1999). Control of the chlorine dioxide-iodine-malonic acid oscillating reaction by illumination.

[12] S. Nettesheim, A. von Oertzen, H. H. Rotermund, and G. Ertl, J. Chem. Phys. **98**, 9977 (1993). Reaction diffusion patterns in the catalytic CO-oxidation on Pt(110): Front propagation and spiral waves.

[13] A. M. Zhabotinsky, Scholarpedia **2**, 1435 (2007). Belousov-Zhabotinsky reaction.

[14] S. K. Scott, *Oscillations, waves, and chaos in chemical kinetics* (Oxford University Press, 1994).

[15] B. A. Grzybowski, *Chemistry in motion* (John Wiley & Sons Ltd, 2009).

[16] M. A. Pellitero, C. A. l. Lamsfus, and J. Borge, J. Chem. Educ. **90**, 82 (2013). The Belousov - Zhabotinskii reaction: Improving the Oregonator Model with the Arrhenius Equation.

[17] I. R. Epstein, J. A. Pojman, *An introduction to nonlinear chemical dynamics* (Oxford University Press, Oxford, 1998).

[18] R. J. Field, E. Korös, and R. M. Noyes, J. Am. Chem. Soc. **94**, 8649 (1972). Oscillations in chemical systems. II. Thorough analysis of temporal oscillation in the Bromate-Cerium-Malonic acid system.

[19] R. J. Field and R. M. Noyes, J. Chem. Phys. **60**, 1877 (1974). Oscillations in chemical systems. IV. Limit cycle behavior in a model of a real chemical reaction.

[20] R. J. Field, Scholarpedia **2**, 1386 (2007). Oregonator.

[21] J. J. Tyson, and P. C. Fife, J. Chem. Phys. **73**, 2224 (1980). Target patterns in a realistic model of the Belousov–Zhabotinskii reaction.

[22] D. Barkley, Physica D **49**, 61 (1991). A model for fast computer simulation of waves in excitable media.

[23] S. H. Strogatz, *Nonlinear dynamics and chaos: With applications to physics, biology, chemistry, and engineering* (1st Edition, Westview Press, 1994).

[24] W. C. Press, S. A. Teukolsky, W. T. Vetterling, and B. P. Flannery, *Numerical recipes in FORTRAN: The art of scientific computing* (Cambridge University Press, Second Edition, 1992).

[25] C. T Hamik, and O. Steinbock, New J. Phys. **5**, 58, (2003). Excitation waves in reaction–diffusion media with non-monotonic dispersion relations

[26] J. Jalife, M. Delmar, J. Anumonwo, O. Berenfeld, and J. Kalifa, *Basic cardiac electrophysiology for the clinician* (Wiley-Blackwell, Oxford, UK, second edition, 2009).

[27] V. G. Fast, and A. G. Kleber, Cardiovasc Res. **33**, 258 (1997). Role of wavefront curvature in propagation of cardiac impulse.

[28] P. Foerster, S. C. Müller, and B. Hess, Development **109**, 11 (1990). Curvature and spiral geometry in aggregation patterns of dictyostelium discoideum.

[29] H. Dierckx, and H. Verschelde, Phy. Rev. E **88**, 062907 (2013). Effective dynamics of twisted and curved scroll waves using virtual filaments.

[30] Z. A. Jiménez, and O. Steinbock, Phy. Rev. Lett. **109**, 098301 (2012). Stationary vortex loops induced by filament interaction and local pinning in a chemical reaction-diffusion system.

[31] E. M. Cherry, and F. H. Fenton, New J. Phys. **10**, 125016 (2008). Visualization of spiral and scroll waves in simulated and experimental cardiac tissue.

[32] Z. A. Jiménez, and O. Steinbock, Phy. Rev. E **86**, 036205 (2012). Scroll wave filaments self-wrap around unexcitable heterogeneities.

Chapter 3

A detailed study of spiral waves in concentration variant Belousov-Zhabotinsky reaction

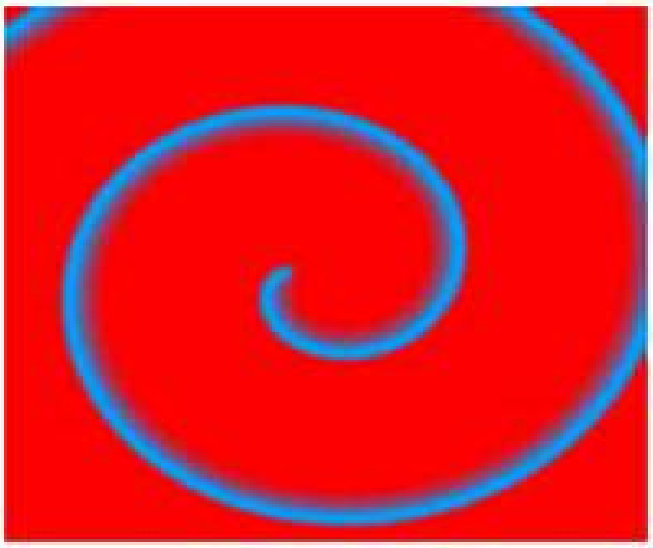

3.1 Introduction

Rotating spiral waves have been observed ubiquitously in thin layers of excitable media like aggregating slime molds [1, 2], cardiac tissue [3, 4], yeasts extracts [5], frog oocyte [6], chemical media [7, 8], etc. Spirals of electrical activity have been suggested to be responsible for cardiac arrhythmias, instabilities of which may further lead to ventricular fibrillation, the leading cause of heart failure in the modern world [3, 9, 10]. The first experimental evidence of spiral waves in an RD system was found in the Belousov-Zhabotinsky (BZ) reaction by Zhabotinsky and Zaikin [11]. Since then the BZ system has been a subject of particular interest of study due to its resemblance to other biological excitable systems. A significant feature of spiral waves is the point of initiation center or pacemaker, known as the spiral center or core. Intensive investigation has shown that the dynamics of a spiral wave can be described by the motion of its tip. Initial studies revealed that spiral tips follow circular paths until Winfree showed that under certain conditions, spirals can also be meandering (cycloidal curves) [12]. Since then, many results on meandering spiral waves have been published [13, 14, 15, 16, 17]. Experimental and theoretical analysis have shown that spirals follow epicycloid orbits (flowerlike orbits with inward petals) or hypocycloid orbits (flowerlike orbits with outward petals) [7, 18, 19]. The dependence of the spiral tip on system parameters has been studied earlier in numerical simulations using reaction diffusion models, especially the Oregonator model [12, 20]. Some studies have been reported by Müller et. al, which demonstrated the dependence of the geometry of the spiral on the concentration of the acid. They found that in highly acidic conditions, spirals are Archimedean, whereas there occur deviations from the trend with decreasing acidity [21]. Belmonte et. al [22] have carried out a systematic study of spiral waves in the BZ reaction in an open reactor with varying concentrations of the substrates. They reported a range of concentration values where spiral wave formation occurs. In this chapter, we study in detail the effect of substrate concentration on the dynamics of spiral waves. We use a thin layer of the BZ reaction for generating spirals and vary the concentration of the reactants in a controlled manner to monitor how the primary wave characteristics like wavelength and time-period change. Also, we

study in detail the tip trajectory of the spiral waves, and we are able to find a trend in the properties of the trajectory with the changing concentration of the reactants. Our experimental results are able to verify some earlier mathematical conclusions drawn about the Oregonator model that relates it to the actual concentration of chemical species in the reaction. We show that such relationships are not restricted to the average wave properties alone, but also to the dynamics of the spiral tip. We have also been able to find spirals in the concentration ranges where earlier studies had reported no such waves [22].

3.2 Numerical Simulations

The Oregonator model, first proposed by Field and Noyes [23], is widely used to study spatio-temporal pattern formation in BZ reaction. The model in presence of diffusion can be described as below:

$$\frac{\partial u}{\partial t} = \frac{1}{\epsilon}[u(1-u) - \frac{fv(u-q)}{(q+u)}] + D_u \nabla^2 u \tag{3.1}$$

$$\frac{\partial v}{\partial t} = u - v + D_v \nabla^2 v \tag{3.2}$$

Here, the time dependent variables u and v are dimensionless forms corresponding to [$HBrO_2$] and [M_{ox}] respectively, q and f are kinetic parameters, and $D_u = 1.0$ and $D_v = 0.6$ are the respective diffusion coefficients of u and v. ϵ represents the ratio of the time scales of the dynamics of the fast and slow variables. The detailed mechanism is given in chapter 2 [equations (2.10) - (2.21)]. Winfree in one of his papers suggested the relation between ϵ and concentration of the different chemical species in the BZ reaction which is as given below [7]:

$$\epsilon = \frac{k_5}{k_3} \frac{[organics]}{[H^+][BrO_3^-]} \tag{3.3}$$

Where [organics] = [BrMA] + [MA] (MA stands for malonic acid), $k_5 = 0.4\ M^{-1}s^{-1}$, $k_3 = 40\ M^{-2}s^{-1}$. Andrew et al. also suggested an equation explaining the dependence of ϵ on the concentrations of the reactants which is given below [22]:

$$\epsilon = \frac{k_j}{k_6} \frac{[organics]}{[H^+][BrO_3^-]} \tag{3.4}$$

Where [organics] = [BrMA] + [MA], $k_j = 1\ \mathrm{M^{-1}s^{-1}}$, $k_6 = 10\ \mathrm{M^{-2}s^{-1}}$. There is not much difference in the formulation provided in these two independent works. The value of epsilon for each set of reaction can be calculated from any of the above two equations. Both the equations give similar results. Thus, we calculated ϵ for each set of reaction condition, and tried to see the nature of various wave properties as a function of ϵ.

For simulations, equations (3.1) and (3.2) were integrated using explicit Euler scheme for a two dimensional lattice of 300×300 grid points having zero flux boundaries along all the four walls. A time step of $dt = 0.0012$ and a grid spacing of $dx = 0.5$ were employed. The above set of conditions produced spirals whose tips are either meandering or stationary depending on the value of ϵ, f, and q. The tip of the spiral was identified at the isoconcentration points of u and v.

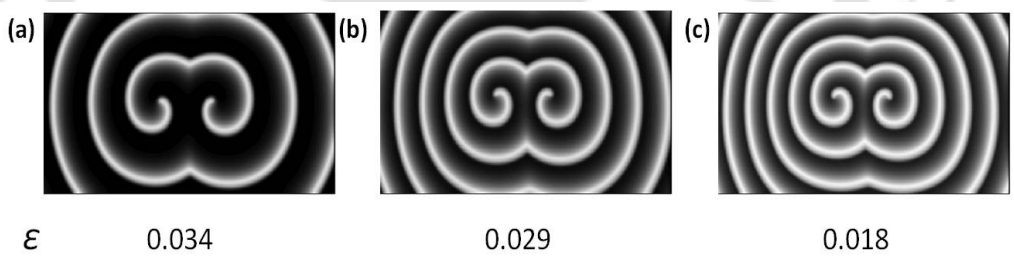

FIG. 3.1: Snapshots of spiral wave generated using Oregonator model for three different values of ϵ: (a) = 0.034, (b) = 0.029, and (c) = 0.018.

Simulations were performed varying ϵ from 0.01-0.1. In Fig. 3.1, snapshots of spiral waves for three different values of ϵ are shown. The figure shows that the wavelength decreases with decrease in ϵ. The dynamics of a spiral wave mostly depends on its tip, i.e., the area around which the core rotates. Therefore, we traced the trajectory for different values of ϵ.

In the Oregonator model, the tip of a spiral either follows a circular path or meanders giving rise to a flower like pattern with petals of varying size depending on the value of the kinetic terms and ϵ. For parameter values $f = 3.3$ and $q = 1.0$ and ϵ varying in

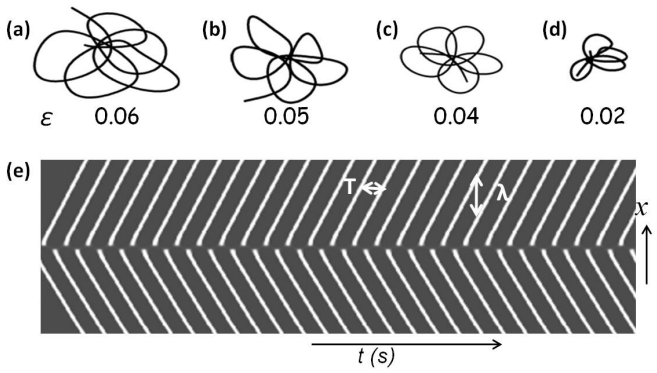

FIG. 3.2: (a - d) Tip trajectories of spiral waves for ϵ values (a) 0.06, (b) 0.05, (c) 0.04 and (d) 0.02, f = 3.3 and q = 1.0, generated with the help of MATLAB codes. (e) Time space plot generated from simulation.

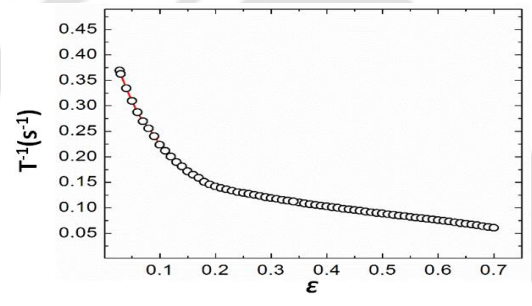

FIG. 3.3: Frequency as a function of epsilon. In the plot, ϵ ranges from 0.02 to 0.7.

the range of 0.001 to 0.13, the spiral meanders with outward petals. The trajectory of spirals for some of the ϵ values are shown in Fig. 3.2. The simulation results show that the core size of the trajectory decreases with decreasing value of ϵ. The period for different ϵ is calculated from the time-space plot as shown in Fig. 3.2 (e).

Frequency, which is related inversely to the time-period, is plotted against ϵ [Fig. 3.3]. The figure illustrates that frequency decays with increase in ϵ. The relation of epsilon and core size has already been studied theoretically [7]. The trend shows that as ϵ value is increased the core size is increased.

3.3 Experimental Section

All experiments were performed in a thin layer of ferroin-catalyzed BZ system using malonic acid as the organic substrate. A series of experiments were carried out with

Table 3.1: List of the set of concentrations of different species in the Belousov-Zhabotinsky reaction for which experiments were performed. $[H_2SO_4] = 0.16 - 0.32$ M, $[NaBrO_3] = 0.04 - 0.12$ M and [MA] = 0.04 M, [Ferroin] = 0.001 M.

$[H_2SO_4]$ M	$[MA]$ M	$[NaBrO_3]$ M
0.16	0.04	0.04
		0.06
		0.08
		0.1
		0.11
		0.12
0.2	0.04	0.04
		0.06
		0.08
		0.1
		0.11
		0.12
0.24	0.04	0.04
		0.06
		0.08
		0.1
		0.11
		0.12
0.28	0.04	0.04
		0.06
		0.08
		0.1
		0.11
		0.12
0.32	0.04	0.04
		0.06
		0.08
		0.1
		0.11
		0.12

Table 3.2: List of the set of concentrations of the various species in the Belousov-Zhabotinsky reaction for which experiments were performed. $[H_2SO_4] = 0.16 - 0.32$ M, $[NaBrO_3] = 0.04 - 0.12$ M and [MA] $= 0.04 - 0.12$ M, [Ferroin] $= 0.001$ M.

$[H_2SO_4]$ M	$[NaBrO_3]$ M	$[MA]$ M
0.16	0.04	0.04
		0.06
		0.08
		0.1
		0.11
		0.12
0.2	0.04	0.04
		0.06
		0.08
		0.1
		0.11
		0.12
0.24	0.04	0.04
		0.06
		0.08
		0.1
		0.11
		0.12
0.28	0.04	0.04
		0.06
		0.08
		0.1
		0.11
		0.12
0.32	0.04	0.04
		0.06
		0.08
		0.1
		0.11
		0.12

concentrations of different reactants in the following range: $[H_2SO_4] = 0.16 - 0.32$ M, $[NaBrO_3] = 0.04 - 0.12$ M and $[MA] = 0.04 - 0.12$ M. [Ferroin] = 0.001 M was kept constant for each reaction. Across these ranges wave fronts can be generated to initiate spiral waves. Reaction mixture outside the above range are either of high or low excitability. Therefore, only traveling waves or turbulent waves can be seen. To study the details, we carried out a series of experiments by varying the concentrations of H_2SO_4, $NaBrO_3$, and MA, the complete set of which is shown in table 1 and 2 for which spiral waves are generated. The BZ solution was prepared with all the ingredients and transferred to a petri dish of 8 cm diameter. The thickness of the solution layer was about 2 mm. The mixture was swirled while allowing one oscillation to complete and then kept undisturbed to attain a homogeneous state. A circular wave was generated by dipping for a few seconds, the tip of a silver wire in the middle of the petri dish to prevent boundary effects. The main reason behind using the silver wire is the removal of the inhibitor Br^- from the vicinity as AgBr. The wave front when cleaved results in the formation of a pair of spiral waves with two tips of opposite chirality. The petri dish was covered to prevent any undesired hydrodynamics. In the above solution, oscillations continue for four hours or more. To capture images of our experiment, a charge coupled device (CCD) camera (mvBlueFOX 22a) was mounted above the system which was illuminated from below by a cold white light source. Snapshots were recorded onto a computer every two seconds and the data analyzed using MATLAB codes.

3.4 Results and Discussion

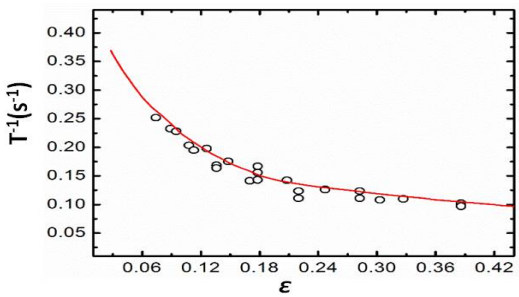

FIG. 3.4: Frequency against epsilon curve. In the graph ϵ ranges from 0.06 to 0.43.

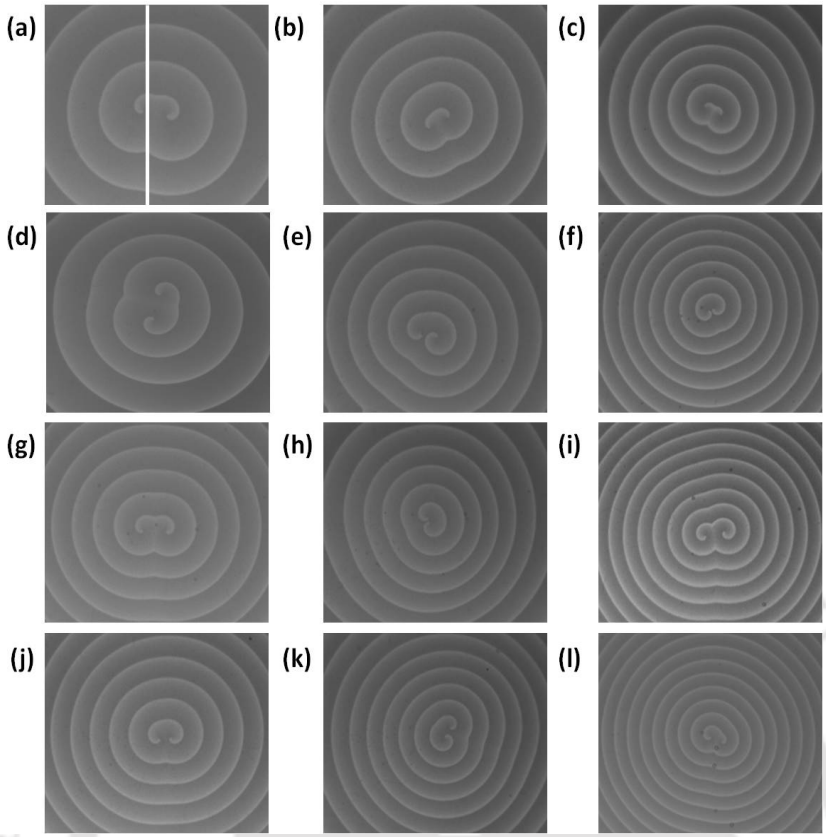

FIG. 3.5: Snapshots of spirals generated in the BZ reaction by disrupting a circular chemical wave. Each snapshot corresponds to a different set of concentrations of the chemical species present in the medium. H_2SO_4 concentration value varies across the columns as: = 0.16 M, 0.2 M, 0.24M, and 0.28M respectively, (a), (d), (g) (f), $[NaBrO_3]$ = 0.06 M, (b), (e), (h), (k) correspond to $[NaBrO_3]$ = 0.08 M, and (c), (f), (i), (l) correspond to $[NaBrO_3]$ = 0.012 M. [MA] = 0.04 M, and [Ferroin] = 0.001 M is same for each experiment in the figure. Each snapshot has an area of 6.4 × 4.8 cm^2.

The value of ϵ for each experiment was calculated from equation (3.3) and plotted against frequency. Figure 3.4 shows the plot of frequency versus epsilon and it is observed that frequency decays exponentially with increasing value of epsilon. Thus, it follows the same trend as shown in Fig. 3.3.

In Fig. 3.5, spirals for twelve different sets of reaction mixture are shown. Each column corresponds to different concentration of $NaBrO_3$ and each row corresponds to a varied concentration of H_2SO_4. Figure 3.6 shows the time-space plots for some of these experiments. These are obtained as a time variation of a cross-section [white line

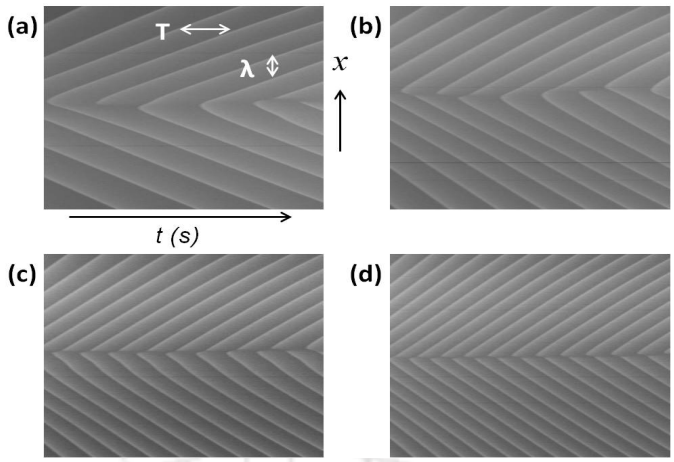

FIG. 3.6: Time space plot generated from the cross-section of two dimensional images. Each plot corresponds to different concentrations of H_2SO_4. In figure (a), (b), (c) and (d), $[H_2SO_4]$ = 0.16 M, 0.2 M, 0.24 M and 0.28 M respectively. $[NaBrO_3]$ = 0.04 M, [MA] = 0.04 M, and [Ferroin] = 0.001 M.

in Fig. 3.5(a)] of the two-dimensional projection image of the experimental system captured from above. As can be seen in Fig. 3.5 and 3.6, the frequency increases with increase in concentration of H_2SO_4 and $NaBrO_3$ i.e., wavelength decreases. The dynamic behavior of spirals depends on the initial concentrations of H_2SO_4, $NaBrO_3$, and MA.

The time-period and wavelength were calculated from the time-space plot. Frequency varies inversely with time-period and the velocity was measured from the equation given below:

$$v = \frac{\lambda}{T} \tag{3.5}$$

where v is velocity, λ is wavelength and T is the period of a wave.

Figures 3.7 and 3.8 summarize the results of our experiments. Figure 3.7 shows the graph of time-period, wavelength, velocity and frequency for the variation of $[H_2SO_4]$ and $[NaBrO_3]$. It is observed that when $[H_2SO_4]$ is increased, both the time-period and wavelength decrease whereas velocity and frequency increase. The same trend is followed with increase in concentration of $NaBrO_3$. Figure 3.8 shows the graph of time-period, wavelength, velocity and frequency for the variation of $[H_2SO_4]$ and [MA]. Just like the previous result, here too the wavelength and time-period decrease

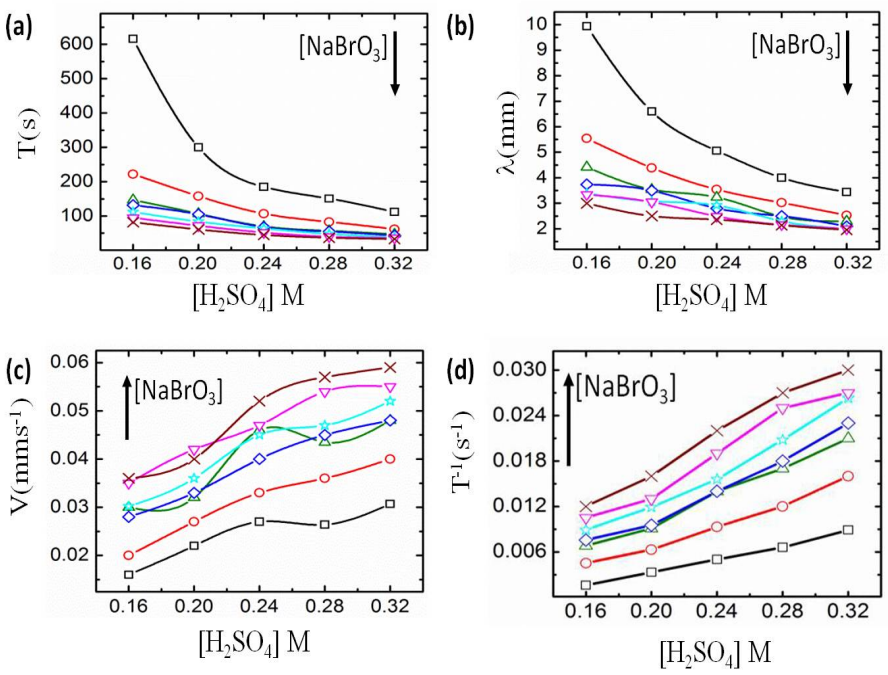

FIG. 3.7: (a) Time period, (b) wavelength (c) velocity, and (d) frequency against $[H_2SO_4]$. Each curve corresponds to different $[NaBrO_3]$, square (black) = 0.04 M, circle (red) = 0.06 M, upper triangle (olive) = 0.08 M, diamond (blue) = 0.09 M, star (cyan) = 0.1 M, lower triangle (pink) = 0.11 M and cross (wine red) = 0.12 M respectively, [MA]= 0.04 M, [Ferroin] = 0.001 M.

whereas velocity and frequency increase with increase in $[H_2SO_4]$. However in the case when [MA] is varied, no appreciable change in the trends is seen for the properties of the spiral waves. From the kinetic studies it has been established that the rate is directly proportional to the product of the concentration of H^+ and BrO_3^-. On the other hand the rate is found to be independent of the concentration of malonic acid and ferroin [23, 24, 25]. Thus, it is quite significant that there will be no effect on the properties of wave such as wavelength (λ), frequency (ν) and time-period (T), with increase in [MA]. Thus, it can be said that the dynamical properties mostly depend on the concentration of H_2SO_4 and $NaBrO_3$.

The most interesting feature of a spiral wave is its tip. From Oregonator model simulations, it is seen that the core can trace different types of floral paths which depend on the kinetic parameters [Fig. 3.2]. For our experiments, we write some programs in MATLAB to trace the trajectories. Figure 3.9 and 3.10 show some examples of

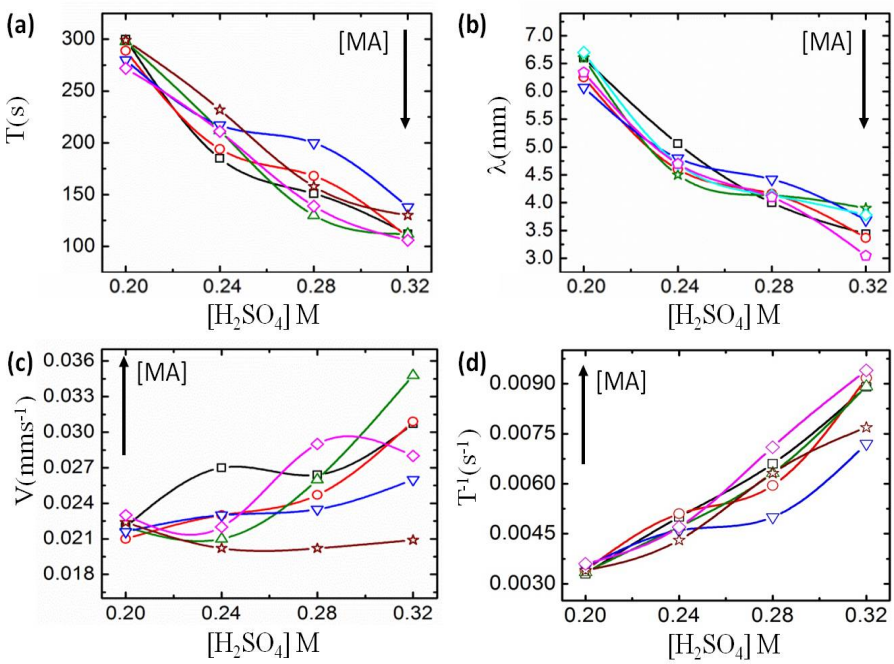

FIG. 3.8: (a) Time period, (b) wavelength, (c) velocity, and (d) frequency against $[H_2SO_4]$. Each curve corresponds to different [MA], square (black) =0.06 M, circle (red) = 0.08 M, upper triangle (olive) = 0.09 M, lower triangle (blue) = 0.1 M, star (wine red) = 0.11 M and diamond (pink) = 0.12 M respectively, $[NaBrO_3]$= 0.04 M, [Ferroin] = 0.001 M.

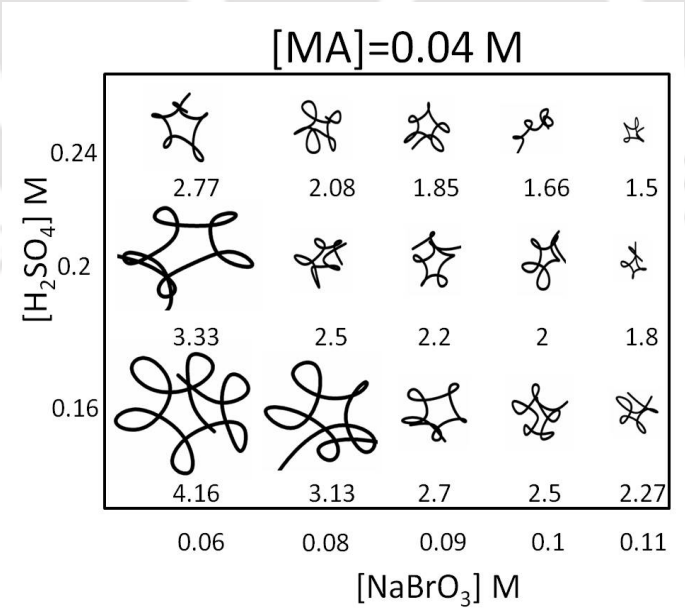

FIG. 3.9: Tip trajectories of spiral waves for different values of $[H_2SO_4]$ and $[NaBrO_3]$, while [MA] = 0.04 M and [Ferroin] = 0.001 M. The number below the trajectory is the calculated value of epsilon.

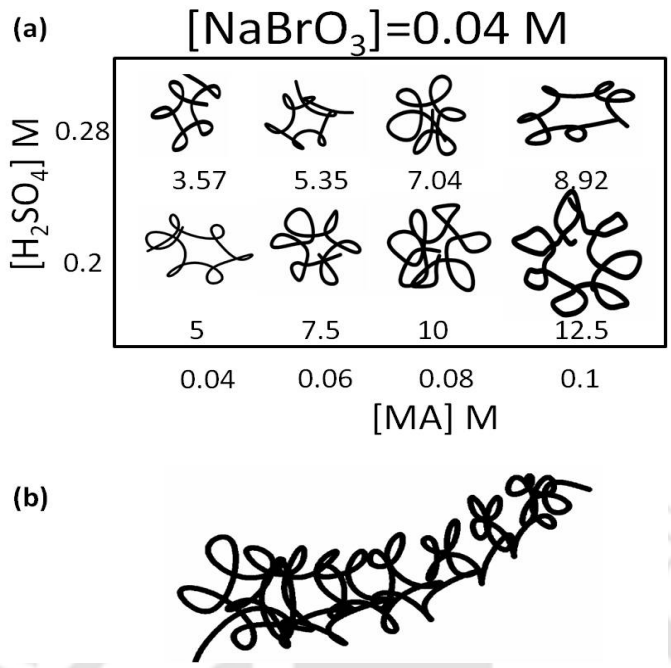

FIG. 3.10: (a) Tip trajectories of spiral waves for different values of [MA] and [H_2SO_4], while [$NaBrO_3$] = 0.04 M and [Ferroin] = 0.001 M. The number below the trajectory is the calculated value of ϵ. (b) Trajectory of a meandering spiral wave for [$NaBrO_3$] = 0.08 M, [H_2SO_4] = 0.16 M, [MA] = 0.04 and [Ferroin] = 0.001 M.

spiral trajectories. It summarizes the results of experiments having increasing concentration of H_2SO_4, $NaBrO_3$ and MA. The tip gives rise to a floral pattern with the petals facing outward. In Fig. 3.9, it is seen that for a particular concentration of H_2SO_4, the number of petals decreases for increased concentration of $NaBrO_3$. It can also be noticed that the core size of the tip gets smaller in this case. Furthermore, for increasing concentration of H_2SO_4, the core size also gets smaller and the number of petals decreases.

On the other hand, for the same concentration of H_2SO_4, it is seen that the number of petals and the core size increase with increasing concentration of MA [Fig. 3.10 (a)]. However, in this case also, the number of petals and the core size reduce with increasing [H_2SO_4].

Again, for some concentrations of the reactants, it was found that the tip drifts from its original position [Fig. 3.10 (b)].

Thus, changing the excitability can induce changes in the dynamics of a spiral wave.

From the figures, it is seen that core size decreases with decrease in ϵ. This result

is closely related to the simulation result shown earlier [Fig. 3.2]. We noticed that ϵ value keeps on decreasing when concentration of H_2SO_4 and $NaBrO_3$ are increased, whereas it increases with increase in concentration of MA.

3.5 Conclusions

We have studied the dynamics of spiral waves in a thin layer of the BZ system varying the concentrations of various species in a set of reaction solution. The properties of spiral waves were studied from analysis of the time space plots. The period and wavelength decreased with increased concentration of H_2SO_4 and $NaBrO_3$, whereas the velocity and frequency increased. In contrast, the trend was opposite, showing no significant changes for changes in concentration of MA. The detailed study of the spiral tip trajectory also gave us newer insights of the spiral wave dynamics. The core of the spiral became smaller with increase in $[H_2SO_4]$ and $[NaBrO_3]$, whereas it enlarges for increase in [MA]. Hence, we can surmise that the excitability increases with increasing H_2SO_4 and $NaBrO_3$ concentration, as evident from higher frequency values, and the excitability is negatively affected by MA. Our experiments give a direct demonstration that the value of "ϵ" as reported by earlier researchers is valid not only in the qualitative sense, but also in the detailed dynamics of the spiral tip. Again, the excitability is not so sensitive to the changes in MA concentration as it is to the changes in $[H_2SO_4]$ and $[NaBrO_3]$ as is evident from the Figs. 3.7 and 3.8. There is a future scope to study BZ reaction in more details with the help of these established results and we expect these results to give us newer direction and path to know more about the unknown facts of spiral wave dynamics.

Bibliography

[1] F. Siegert, and C. J. Weijer, Physica D **49**, 224 (1991). Analysis of optical density wave propagation and cell movement in the cellular slime mould Dictyostelium discoideum.

[2] S. Sawai, P. A. Thomason, and E. C. Cox, Nature **433**, 323 (2005). An autoregulatory circuit for long-range self-organization in Dictyostelium cell populations.

[3] R. A. Gray, A. M. Pertsov, and J. Jalife, Nature **392**, 75 (1998). Spatial and temporal organization during cardiac fibrillation.

[4] G. Bub, A. Shrier, and L. Glass, Phy. Rev. Lett. **88**, 058101 (2002). Spiral wave generation in heterogeneous excitable media.

[5] S. C. Müller, T. Mair, and O. Steinbock, Biophys. Chem. **72**, 37 (1998). Travelling waves in yeast extract and in cultures of Dictyostelium discoideum.

[6] J. Lechleiter, S. Girard, E. Peralta, and D. Clapham, Science **252**, 123 (1991). Spiral calcium wave propagation and annihilation in Xenopus laevis oocytes.

[7] A. T. Winfree, Science **175**, 634 (1972). Spiral waves of chemical activity.

[8] C. Luengviriya, U. Storb, M. J. B. Hauser, and S. C. Müller, Phys. Chem. Chem. Phys. **8**, 1425 (2006). An elegant method to study an isolated spiral wave in a thin layer of a batch Belousov-Zhabotinsky reaction under oxygen-free conditions.

[9] J. Jalife, R. A. Gray, G. E. Morley, and J. M. Davidenko, Chaos **8**, 79 (1998). Self-organization and the dynamical nature of ventricular fibrillation.

[10] L. Gaztañaga, F. E. Marchlinski, and B. P. Betenskya, Rev. Esp. Cardiol. **65**, 174 (2012). Mechanisms of cardiac arrhythmias.

[11] A. N. Zaikin, and A. M. Zhabotinsky, Nature **225**, 535 (1970). Concentration wave propagation in two-dimensional liquid-phase self-oscillating system.

[12] W. Jahnke, W. E. Skaggs, and A. T. Winfree, J. Phys. Chem. **93**, 740 (1989). Chemical vortex dynamics in the Belousov-Zhabotinsky reaction and in the two-variable Oregonator model.

[13] G. Li, Q. Ouyang, V. Petrov, and H. L. Swinney, Phy. Rev. Lett. **77**, 2105 (1996). Transition from Simple Rotating Chemical Spirals to Meandering and Traveling Spirals.

[14] G. S. Skinner, and H. L. Swinney, Physica D **48**, 1 (1991). Periodic to quasiperiodic transition of chemical spiral rotation.

[15] M. Braune, and H. Engel, Chem. Phys. Lett. **211**, 534 (1993). Compound rotation of spiral waves in active media with periodically modulated excitability.

[16] Z. N. Ungvarai, J.Ungvarai, and S. C. Müller, Chaos **3**, 15 (1993). Complexity in spiral wave dynamics.

[17] J. Luengviriya, P. Porjai, M. Phantu, M. Sutthiopad, B. Tomapatanaget, S. C. Müller, and C. Luengviriya, Chem. Phys. Lett. **588**, 267 (2013). Meandering spiral waves in a bubble-free Belousov-Zhabotinsky reaction with pyrogallol.

[18] D. Barkley, Phy. Rev. Lett. **72**, 164 (1994). Euclidean symmetry and the dynamics of rotating spiral waves.

[19] D. Barkley, and I. G. Kevrekidis, Chaos **4**, 453 (1994). A dynamical systems approach to spiral wave dynamics.

[20] W. Jahnke, and A. T. Winfree, Int. J. Bifurcat. Chaos **1**, 445 (1991). A survey of spiral-wave behaviors in the Oregonator model.

[21] T. Plesser, S. C. Müller, and B. Hess, J. Phys. Chem. **94**, 7501 (1990). Spiral wave dynamics as a function of proton concentration in the ferroin-catalyzed Belousov-Zhabotinskii reaction.

[22] A. L. Belmonte, Q. Ouyang, and J. M. Flesselles, J. Phys. II France **7**, 1425 (1997). Experimental survey of spiral dynamics in the Belousov-Zhabotinsky reaction.

[23] R. J. Field, and R. M. Noyes, J. Chem. Phys. **60**, 1877 (1974). Oscillations in chemical systems. IV. Limit cycle behavior in a model of a real chemical reaction.

[24] R. J. Field, E. Korös, and R. M. Noyes, J. Am. Chem. Soc. **94**, 8649 (1972). Oscillations in chemical systems. II. Thorough analysis of temporal oscillation in the Bromate-Cerium-Malonic acid system.

[25] R. M. Noyes, R. J. Field and E. Korös, J. Am. Chem. Soc. **94**, 1394 (1972). Oscillations in Chemical Systems. I. Detailed Mechanism in a System Showing Temporal Oscillations.

Chapter 4

Unpinning of scroll waves under the influence of a thermal gradient

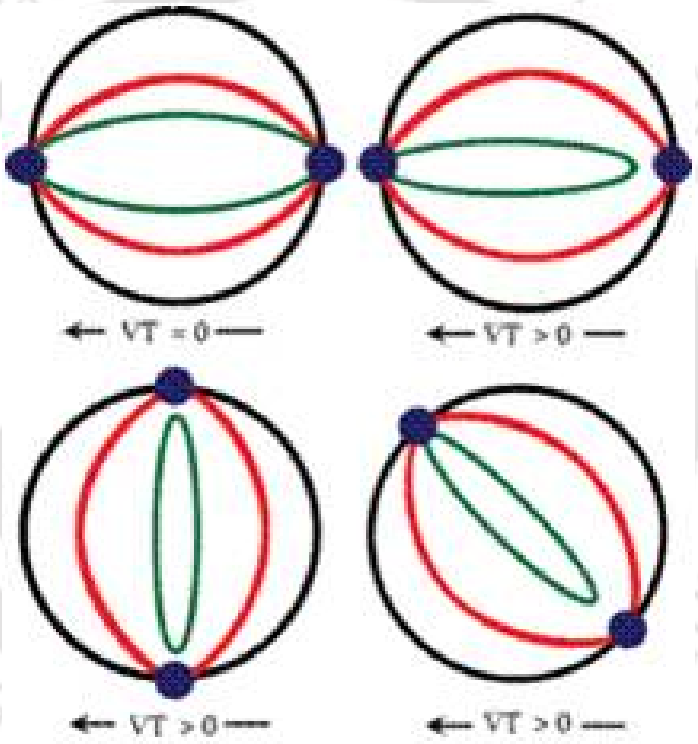

4.1 Introduction

Recent studies have shown that the scroll waves can attach themselves to unexcitable, heterogeneous obstacles [1, 9, 3, 4]. This process known as pinning stabilizes the vortex filaments and highly elongates their lifetimes, sometimes completely stopping their collapse. The presence of inert obstacles like scar tissues within the excitable cardiac muscles can initiate the formation of scroll waves [5, 6]. These vortices can also pin themselves to the inert, heterogeneous anomalies which highly elongate their lifetimes [7]. This is further detrimental to cardiac health. Thus a better understanding of the process of pinning and possible methods of unpinning of scroll waves from obstacles is highly desirable.

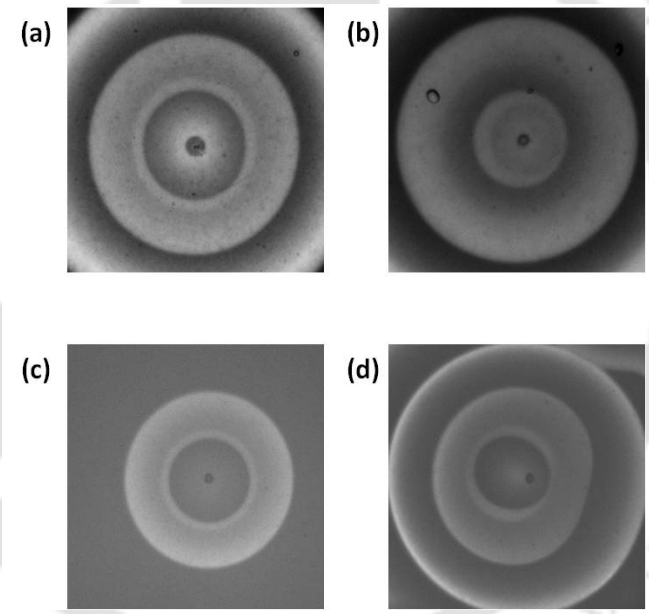

FIG. 4.1: (a, b) Snapshots of scroll wave under the influence of thermal gradient, (a) before and (b) after the advent of thermal gradient. (c, d) Snapshots of scroll wave under the influence of electric field, (c) before and (d) after the application of electric field.

Earlier studies have shown that the excitability of reaction diffusion systems can be influenced by various perturbations like electric fields, thermal and concentration gradients [8, 9, 10, 11] [Fig. 4.1]. Similarly it is also known that, free (unpinned) scroll waves can be expanded, reoriented, or even annihilated by imposing gradients and excitation fields over the reaction system [12, 13, 14]. Whether such external

or internal perturbations can be employed to unpin the stable filaments attached to unreactive obstacles is a question worth exploring.

Quantitative studies of mathematical models have revealed that an advective field can unpin vortices that are pinned to inert obstacles [15]. In a recent experimental study of the BZ system, the effect of electric field gradient on pinned scroll waves have been explored [16]. This has shown that unpinning of scroll wave filaments from such heterogeneities is possible. This method has a close resemblance to the defibrillation techniques used in removing the intruding scroll waves from the heart tissue, in the fact that it uses a high pulse of electric field to unpin the vortices. In the case of defibrillation of the heart, a strong electric field is also employed, that at often times have lasting effect on the cardiac muscles. This may result in tissue damage and be a cause of further arrhythmias [17]. So, we are in search of a milder technique to control scroll waves and bring about their unpinning. In this chapter, we explore the possibility that a thermal gradient can be used to unpin the scroll waves.

4.2 Experimental Section

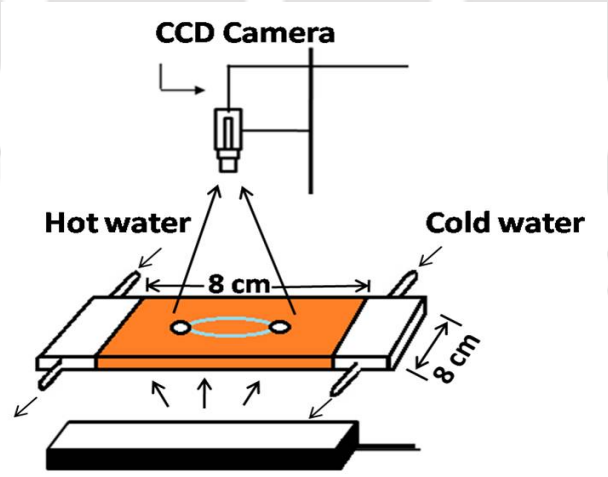

FIG. 4.2: Schematic diagram of our experimental set-up.

We carried out experiments using the Ferroin-catalyzed Belousov-Zhabotinsky reaction. All solutions were made in Millipore water and the experiments carried out at room temperature. The initial concentrations of the different components of the Ferroin-catalyzed BZ system were as follows: sodium bromate 0.04 M, malonic acid

0.04 M, sulphuric acid 0.2 M and ferroin indicator solution 0.8 mM. The reaction was embedded in a 0.8 % w/v agar gel matrix. The experimental system consisted of two layers, each about 4 mm in height. After the gelation of the first layer, the tip of a silver wire was inserted in its center for a few seconds. This initiated a semi-spherical wave. When the wave reached the desired dimensions, we poured another layer of BZ gel over it, at temperatures slightly above its gelling temperature, and allowed it to gel over the first layer. This allowed for the semi-spherical wave generated in the lower layer to curl up into the top layer, and form a scroll wave with a circular filament. For pinning purposes, we inserted two spherical glass beads half-way into the lower layer at the time of its gelation. In this case, the wave was initiated in between the beads. When the distance between the beads and their radius was of correct dimensions, we achieved pinning of the scroll wave to the beads [1]. In our case, we chose glass beads of radii 1 mm and placed them at a distance of 8.3 mm (centre-centre distance).

For the studies in the presence of a thermal gradient, we designed a square reaction chamber (8 cm $\times$ 8 cm) that had two heat-exchangers on its two sides connected to two circulating baths that were thermostat-controlled [Fig. 4.2]. This enabled us to have a horizontal gradient of temperature across our gel layer. We could maintain a temperature difference of 4 to 32 °C between the two sides of the gel layer, thus generating a gradient in the range of 0.5 - 4 °C cm $^{-1}$. The reaction system was monitored from above by a charge coupled device (CCD) camera (mvBlueFOX 220a) through a blue filter, while it was illuminated from below with a diffused white light. The images were recorded onto a personal computer at an interval of 2 s and the data analyzed using MATLAB codes.

4.3 Results and Discussion

We generate pinned scroll waves and study them by visual inspection of their snapshots [Fig. 4.3 (a, b)] and time-space plots [Fig. 4.3 (c, d)]. The latter is obtained as a time-variation of a cross-section [black lines in Fig. 4.3 (a)] of the two dimensional

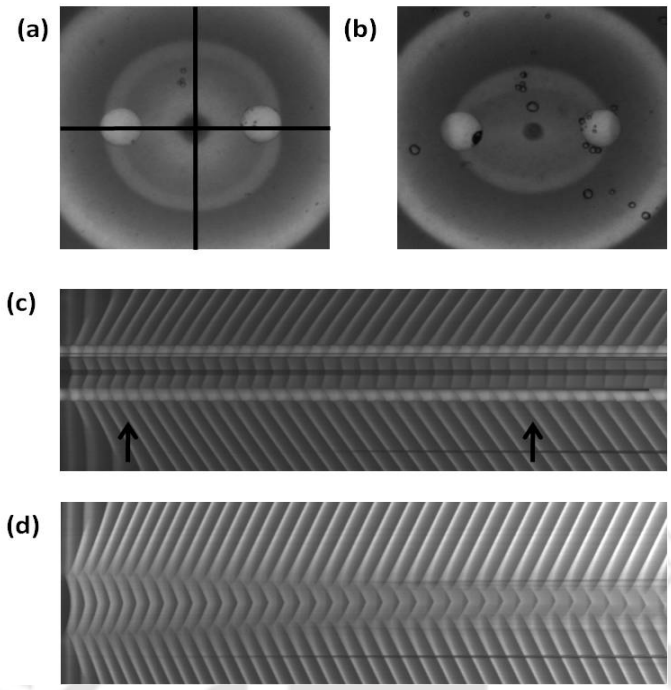

FIG. 4.3: A pinned, stable vortex is shown in (a) and (b). The shining round-shaped objects are glass beads of 1 mm radius that act as our inert obstacles. The time-space plots (time going left to right) span time interval of 220 min in both (c) and (d). Straight horizontal and vertical black lines on the snapshot (a) show the stripe along which the corresponding time-space plot has been generated for (c) and (d) respectively. The two arrows mark the position of the snapshots (a) and (b).

projection image of the experimental system captured from above [Fig. 4.3 (a)]. From the previous chapters, we know that in the BZ reaction system, free scroll waves with circular filaments (with positive filament tension) have a limited lifetime. A free scroll of initial diameter 7 mm has a life time of about 2 hours, while a pinned scroll wave has an infinitely longer lifetime. Fig. 4.3 (c) and (d) shows the time-space plot for such a pinned scroll for the initial four hours.

Fig. 4.3 (c) shows the time-space plot along the horizontal line in frame (a), and Fig. 4.3 (d) shows the time-space plot along the vertical line in frame (a) of Fig. 4.3. After about six hours, the experiment starts losing the contrast since we are using a closed system, and the BZ chemicals start getting depleted. When we apply a thermal gradient to a pinned scroll wave, after the filament has been stabilized (1 hour from wave initiation), it is seen that the otherwise stable filament now gets unpinned from

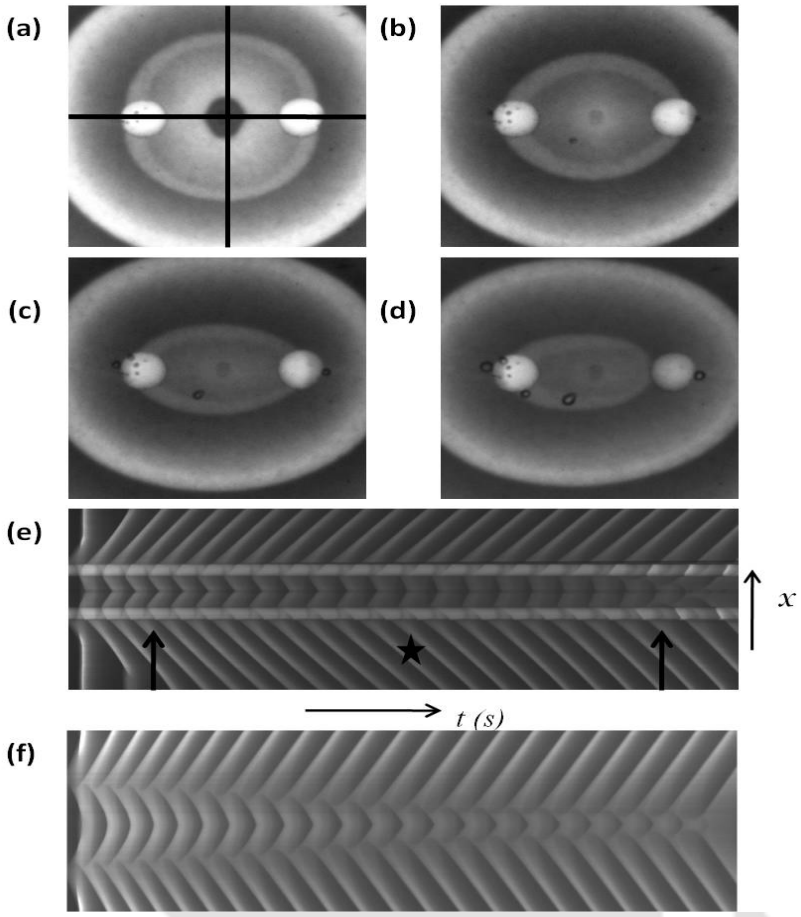

FIG. 4.4: Unpinning of scroll waves under a constant temperature gradient. Snapshots (a), (b), (c), (d) and time-space plot (e), (f) along horizontal and vertical direction respectively. Each snapshot has an area of 16 mm $\times$ 16 mm. Straight black lines on the snapshot show the stripe along which the corresponding time-space plot has been generated. The shining round-shaped objects are glass beads of 1 mm radius that act as our inert obstacles. In this experiment, the angle between the inter-bead axis and gradient vector (θ) is 0°. In each of the snapshots, the left side is the hot end and the temperature gradient is 2 °C cm^{-1}. The star on the time-space plot marks the time at which the thermal gradient has been applied on the system. The two arrows mark the position of the snapshots (a) and (d), one taken before the application of thermal gradient and the other after at least one end of the scroll has detached itself from the pinning obstacles. The time-space plots (time going left to right) span a time interval of 130 min.

the obstacles. Examples of such experiments are shown in Figs 4.4 - 4.8.

In all these experiments, the thermal gradient (2 °C cm^{-1}) is in the horizontal di-

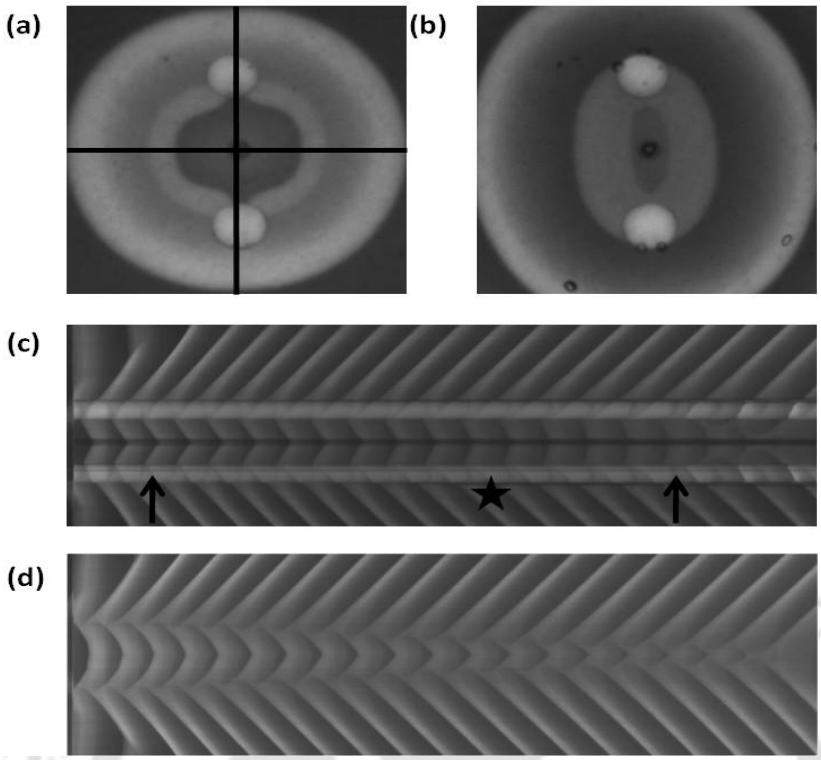

FIG. 4.5: Unpinning of scroll waves under a constant temperature gradient when the angle between the inter-bead axis and gradient vector (θ) is 90°. (a), (b) Snapshots and (c), (d) time-space plots along horizontal and vertical direction respectively. Each snapshot has an area of 16 mm × 16 mm. Straight black lines on the snapshot shows the stripe along which the corresponding time-space plot has been generated. The time-space plots (time going left to right) span a time interval of 95 min. The star on the time-space plot marks the time at which the thermal gradient has been applied on the system. The two arrows mark the position of the snapshots (a) and (b), one taken before the application of thermal gradient and the other after at least one end of the scroll has detached itself from the pinning obstacles.

rection, with the left side being the hot end and right side the cold end. In Fig. 4.4 (a - f), the line joining the beads is parallel to the gradient vector. Fig. 4.4 (e) and (f) are the corresponding time-space plot of the experiment along the horizontal and vertical lines in frame (a) respectively, the two arrows showing the time at which the snapshots were taken. Similarly, in Fig. 4.4 (a - d), the inter-bead axis is perpendicular to the gradient vector and in Fig. 4.5 (a - d), the axis is at an angle of about 45° to the gradient. The snapshot images demonstrate that the deformation of the scroll

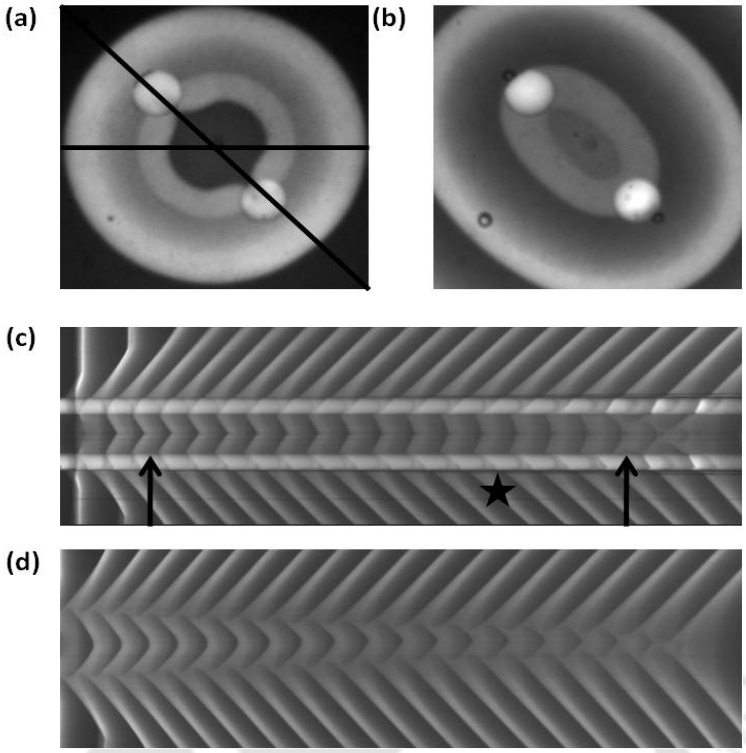

FIG. 4.6: Unpinning of scroll waves under a constant temperature gradient when the angle between the inter-bead axis and gradient vector (θ) is 45°. (a), (b) Snapshots and (c), (d) time-space plots along horizontal and vertical direction respectively. Each snapshot has an area of 16 mm × 16 mm. Straight black lines on the snapshot (a) show the stripe along which the corresponding time-space plot has been generated. The star on the time-space plot marks the time at which the thermal gradient has been applied on the system. The two arrows mark the position of the snapshots (a) and (b), one taken before the application of thermal gradient and the other after at least one end of the scroll has detached itself from the pinning obstacles. The time-space plots (time going left to right) span a time interval of 90 min.

wave in each case is different. When the inter-bead axis is parallel to the thermal gradient vector ($\theta = 0°$), the wave gets unpinned from the bead that lies towards the colder end (right side) of the reaction chamber [Fig. 4.4 (d)]. For low gradients (∇T < 2 °C cm $^{-1}$), it remains attached to the bead on the left side till the end. While in the case of perpendicular alignment of the inter bead axis with respect to the gradient vector ($\theta = 90°$), the scroll wave gets simultaneously detached from both the beads [Fig. 4.5 (b)], before it disappears. When the beads are placed at an angle

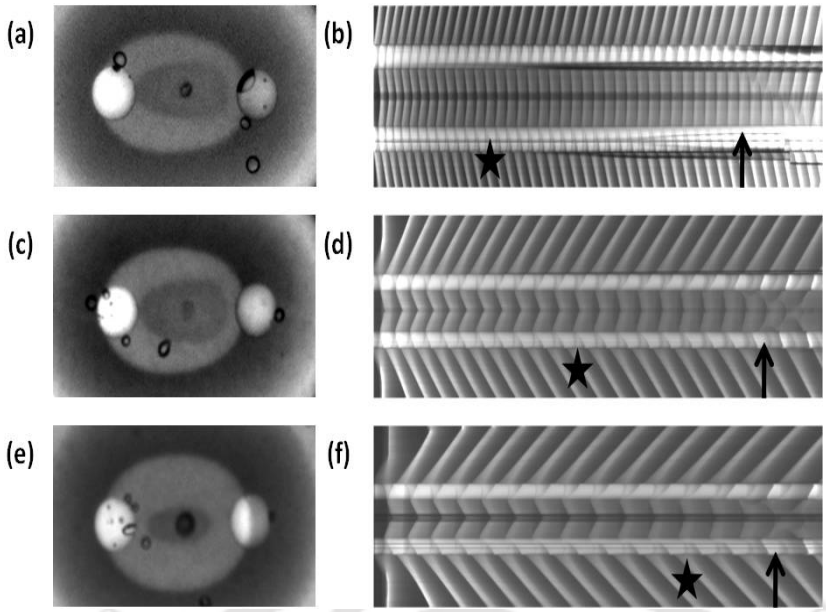

FIG. 4.7: Variation of gradient strength and its effect on unpinning. (a, b), (c, d) and (e, f) are snapshots (area 16 mm × 8 mm) and time-space plots of three different experiments with thermal gradients of 1 °C cm^{-1}, 2 °C cm^{-1} and 3 °C cm^{-1} respectively. The time-space plots (time going left to right) span time intervals of 240 min (b), 133 min (d) and 82 min (f). Each frame has been chosen at the instant when one end of the scroll wave has detached itself from the heterogeneous obstacles for the first time, denoted by the arrow in the corresponding time space plot. The star on the time-space plot denotes the advent of thermal gradient.

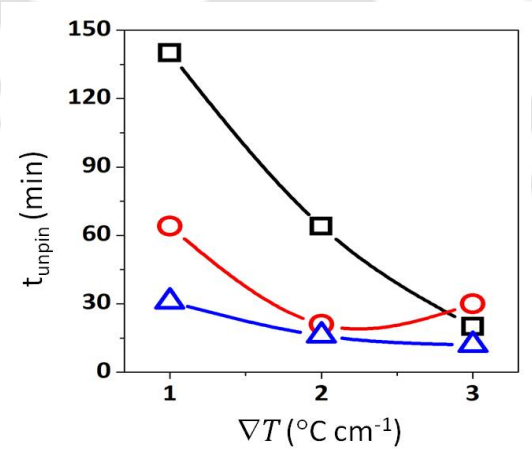

FIG. 4.8: Time required for unpinning (tunpin) as a function of the temperature gradient. Squares (black line) stand for $\theta = 0°$, circles (red curve) for $\theta = 90°$ and triangles (blue line) for $\theta = 45°$.

to the gradient vector ($\theta = 45°$), the scroll wave again gets detached from the cold end first [Fig. 4.5 (b)]. After a couple of rotations, it also gets detached from the other bead before it vanishes completely. Depending on the relative position of the pinning beads to the direction of thermal gradient, the time required for unpinning of the scroll wave varies. The time-space plots [Fig. 4.4 (e), 4.5 (c) and 4.6 (c)] shows that the time required for the scroll to unpin from at least one bead is different for different relative bead positions. The star denotes the time when the thermal gradient has been introduced into the system. In the first case ($\theta = 0°$), it requires 64 min for the scroll to get unpinned from one bead [Fig. 4.4 (e)], in the case when $\theta = 90°$, the scroll gets unpinned from both the beads simultaneously, 21 min after the application of the thermal gradient [Fig. 4.5 (c)] and when $\theta = 45°$, the time taken for advent of unpinning is 16 min [Fig. 4.6 (c)].

We also varied the strength of the thermal gradient and studied its effect on the unpinning of the scroll wave. Figure 4.7 shows how a scroll wave is deformed differently under the influence of thermal gradient of different strengths. The snapshots show the deformed waves after the unpinning has occurred for thermal gradients of 1, 2 and 3 °C cm^{-1} for the case where $\theta = 0°$ [Figs. 4.6 (a, c, e)]. The corresponding time-space plots show the unpinning of the scroll from one or both beads in a time scale [Figs. 4.6 (b, d, f)]. The unpinning starts at 140 min [Fig. 4.7 (b)], 64 min [Fig. 4.7 (d)] and 20 min [Fig. 4.7 (f)] after the application of thermal gradient. It is seen that in the first case [Fig. 4.7 (a, b)], ∇T = 1 °C cm^{-1}, the scroll gets unpinned from the right bead before it vanishes at the left one. For the second case (Fig. 4.7 (c, d), ∇T = 2 °C cm^{-1} , in the beginning it gets unpinned from the right bead followed by the left one after a while, before it quickly disappears. When ∇T = 3 °C cm^{-1} [Fig. 4.7 (e, f)], the scroll gets unpinned simultaneously from both the beads. We also varied the position of the beads ($\theta = 90°, 45°$) for similar experiments under different temperature gradients. Figure 4.8 summarizes the result of nine experiments. The time required for the scroll to unpin from the first bead (sometimes two simultaneously) is plotted as a function of the strength of thermal gradient. As expected, stronger thermal gradients led to a quicker unpinning and annihilation of

the scroll waves. The time required for unpinning also varies with θ. Unpinning is fastest for $\theta = 45°$, and slowest for $\theta = 0°$. We also carried out few experiments to study the effect of high and low temperature on the dynamics of a pinned scroll wave and found that the scroll remains stationary at all temperatures and unpinning occurs only in the presence of thermal gradient (see Appendix A).

4.4 Numerical Simulations

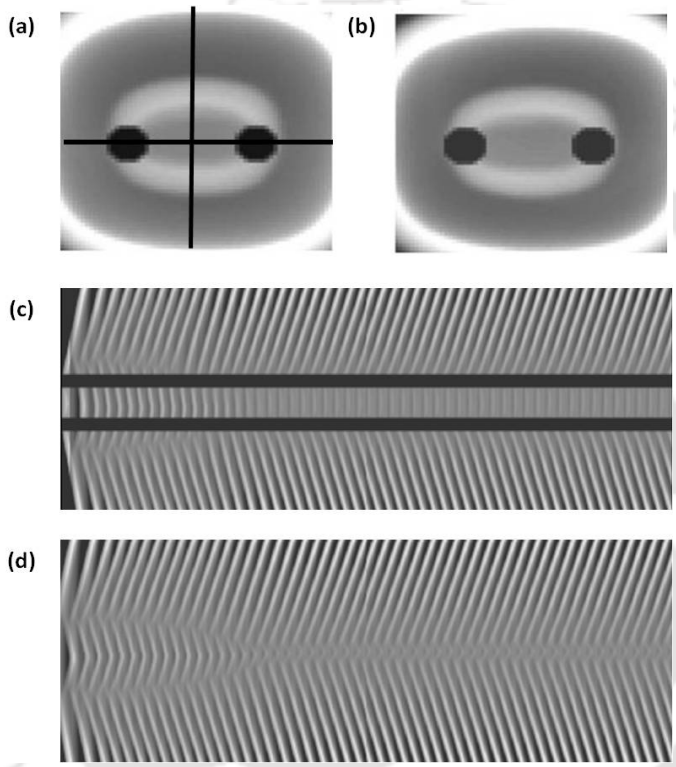

FIG. 4.9: Simulation studies for pinning of scroll wave. (a, b) shows the stabilization of a scroll that is attached to two inert obstacles (black spheres) in the absence of temperature gradient. (c, d) The time-space plots (time going left to right) corresponding to (a) and (b). Straight horizontal and vertical black lines on the snapshot (a) show the stripe along which the corresponding time-space plot has been generated for (c) and (d) respectively.

In order to gain a better understanding of the phenomenon, we carried out numerical simulations of the Barkley model for a two-variable reaction-diffusion system [18]. This model is frequently employed to study the dynamics of reaction-diffusion systems. The influence of the thermal gradient can be incorporated into the system

by introducing a thermodiffusion term as used in earlier studies [9, 19]. The system is as follows:

$$\frac{\partial u}{\partial t} = \frac{1}{\epsilon}\left\{u(1-u)\left(u-\frac{v+b}{a}\right)\right\} - \nabla J_u \quad (4.1)$$

$$\frac{\partial v}{\partial t} = u - v - \nabla J_v \quad (4.2)$$

where the flux in the presence of thermal gradient is given by $J_u = D_u\nabla u + D_{T_u}u(1-r_u)\nabla T$ and $J_v = D_v\nabla v + D_{T_v}v(1-r_v)\nabla T$. D_u = 1.0 and D_v = 0.0 are the translational diffusion coefficients of u and v respectively, and $D_{T_i} = (D_i S_{T_0})/(1+k_s c_i)$ is the thermal diffusion coefficient of species i (u or v). c_i (=u or v) is the concentration of the i^{th} species and r_i is its relative concentration given by $r_i = c_i/c_T$; and c_T = 1.2. S_{T_0} = -0.1 is the Soret coefficient and its negative value emphasizes the movement of the particles towards the hot end of the reaction chamber. k_s=1.0 is a phenomenological constant. ∇T is the thermal gradient along x-direction of the reaction system, and is a constant for a particular experiment. a = 1.1, b = 0.18, ϵ = 0.01, are the system parameters [20]. This set of parameters was chosen so that the drift of the scroll in the binormal direction is negligible over time. We use the Euler method for integrating the equations in a finite system size of $160\times160\times100$ grid points and zero-flux boundary conditions. A time interval Δt = 0.012 and space step of Δx = 0.35 are employed. The pining obstacles of radii 4 space units have been introduced by fixing u and v at 0. The filament of the scroll is identified at regions having u = 0.5 and $v = a/2-b$.

We carry out simulations for varying strengths of the thermal gradient and relative position of the inter-bead axis with respect to the direction of the gradient. Figure 4.9 - 4.13 summarizes the results of the simulations. At zero thermal gradient, the scroll wave attaches itself to the two obstacles, and gains an infinite lifetime [Figs. 4.9 (a,b)]. Figure 4.9 (c) shows the time-space plot along the horizontal line in frame (a) and Fig. 4.9 (d) show the time-space plot along the vertical line in frame (a).

With the introduction of a finite thermal gradient beyond a particular value, the filament of the scroll wave starts to get unpinned from these obstacles [Figs. 4.10 - 4.11)]. This finally leads to annihilation of the scroll, like in the case of a free scroll

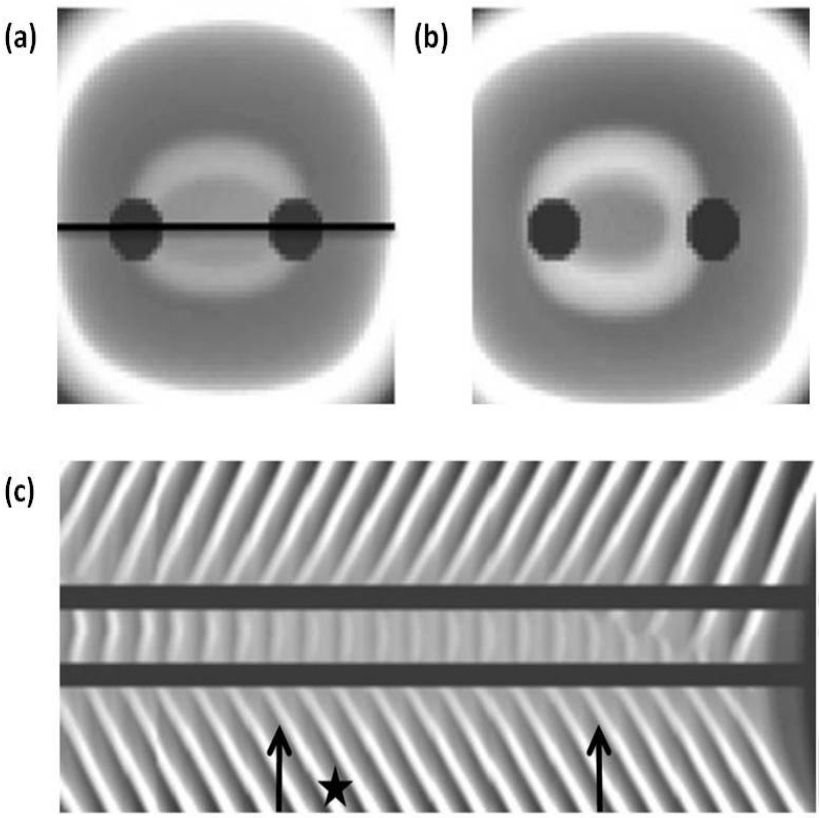

FIG. 4.10: Simulation studies of unpinning of a scroll vortex under the influence of a thermal gradient. Two-dimensional snapshots (a-b) of area 65 space units × 65 space units and a representative time space plot (c) generated from simulation of the three dimensional Barkley model. The simulations have been carried out for $\nabla T = 10$. One snapshot is for the stable scroll before the introduction of thermal gradient (a) and the other snapshot is after the advent of unpinning (b). The time-space plot (c) (time increasing from left to right) corresponds to the case where $\theta = 0^\circ$ along the black line shown in (a). The star on the time-space plot marks the time at which the thermal gradient has been applied on the system. The two arrows mark the position of the snapshots, one taken before the application of thermal gradient and the other after one end of the scroll has detached itself from the pinning obstacle.

wave. In Fig. 4.10 (a), snapshot of a pinned and in Fig. 4.10 (b), snapshot of an unpinned scroll wave are shown when the inter-bead axis is parallel to the thermal gradient vector ($\theta = 0^\circ$). From the simulation results also, we found that when the beads are parallel to the thermal gradient, the wave first gets unpinned from the right bead. The time-space plot [Fig. 4.10 (c)] generated along the horizontal line as shown

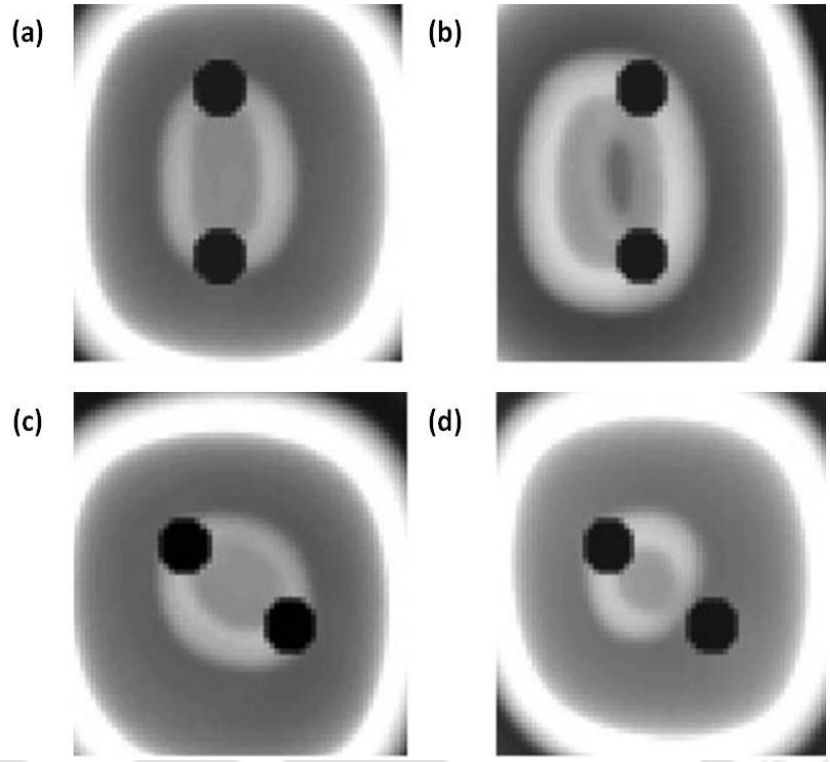

FIG. 4.11: Simulation studies of unpinning of a scroll vortex under the influence of a thermal gradient for two different orientations. (a, b) for $\theta = 90°$ and (c, d) for $\theta = 45°$. Two-dimensional snapshots (a-d) of area 65 space units x 65 space units. Each set of simulations have been carried out for $\nabla T = 10$. Each set shows one snapshot for the stable scroll before the introduction of thermal gradient (a, c) and one snapshot after the advent of unpinning (b, d).

in Fig. 4.10 (a) shows a similar behavior as in the case of experiments where $\theta = 0°$ [Fig. 4.4(e)].

In Fig. 4.11, simulation results for two different orientations of the obstacles are shown. These simulations are performed similar to the previously described experimental results of our experiments. Figure 4.11 (a, b) shows the result when the beads are at angle of $\theta = 90°$ with the gradient and Fig. 4.11 (c, d) are the snapshots shown for $\theta = 45°$. As previously mentioned in experimental results, we found that the wave gets unpinned from both the beads for $\theta = 90°$ orientation of the beads and again, the unpinning was fastest $\theta = 45°$.

In Fig. 4.12 and Fig. 4.13, we have tried to look at the three dimensional projection of filament of the scroll wave at various instants before and after the introduction of the

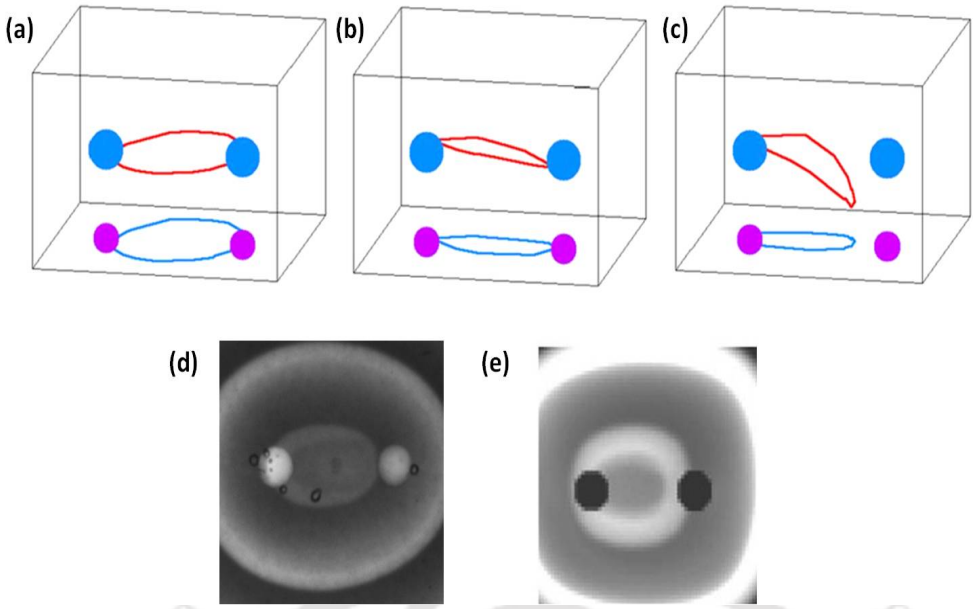

FIG. 4.12: Filament dynamics of unpinning for $\theta = 0^\circ$ orientation of inert obstacles. Results (a, b, c) for the three dimensional Barkley model for $\theta = 0^\circ$. The curves (red) in the center of the cube are the filaments, the spheres (blue) the pinning obstacles, and the curves (blue) along with the circles (purple) at the bottom of the box are the two-dimensional projections of the filament and the obstacle. In (a, b, c), the inter-bead axis is parallel to the gradient vector. In (a), the vortex filament is shown attached to the two unexcitable obstacles before the application of thermal gradient. (b) Shows the distortion of the filament under the influence of thermal gradient, finally leading to unpinning in (c). (d, e) Snapshots from experiment and simulation where filament is similar to (c).

thermal gradient. From these figures, it is seen that the filament loses planarity and tries to align itself perpendicular to the direction of the thermal gradient [Fig. 4.12 (b, c) and Fig. 4.13 (b, c)]. This could be the reason why in the case when the inter-bead axis is parallel to the gradient vector [Figs. 4.12 (b, c)], the scroll always gets unpinned from the bead farther away from the hot end. It is known that a free scroll under thermal gradient moves in the direction of lower excitability, meaning the hot end of the reaction vessel. So, we may safely surmise that it detaches itself from the cold end, while it still remains attached to the bead on the left (hot) side. The contour of the filament [Fig. 4.12 (c)] shows a striking similarity with the experimental result

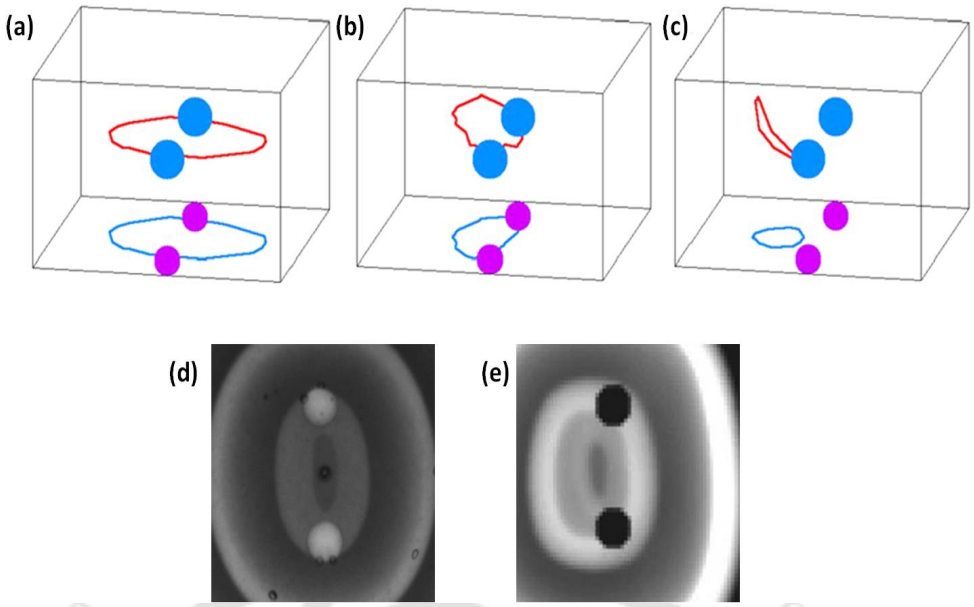

FIG. 4.13: Filament dynamics of unpinning for 90° orientation of inert obstacles. Results (a, b, c) for the three dimensional Barkley model for $\theta = 90°$. The curves (red) in the center of the cube are the filaments, the spheres (blue) the pinning obstacles, and the curves (blue) along with the circles (purple) at the bottom of the box are the two-dimensional projections of the filament and the obstacle. In (a, b, c), the inter-bead axis is perpendicular to the gradient vector. In (a), the vortex filament is shown attached to the two unexcitable obstacles before the application of thermal gradient. (b) Shows the distortion of the filament under the influence of thermal gradient, finally leading to unpinning in (c). (d, e) Snapshots from experiment and simulation for a filament similar to (c).

[Fig. 4.4 (d)]. When the inter-bead axis is perpendicular to the thermal gradient [Figs. 4.12(a-c)], the filament of the scroll wave shows similar behavior with respect to the excitability of the medium. But its reflection on the unpinning of the wave is not the same. As is seen in Fig. 4.13 (c), the wave detaches simultaneously from both the beads. Similar observation was made in the experiments [Fig. 4.5 (b)]. Fig. 4.12 (d, e) and 4.12 (d, e) are the snapshots two dimensional projection of the scroll wave which corresponds to the unpinning of the filament shown in Figs. 4.12 (c) and 4.13 (c) respectively for experiment and sinulation.

It is known from an earlier experimental study that when a thermal gradient is ap-

plied to a circular scroll ring, there is a gradient-induced drift velocity that acts perpendicular to both the filament as well as the gradient. This gives rise to motion along opposite directions at opposite points of the filament [12]. There develops a net torque in the system that reorients a free circular filament, perpendicular to the direction of the thermal gradient. In the case, where the scroll ring is pinned to two beads whose inter-bead axis is parallel to the gradient ($\theta = 0°$), the pinning will restrict this rotatory motion [Fig. 4.12 (b)]. Whereas, in the case when inter-bead axis is perpendicular to the gradient ($\theta = 90°$), the scroll ring can easily reorient while still being attached to the two beads [Fig. 4.13]. This may be the reason that the time required for unpinning is more in the earlier case [Fig. 4.7].

Similar to the thermal gradient, other external fields like electric field can also bring about anisotropy in the medium and initiate chirality-dependent drift of the filaments. So the basic mechanism of unpinning remains the same. In the presence of a homogenous electric field, a free scroll ring is reoriented perpendicular to the field and the filament further moves toward the anode [13]. However, the time required for unpinning by an electric-field is the least for $\theta = 0°$ and highest for $\theta = 90°$ [16]. This is unlike what we see in our experiments. Our numerical simulation results have been able to explain the trend in the case of thermal gradient induced unpinning. Similar detailed numerical simulations also require to be done for electric-field-controlled unpinning to explain the different observations in their case.

4.5 Conclusions

In our present study, we have shown that scroll waves pinned to heterogeneous obstacles can be unpinned by the employment of a thermal gradient. Stronger the gradient, lesser is the time taken by the scroll to get unpinned. This could be because, a stronger gradient is quicker to reorient the vortex perpendicular to itself, thus resulting in a faster unpinning. We have carried out experiments for gradients as low as 0.5 °C cm^{-1}, where unpinning takes place after a period of time much longer than three hours. Further studies are required to find if there is a lower threshold of the

gradient strength below which unpinning does not occur.

The relative position of the beads with the thermal gradient also plays a major role in determining the time required for the unpinning and the shape of the unpinned scroll waves. Our numerical simulations are in close conjunction with the experiments. In addition, they allow us to have a three dimensional insight into the process of filament distortion and unpinning in the presence of a thermal gradient.

There is scope for further investigation into the details of this problem. Studies could be carried out by making changes to the size and shape of the obstacles, and the inter-bead distance. The probability and nature of unpinning would also change with the number of pinning obstacles.

Bibliography

[1] Z. A. Jiménez, and O. Steinbock, Phys. Rev. Lett. **109**, 098301 (2012). Stationary vortex loops induced by filament interaction and local pinning in a chemical reaction-diffusion system.

[2] Z. A. Jiménez, and O. Steinbock, Europhys. Lett. **91**, 50002 (2010). Pinning of vortex rings and vortex networks in excitable systems.

[3] Z. A. Jiménez, and O. Steinbock, Phys. Rev. Lett. **102**, 244101 (2009). Pinned scroll rings in an excitable system.

[4] S. Dutta, and O. Steinbock, J. Phys. Chem. Lett. **2**, 945 (2011). Topologically mismatched pinning of scroll waves.

[5] J. M. Davidenko, A. V. Pertsov, R. Salomonsz, W. Baxter, and J. Jalife, Nature **355**, 349 (1992). Stationary and drifting spiral waves of excitation in isolated cardiac muscle.

[6] A. Arenal, J. Hernández, E. P. David, J. L. R. Guvernau, M. J. L. Carbayo, and F. F. Avilés, Cardio. Res. **94**, 324 (2012). Do the spatial characteristics of myocardial scar tissue determine the risk of ventricular arrhythmias?

[7] J. Jalife, R. A. Gray, G. E. Morley, and J. M. Davidenko, Chaos **8**, 79 (1998). Self-organization and the dynamical nature of ventricular fibrillation.

[8] H. Sevčíková, M. Marek, and S. C. Müller, Science **257**, 951 (1992). The reversal and splitting of waves in an excitable medium caused by an electric field.

[9] S. Dutta, and D. S. Ray, Phys. Rev. E **75**, 066206 (2007). Thermodiffusion induced instabilities in reactive systems.

[10] S. Mironov, M. Vinson, S. Mulvey, and A. Pertsov, J. Phys. Chem. **100**, 1975 (1996). Destabilization of three-dimensional rotating chemical waves in an inhomogeneous BZ reaction.

[11] P. Sadeghi, and H. H. Rotermund, Chaos **21**, 013125 (2011). Gradient induced spiral drift in heterogeneous excitable media.

[12] M. Vinson, S. Mironov, S. Mulvey, and A. Pertsov, Nature **386**, 477 (1997). Control of spatial orientation and lifetime of scroll rings in excitable media.

[13] C. Luengviriya, S. C. Müller, and M. J. B. Hauser, Phys. Rev. E **77**, 015201 (2008). Reorientation of scroll rings in an advective field.

[14] T. Amemiya, P. Kettunen, S. Kádár, T. Yamaguchi, and K. Showalter, Chaos **8**, 872 (1998). Formation and evolution of scroll waves in photosensitive excitable media.

[15] D. Pazó, L. Kramer, A. Pumir, S. Kanani, I. Efimov, and V. Krinsky, Phys. Rev. Lett. **93**, 168303 (2004). Pinning force in active media.

[16] Z. A. Jiménez, Z. Zhang, and O. Steinbock, Phys. Rev. E **88**, 052918 (2013). Electric-field-controlled unpinning of scroll waves.

[17] F. X. Witkowski, L. J. Leon, P. A. Penkoske, W. R. Giles, M. L. Spano, W. L. Ditto, and A. T. Winfree, Nature (London) **392**, 78 (1998). Spatiotemporal evolution of ventricular fibrillation.

[18] D. Barkley, M. Kness, and L. S. Tuckerman, Phys. Rev. A **42**, 2489 (1990). Spiral-wave dynamics in a simple model of excitable media: The transition from simple to compound rotation.

[19] S. Duhr, and D. Braun, Proc. Nat. Acad. Sci. **103**, 19678 (2006). Why molecules move along a temperature gradient?

[20] S. Alonso, R. Kähler, A. S. Mikhailov, and F. Sagués, Phys. Rev. E **70**, 056201 (2004). Expanding scroll rings and negative tension turbulence in a model of excitable media.

Chapter 5

Control of three dimensional vortex by multiple external fields

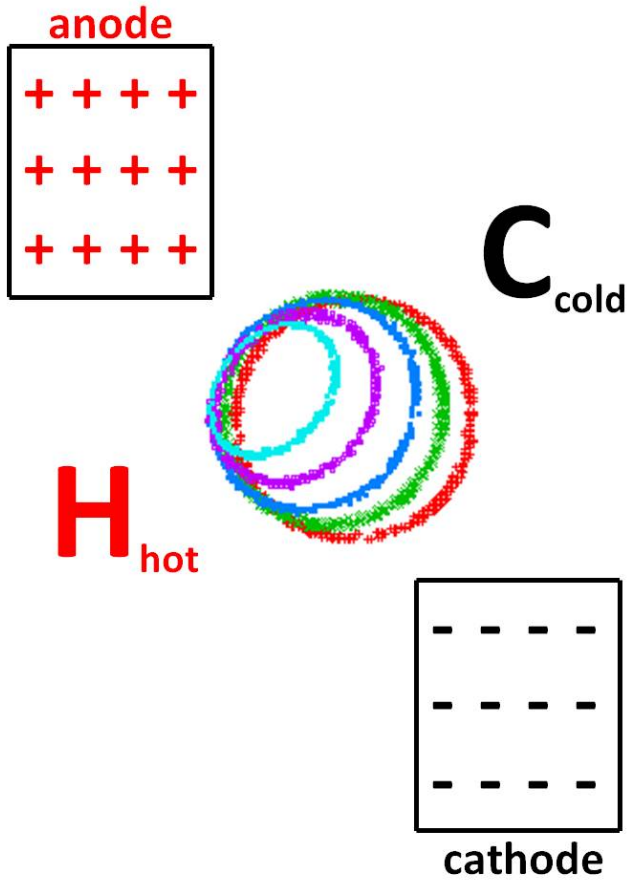

5.1 Introduction

In the cardiac system, the spiral and scroll waves are responsible for malfunctioning of the heart [1]. Once formed, these high frequency wave sources take over the normal cardiac activity and causes arrhythmias. Further interaction of these waves with themselves and other heterogeneities in the heart may lead to the onslaught of chaos, which is reflected in cardiac tissues as atrial and ventricular fibrillation, the latter being a major cause of cardiac arrest [2]. This makes the understanding and control of the scroll waves a subject of interest to physicians, biologists, and physicists. Current methods of cardioversion employs the application of high-voltage electric shocks, that may lead to tissue damage and pain [3]. Hence, it is required to control the scroll waves by milder techniques, which will not have such undesirable side effects.

Earlier studies on model experimental systems have shown that scroll waves reorient themselves under the influence of low-voltage electric fields and pulses and mild thermal gradients [Fig. 4.1] [4, 5, 6, 7]. It was seen that scroll waves may also expand and their lifetimes may change depending on the strength of the gradient [8, 9, 10, 11, 12, 13]. In this chapter, we try to study the behavior of the scroll waves under the influence of dynamic and multiple external gradients. We employ electric field and thermal gradients to control scroll waves. We use the BZ reaction as our experimental system for generating and sustaining the scroll waves. It is a redox reaction diffusion system, which can sustain spiral and scroll waves, in an unstirred condition. The BZ system is one of the most widely used laboratory model systems for studying the dynamics of spiral and scroll waves [14, 15]. Though it has several dissimilarities with the cardiac system, due to the latter's heterogenous nature and the differences in wave properties, still the physics that governs the spiral and scroll waves in both systems is the same. In our current study, we use moving electric fields and also sometimes thermal gradients perpendicular to the electric field to control the position of the scroll vortices in the two dimensional reaction space. We are able to make the vortices trace cyclic trajectories by the use of these external gradients. Numerical simulations on the Barkley model are carried out that lends support to our experimental findings.

5.2 Experimental Section

For our experiments, we used the three-dimensional Belousov-Zhabotinsky reaction which is a simple laboratory model to generate scroll waves [16]. The BZ solution used for our experiments contained 0.04 M sodium bromate, 0.04 M malonic acid, 0.16 M sulphuric acid and 0.5 mM ferroin. The solutions were prepared in Millipore water and all experiments were carried out at room temperature. To avoid convection, the reaction mixture was embedded in a 0.8 % w/v agar gel matrix. The experimental system consisted of two layers, each about 4 mm in height and were placed one above the other to make a three dimensional reaction environment. After the gelation of the first layer, a circular wave was generated in the middle of the first gel layer, by inserting the tip of a thin silver wire. A second gel layer was then poured over it whereupon the circular wave curled up into the top layer and formed a scroll ring.

Since our experiments aim at studying the effects of external fields on scroll waves, we had to incorporate electric fields as well as thermal gradients into our reaction system. For this purpose, the reaction chamber was designed as a square petri dish (8 cm $\times$ 8 cm) that had two heat exchangers on its either side. These were connected with circulating baths kept at desired temperatures, that enabled us to maintain a fixed temperature gradient in the range of 0.5 - 4 °C cm^{-1} between two sides of the reaction chamber [Fig. 5.1]. However, this arrangement did not allow us to change the direction of the thermal gradient during the course of an experiment. An electric field was applied to the system using a pair of copper electrodes [7 cm (length) $\times$ 4 cm height $\times$ 0.02 cm (width)], which were inserted into the gels, at opposite ends of the reaction chamber. These electrodes were placed parallel to each other and connected to a DC power source (Scientific Multipurpose Power Supply PSD3304). Experiments were performed for electric field potentials of 1 - 3 $V\ cm^{-1}$. For experiments involving moving electric fields, we used two such pairs of electrodes placed perpendicular to each other. Electric field was applied through any one of the electrode pairs at a given time. We used a charge-coupled device (CCD) camera (mvBlueFOX 220a) to monitor our experiments from above. A blue dichroic filter was attached to the camera for better imaging. The reaction system was illuminated from below by using

a diffused, cold white light source. We recorded the images onto a personal computer at a regular interval of 10 s. The images were later analyzed using some in-house MATLAB codes.

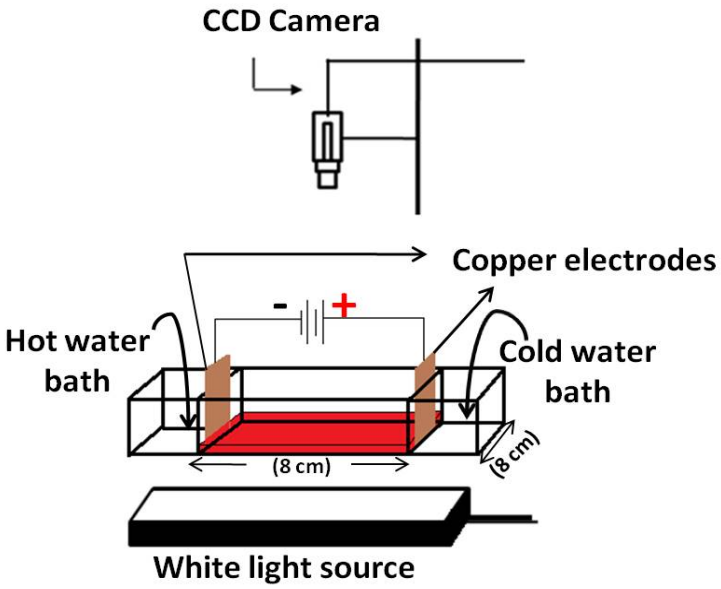

FIG. 5.1: Schematic diagram of our experimental set-up.

5.3 Results and Discussion

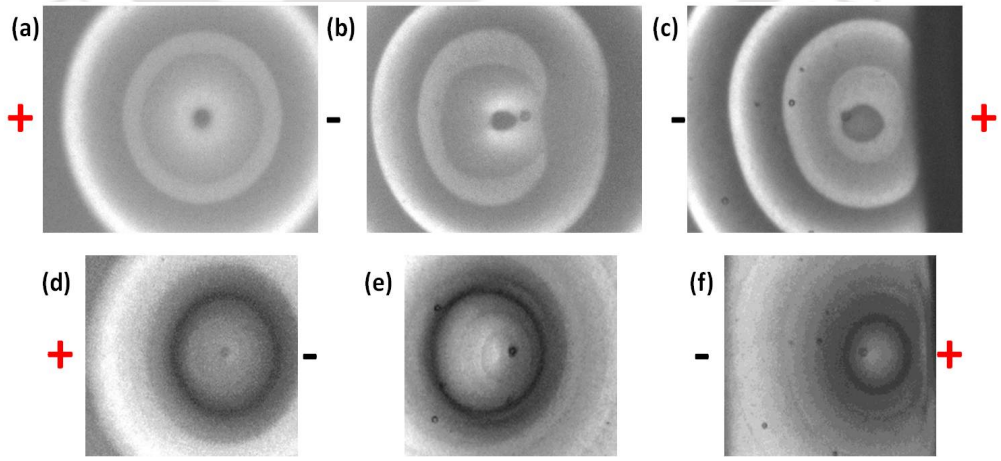

FIG. 5.2: (a, b, c) Movement of scroll waves under changing orientations of the electrode. (d, e, f) Filaments corresponding to (a, b, c). Positive and negative symbols mark the position of anode and cathode respectively.

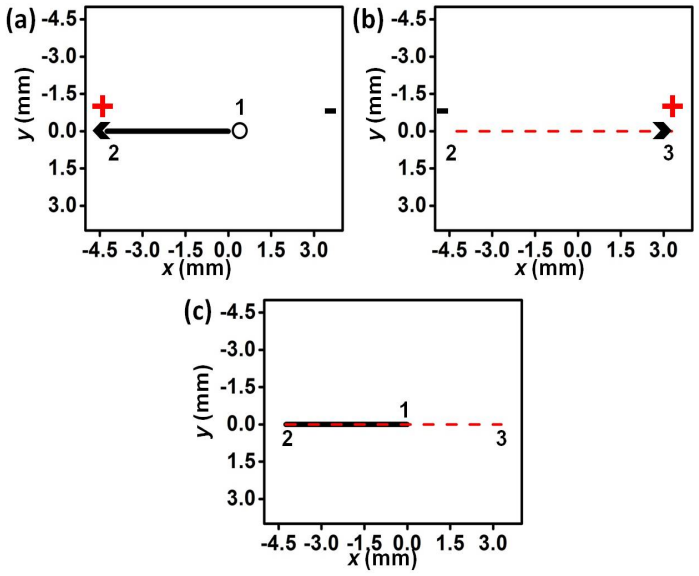

FIG. 5.3: Trajectory of a scroll ring under a moving electric field. The field strength is 1.5 V cm^{-1}. The position of the positive and negative electrodes are exchanged after 20 minutes. Open circle in (a) denotes the initial position of the center of the scroll ring. (a) The initial movement of the scroll ring when the positive electrode on the left and the negative electrode is on the right side of the chamber. The continuous bold line shows the trajectory of the center of the scroll ring for an electric field perturbation of 20 min duration. (b) Positive electrode is now at the right and the negative electrode at the left. Broken red line denotes the trajectory for 60 min. 3 in (b) denotes the final position of the scroll ring. (c) Overall trajectory of the scroll ring.

At first we employ a static homogenous electric field across the reaction chamber. Figures 5.2 and 5.3 summarizes the result of such an experiment. In Fig. 5.2 (a, b, c) snapshots and in (d, e, f) filaments corresponding to the snapshots are shown. At first the anode is placed to the left and the cathode to the right. In Fig. 5.3, the path traced by the centre of the filament is shown. It is seen that the scroll wave moves towards the anode [Fig. 5.2 (b, e) and Fig. 5.3(a)]. After a period of 20 min, we reverse the direction of the electric field gradient [Fig. 5.3 (b)] and consequently the scroll ring traverses back the path it had earlier traced, crosses the initial position and moves further right towards the anode.

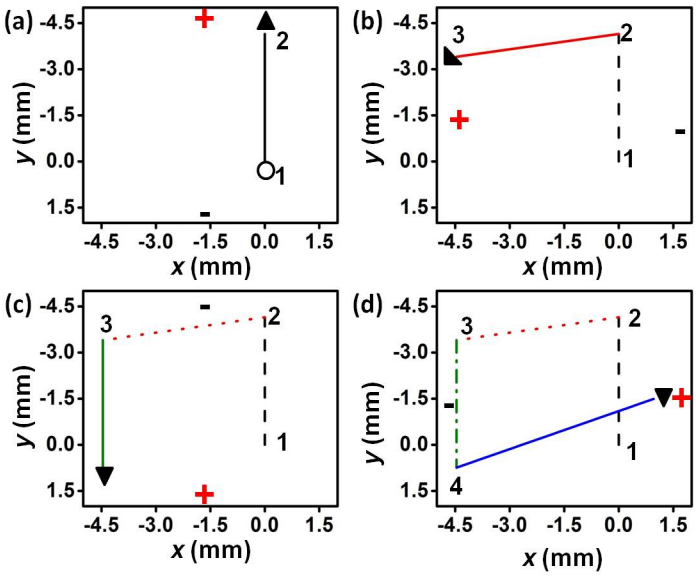

FIG. 5.4: Cyclic movement of a scroll ring under a moving electric potential gradient. The field strength is 1.5 V cm^{-1}, and the position of the electrodes are changed after every 35 minutes. The continuous bold line in every box shows the trajectory for the current position of the electrodes, while broken lines denote past trajectory. Open circle in (a) denotes the initial position of the center of the scroll ring and 5 in (d) is the final position of the ring center. For any orientation of the gradient, it is observed that the scroll ring moves in the direction of the positive electrode.

We then used two pairs of electrodes to change the direction of the electric field in an anticlockwise manner. Figure 5.4 shows the results of one such experiment. It is observed that the scroll ring moves towards the anode for every orientation of the electric field. Here, it can be seen that the scroll wave could be moved around in space to traverse cyclic trajectories.

In order to see the effects of cross fields, we turned on a thermal gradient, perpendicular to the electric field, with the hot end to the left and cold end to the right of the reaction chamber. It was seen that the scroll wave moved in a diagonal direction, between the anode and the hot end [Fig. 5.5]. This evidences the role of thermal gradient in the orientation of the scroll wave. We also varied the strengths of the electric field and thermal gradient to study their relative effect on the dynamics of the scroll wave. Temperature gradient was varied from 1- 3 °C cm^{-1}, and electric field from 1 -

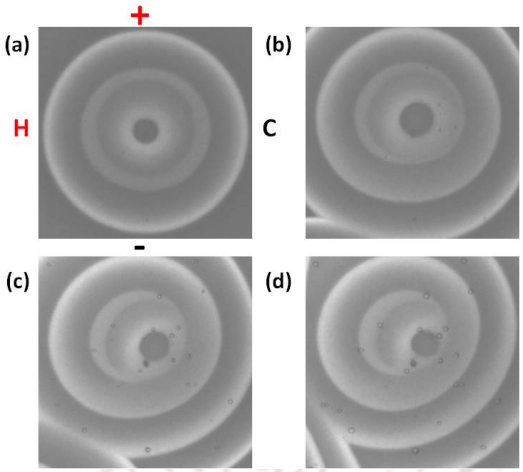

FIG. 5.5: Movements of scroll waves under perpendicular electric field and thermal gradients. Snapshots (a, b, c, d) of scroll wave for an experiment of 4 °C cm^{-1} temperature gradient and 2 V cm^{-1} electric field strength after a period of 24, 52, 80 and 108 mins have evolved. Anode and cathode position is marked by + and - symbols and hot and cold end by H and C respectively.

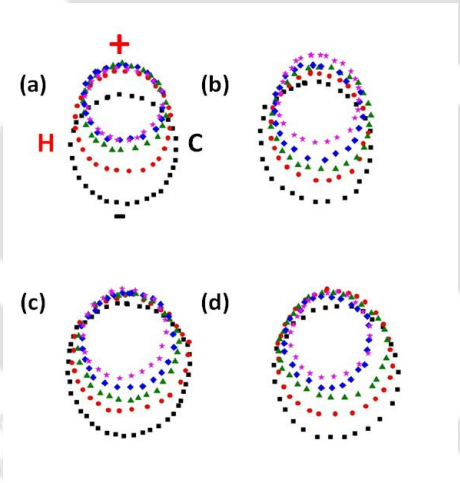

FIG. 5.6: Dynamics of a scroll wave under an electric field and a thermal gradient perpendicular to each other. Different curves correspond to filaments at different times after the start of the thermal and electric field perturbations (black solid squares = 0 min, red solid circles = 21 min, green solid triangles = 42 min, blue solid diamond = 84 min and pink solid stars = 105 min). For field strengths: (a) $E = 1$ V cm^{-1} and $\nabla T = 1$ °C cm^{-1}, (b) $E = 1$ V cm^{-1} and $\nabla T = 2.5$ °C cm^{-1}, (c) $E = 1.5$ V cm^{-1} and $\nabla T = 1$ °C cm^{-1} and (d) $E = 1.5$ V cm^{-1} and $\nabla T = 2.5$ °C cm^{-1}.

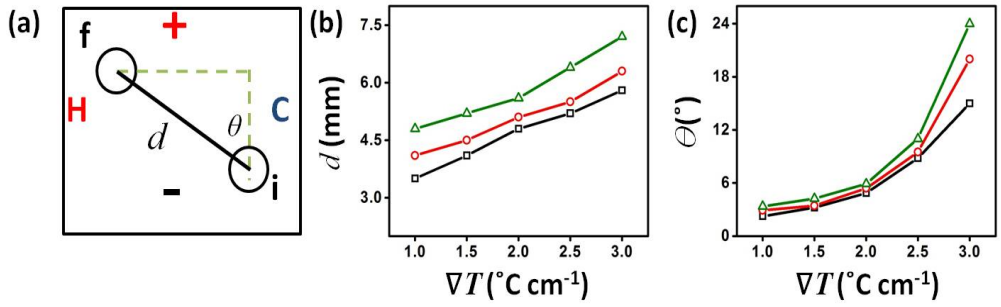

FIG. 5.7: Influence of cross electric potential and thermal gradients on scroll waves. (a) Schematic diagram showing the trajectory of a scroll wave (bold line) from initial position **i** to final position **f**, showing the distance d, and the orientation θ. The anode(+) and cathode(-) are positioned at the top and bottom of the reaction chamber respectively, and the hot(H) and cold(C) end lie to the left and right. (b) and (c) show the variation of the distance traversed in 60 min and the corresponding change in orientation of the scroll ring with varying temperature gradient. Each curve corresponds to a different value of electric field. Squares (black curve) stand for $E = 1$ V cm^{-1}, circles (red curve) stand for $E = 1.5$ V cm^{-1} and triangles (green curve) stand for $E = 2$ V cm^{-1}.

2 V cm^{-1}. Higher strengths of electric field was not considered since it resulted in the breakage of scroll waves on touching the system boundary. Figure 5.6 summarizes the result of our experiments. In order to be able to compare the movement of the scroll for different experiments, we define the quantities d, the distance traversed by the scroll, and θ, the angle by which it deflects from the vertical direction. d increases almost linearly with the increase in thermal gradient [Fig. 5.7 (a)]. The trends for the electric field strength is also similar. However, the orientation changes only with a huge change in thermal gradient [Fig. 5.7 (b)]. For low values of thermal gradient (1-1.5 °C cm^{-1}), the scroll ring moves almost vertically upwards (towards the anode), for all values of electric field. Only for high values of thermal gradient (3 °C cm^{-1}), there is a marked difference in the way varying electric fields influence the movement of the ring. From this we can surmise that the electric field is the stronger of the two fields and mostly controls the movement of the scroll (in the vertical direction). Only when the thermal gradient is very high is it able to deflect it along a diagonal

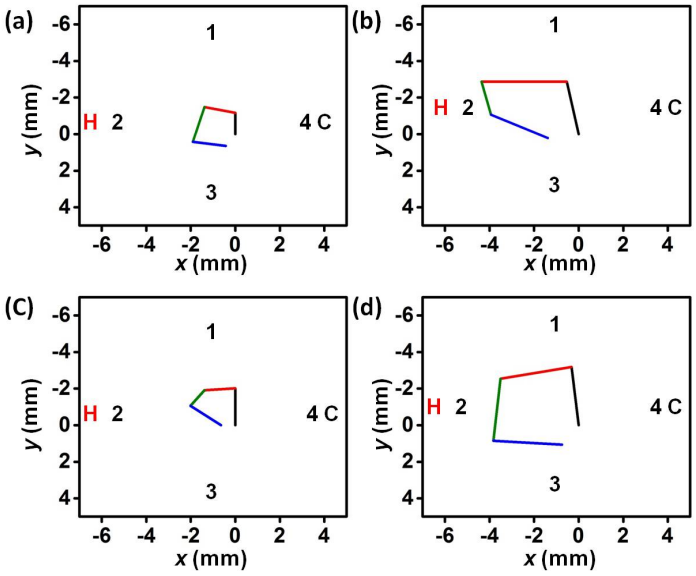

FIG. 5.8: Movement of a scroll vortex in the presence of a static thermal gradient (right to left) and a moving electric field. The anode position is changed after every 20 min. The graph show the trajectory of the scroll for four different positions of the anode (1, 2, 3 and 4) with the cathode placed at its opposite end. The different colors of the line sections (black, red, green and blue respectively) mark the trajectory for different position of the anode. In (a) ∇T= 2 °C cm^{-1} and $E = 0.5$ V cm^{-1}, in (b) ∇T= 2 °C cm^{-1} and $E = 1.5$ V cm^{-1}, in (c) ∇T= 3 °C cm^{-1} and $E = 0.5$ V cm^{-1}, and (d) ∇T= 3 °C cm^{-1} and $E = 1.5$ V cm^{-1}.

direction. Again, for high thermal gradient values, the deflection is maximum for low electric field strength and much lower for higher values of E.

We then explore the movement of the scroll ring in the presence of dynamic cross fields. The experimental set-up does not allow the change in direction of the thermal gradient. So keeping that intact, we vary the electric field position as before [Fig. 5.8]. The field direction is changed cyclically by passing current through alternate pairs of electrodes. It can be seen from the results of the experiments that the scroll vortex moves towards the anode with deflection in the direction of the hot end whenever the thermal gradient is on the higher side [Fig. 5.8 (c) and Fig. 5.8 (d)].

These experiments show that the effect of the electric field on the movement of the scroll is much more as compared to the thermal gradient. Larger thermal gradients

(> 3 °C cm^{-1}) were avoided, else the excitability of the medium is changed drastically leading to the generation of target waves at the hot end.

5.4 Numerical Simulations

In order to validate and understand our experimental observations, we also performed numerical simulations using the two variable Barkley model [17, 18].

$$\frac{\partial u}{\partial t} = \frac{1}{\epsilon}\left\{u(1-u)\left(u-\frac{v+b}{a}\right)\right\} - \nabla J_u, \tag{5.1}$$

$$\frac{\partial v}{\partial t} = u - v - \nabla J_v. \tag{5.2}$$

where the two variables u and v are related with the concentrations of bromous acid and the oxidized form of ferroin, respectively. The flux of the variable u, J_u, in the presence of both thermal gradient and electric field is given by the Soret effect and Nernst equation respectively and can be written as [19, 20],

$$J_u = D_u \nabla u + D_{T_u} u(1-r_u)\nabla T - D_u z_u u E$$

$$J_v = D_v \nabla u + D_{T_v} v(1-r_v)\nabla T - D_v z_v v E$$

where, $D_u = 1.0$ is the translational diffusion coefficient and $D_{T_u} = D_u S_{T_0}/1 + k_s u$ is the thermal diffusion coefficient of u. r_u is the relative concentration of u given by, $r_u = u/c_T$; and $c_T = u+v$. $z_u = 0.0$, is the ionic charge on u. S_{T_0} = -0.1 is the Soret coefficient and its negative value implies the movement of a particle towards the hot end. $k_s = 1.0$ is a phenomenological constant. ∇ T is the thermal gradient between two sides of the reaction vessel and a constant for a reaction. E denotes the electric field or electric potential gradient. The flux of species v also gets similarly modified in the presence of external gradients, with $D_v = 1.0$ $z_v = 3.0$. $a = 0.84$, $b = 0.06$ and $\epsilon = 0.02$ are the system parameters. We used the Euler method for integrating the equations in a finite system size of $300 \times 300 \times 300$ grid points and zero-flux boundary conditions. A time interval $\Delta t = 0.012$ and space step of $\Delta x = 0.35$ were employed. The filament of the scroll was identified at regions having $u = 0.5$ and $v = a/2 - b$.

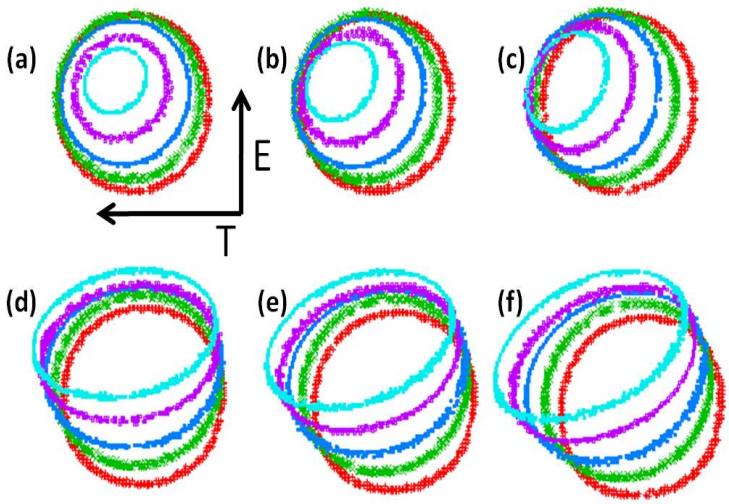

FIG. 5.9: Filament dynamics of a scroll ring vortex under the influence of cross electric and thermal gradients. The filament is constructed from the iso-points of u and v. In each sub-figure, the time evolution of the filament is shown for a particular combination of thermal and electric field gradient. In (a, b, c) applied thermal gradient is 5, 10 and 15 respectively and electric field is 0.02. In (d, e, f) the thermal gradient is 5, 10 and 15 respectively, for an electric field strength of 0.03.

We carried out simulations by varying the strength of thermal gradient and electric potential. Figure 5.9 shows some of the results of our simulation. When both the fields are placed perpendicular to each other, a cross field effect arises, and we can see that the scroll wave under its influence moves in a diagonal direction between the hot end and the positive electrode [Fig. 5.9]. It is evident that when the field strengths are increased, the filament movement increases. The figure also shows that the movement of the scroll is more influenced with the increase in electric potential gradient as compared to the thermal gradient ∇T. This result is similar to what was seen in our experiments with the BZ system [Fig. 5.6].

5.5 Conclusions

In our study, we have been able to successfully control the position of a scroll wave by applying external field perturbations such as electric and thermal gradient. A moving electric field causes a drift of the scroll ring, with its center always trying

to move towards the anode. In the presence of cross electric and thermal gradients, the scroll vortex moved towards the hot end and the anode, thus tracing a diagonal path. When the electric field was moved in an anticlockwise manner, while keeping the thermal gradient constant in time and space, we could see that the nature of the trajectories changed, depending on the comparative strength of both the fields. The results of our experiments as well as simulations allowed for a comparison of the influence of the electric and thermal gradients, as is evident from their impact on the position and orientation of the scroll wave. Though the effect of the electric and thermal field gradients on scroll waves are similar, the electric field gradient takes precedence over the thermal gradient, in the movement of the scroll ring, when both are present simultaneously. Again stronger the field whether it is electric or thermal, the scroll ring drifts through a longer distance from its initial position in a given time interval, because of higher diffusion rate of ions present in the chemical reaction. The conclusions drawn from this work give us newer insights into the behavior of these scroll waves and may pave the way for their control in more complicated biological systems where spiral and scroll waves are found.

Bibliography

[1] N.Sperelakis, y. Kurachi, A. Terzic, and M. V. Cohen, *Heart physiology and patholphysiology* (fourth edition, Academic Press, 1984).

[2] J. Jalife, M. Delmar, J. Anumonwo, O. Berenfeld, and J. Kalifa, *Basic cardiac electrophysiology for the clinician* (Wiley-Blackwell, Oxford, UK, second edition, 2009).

[3] J. Jalife, Annu. Rev. Physiol. **62**, 25 (2000). Ventricular fibrillation: Mechanisms of initiation and maintenance.

[4] C. Luengviriya, S. C. Müller, and M. J. B. Hauser, Phys. Rev. E **77**, 015201(R) (2008). Reorientation of scroll rings in an advective field.

[5] Z. A. Jiménez, Z. Zhang, and O. Steinbock, Phys. Rev. E **88**, 052918 (2013). Electric-field-controlled unpinning of scroll waves.

[6] M. Vinson, S. Mironov, S. Mulvey, and A. Pertsov, Nature **386**, 477 (1997). Control of spatial orientation and lifetime of scroll rings in excitable media.

[7] N. P. Das, D. Mahanta, and S. Dutta, Phys. Rev. E **90**, 022916 (2014). Unpinning of scroll waves under the influence of a thermal gradient.

[8] C. Luengviriya, and M. J. B. Hauser, Phys. Rev. E **77**, 056214 (2008). Stability of scroll ring orientation in an advective field.

[9] Z. A. Jiménez, and O. Steinbock, Phys. Rev. Lett. **109**, 098301 (2012). Stationary vortex loops induced by filament interaction and local pinning in a chemical reaction-diffusion system.

[10] Z. A. Jiménez, and O. Steinbock, Europhys. Lett. **91**, 50002 (2010). Pinning of vortex rings and vortex networks in excitable systems.

[11] Z. A. Jiménez, and O. Steinbock, Phys. Rev. Lett. **102**, 244101 (2009). Pinned scroll rings in an excitable system.

[12] Z. A. Jiménez, and O. Steinbock, Phys. Rev. E **86**, 036205 (2012). Scroll wave filaments self-wrap around unexcitable heterogeneities.

[13] E. Nakouzi, Z. A. Jiménez, V. N. Biktashev, and O. Steinbock, Phys. Rev. E **89**, 042902 (2014). Analysis of anchor-size effects on pinned scroll waves and measurement of filament rigidity.

[14] I. R. Epstein, and J. A. Pojman, *An introduction to nonlinear chemical dynamics* (Oxford University Press, Oxford, 1998).

[15] A. F. Taylor, B. R. Johnson and S. K. Scott, Phys. Chem. Chem. Phys. **1**, 807 (1999). Scroll waves in the Belousov–Zhabotinsky reaction: Exploitation of O_2-effect on the ferroin-catalysed system.

[16] O. Benini, R. Cervellati, and P. Fetto, J. Chem. Educ. **73**, 865 (1996). The BZ reaction: experimental and model studies in the physical chemistry laboratory.

[17] D. Barkley, M. Kness, and L. S. Tuckerman, Phys. Rev. A **42**, 2489 (1990). Spiral-wave dynamics in a simple model of excitable media: The transition from simple to compound rotation.

[18] D. Barkley, Physica D **49**, 61 (1991). A model for fast computer simulation of waves in excitable media.

[19] S. Dutta, and D. S. Ray, Phys. Rev. E **75**, 066206 (2007). Thermodiffusion induced instabilities in reactive systems.

[20] S. Dutta, and D. S. Ray, Phys. Rev. E **73**, 026210 (2006). Electric field induced instabilities: Waves and stationary patterns.

Chapter 6

Interaction of Scroll Waves in Excitable Medium: Reconnection and Repulsion

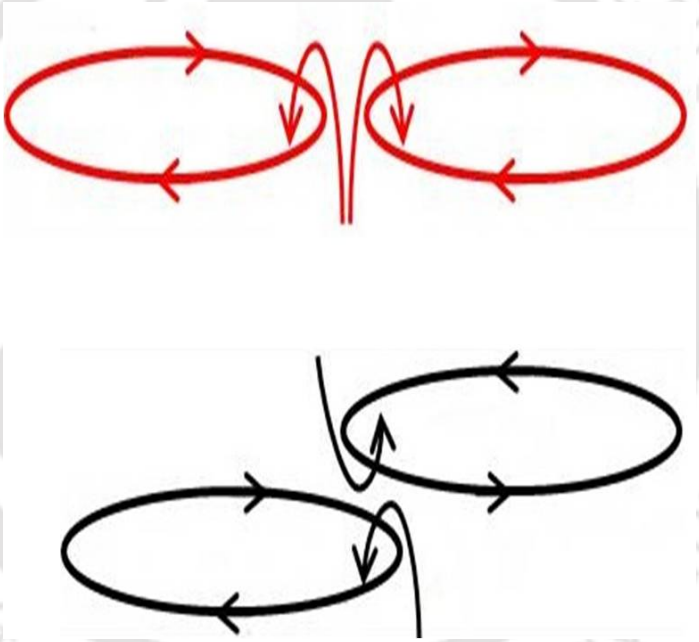

6.1 Introduction

In fluids and liquid crystals, there is evidence of vortex interaction leading to interesting phenomena like filament reconnection [1, 2, 3]. If likewise, scroll rings interact and reconnect, then small rings may merge and form large ones that will have enhanced life-times. If this happens in heart tissues, it will ensure a long life of the filaments, which in turn will have a detrimental effect on cardiac health. The work reported here is motivated by these concerns. Though the study of scroll waves has been ongoing for quite some decades [4], only a few computational studies of their interactions have been made [5, 6, 7]. Some experiments on the interaction of 2D spiral cores [8, 9] and 3D filaments have been carried out more recently [10], but no instances of scroll wave reconnection has yet been demonstrated.

In this chapter, we demonstrate an experimental evidence of scroll wave interaction. Our results demonstrate that when two scroll rings are brought close enough, they can either attract each other and reconnect to form a large scroll ring, or they can repel so that they rupture on touching the boundaries. We also carry out simple numerical simulations that helps explain the filament behavior in our experiments. Both the phenomena will have important consequences on the nature and life-time of the scroll waves.

6.2 Experimental Section

For our studies in scroll-wave interaction, we use the three-dimensional Belousov-Zhabotinsky reaction, which is a simple laboratory model where scroll waves can be directly observed [11, 12, 13, 14, 15, 16]. Our experimental system was embedded in a 0.8% w/v agar gel matrix. The mixture contained 0.04 M sodium bromate, 0.04 M malonic acid, 0.16 M sulphuric acid, 0.5 mM ferroin and 0.1 mM SDS. SDS was added to prevent the formation of CO_2 bubbles during the later stages of the experiment. For the first set of experiments, we initiated two non rotating semi spherical waves some distance apart, touching the tip of a silver wire into a 5 mm thick BZ gel layer. When the two waves expanded to their required size and were approximately 1-2 mm apart,

another layer of BZ gel was poured over this layer. The semi-spherical waves curled into the top layer and formed a pair of scroll waves with circular filaments. Both the filaments were coplanar and had similar sense of rotation. In order to study scroll wave interaction between filaments having opposite sense of rotation, we prepared two gel layers, each with a thickness of about 5 mm, in two separate petridishes. Two non-rotating half-spheres were generated in each one by initiation with a silver wire. When the waves reached desirable dimensions, we placed one petridish over the other. The waves curled into the facing gel layer and formed two scroll rings, whose filaments are placed one over the other. We illuminated our experimental system from below, using diffused white light and monitored it from above with a charge coupled device (CCD) camera (mvBlueFOX 220a) through a blue filter. The images were recorded onto a computer at an interval of 2 s and the data analyzed using MATLAB codes.

6.3 Results and Discussion

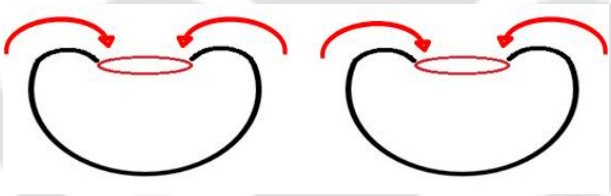

FIG. 6.1: Schematic representation of two scroll waves placed side by side.

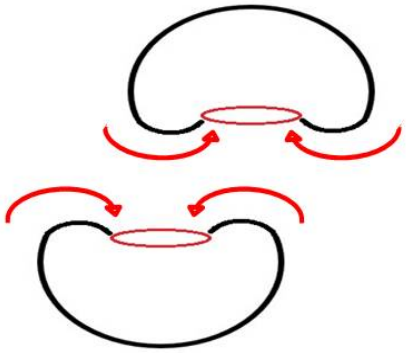

FIG. 6.2: Schematic diagram to represent the idea of two scroll waves placed one above the other.

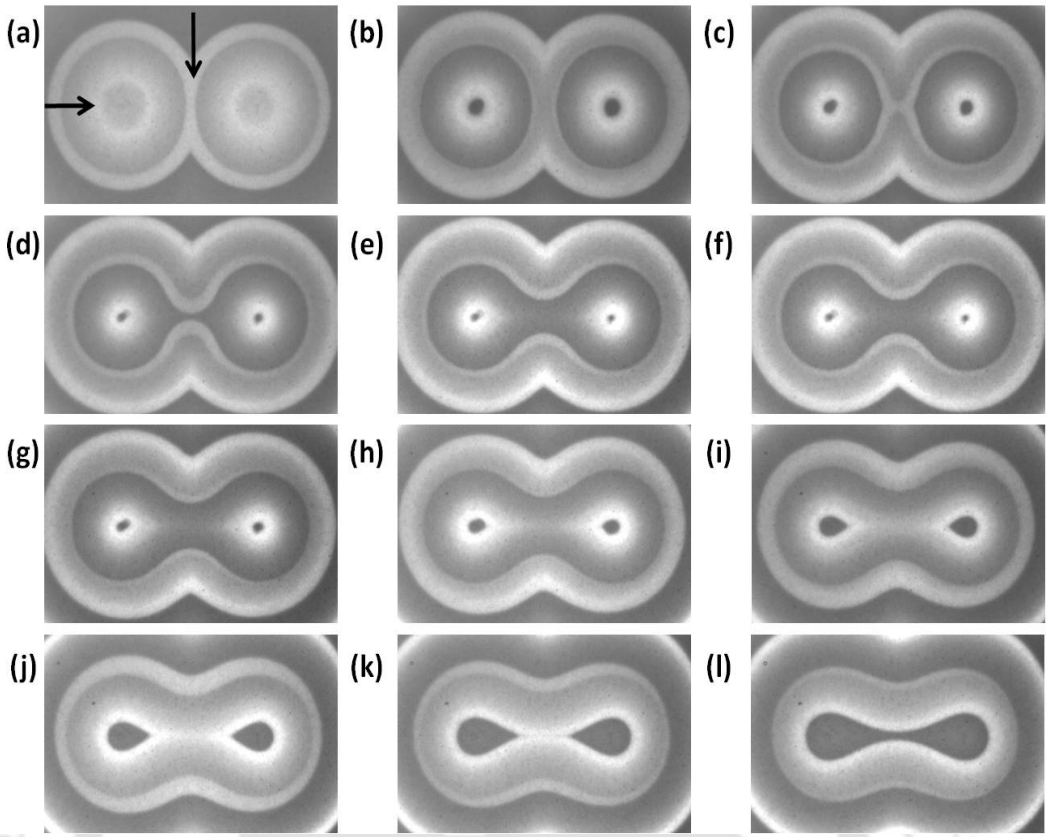

FIG. 6.3: Reconnection of scroll wave filaments. (a - l) Snapshots of a pair of coplanar scroll waves for the first 12 periods after scroll wave initiation. Image area of the snapshots is 3.2 cm x 2 cm.

In our analysis of the filament interactions, we have assigned a direction along the tangent to the filament at a particular point, via the right-hand rule [7]. This utilizes the curl of the motion of the constituent spirals around the said point on the filament [Fig. 6.1, 6.2]. Thus a unique direction of travel along the ring is defined. The two scroll rings that are formed side-by-side on the gel have a clockwise sense of rotation when viewed from the top, while the scroll rings that are formed with their kernels facing each other have opposite sense of rotation. Fig. 6.3 - Fig. 6.6 summarizes the results of an experiment involving interacting scroll rings with the same sense of rotation. During the scroll initiation process, if the half-spherical waves are too close, on pouring the second gel layer over them, the wave fronts merge and a single scroll wave is formed. When we increase the distance between the wave fronts, two independent scroll rings are generated. However in most cases, the distance between them keeps on increasing as they shrink under their positive filament tension, known

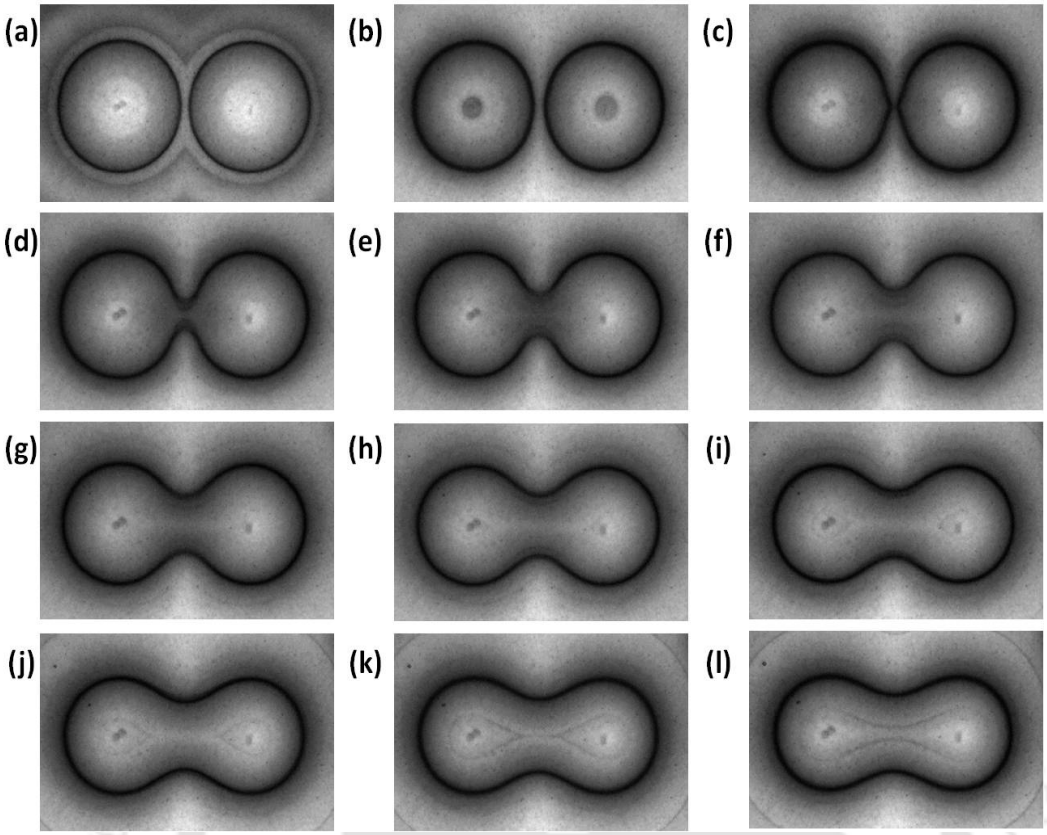

FIG. 6.4: (a - l) Filaments corresponding to the snapshots in Fig. 6.3 (a - l) respectively, each one calculated over one time-period. The dark areas of singularity show the position of the filaments.

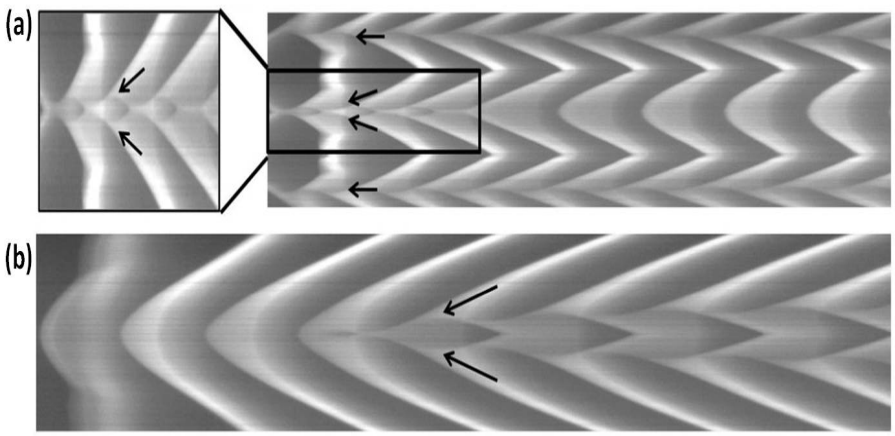

FIG. 6.5: (a) Time-space plot along the horizontal arrow in frame (a) of Fig. 6.3. Magnified area marked by black box. (b) Time-space plot along the vertical arrow in frame (a) of Fig. 6.3. Black arrows in frames (a) and (b) mark the position of filaments. Time evolves from left to right. Time-space plots span a time of 52 min.

to exist for the filaments in the BZ system. Only within a very specific range of inter-filament distance, do the two filaments undergo reconnection.

Figure 6.3 shows such an example where scroll wave reconnection has been observed. Figure 6.4 portrays the corresponding filaments generated by MATLAB for each of the snapshots shown in Fig. 6.3. Figure 6.3 (a) shows the initiation of two scroll waves formed at a close proximity. Dark region in Fig. 6.4 (a) marks the position of the filaments at this stage of the experiment. With time, the filaments attract each other at the point of nearest approach [Fig. 6.3, 6.4 (c)], and a bridge is formed between the two circular wave fronts [Fig. 6.4 (d)]. Eventually this bridge expands and the two filaments evolve into a single one [Fig. 6.3 (e - l), 6.4 (e - l)]. This has been predicted in earlier mathematical studies, and the phenomenon coined *crossover collision* [6, 17]. This ensures that after collision, the two filaments do not reconnect as before, re-establishing the previous filaments. Instead they choose to cross over in space and give rise to two new filament sections. In this case, they join to form a single, large filament. The newly formed vortex filament then undergoes curvature-dependent motion with the bridge expanding at the center, and the two sides shrinking, until it almost forms a hotdog shape [Fig. 6.3 (l)]. This is in keeping with the curvature-flow model [13]. The filament continues to shrink further until it comes to a point and disappears. The time-space plots clearly show the presence of four filament-sections along the horizontal cross-section of the snapshots [Fig. 6.5 (a)] at an early stage of the experiment (first three rotations), while no filaments are encountered along the vertical cross-section [Fig. 6.5 (b)] at this time. In the later part of the reaction, only two filament-sections are encountered along the horizontal axis, while two new filament-sections have now evolved in the vertical cross-section. Thus, circular filaments with the same sense of rotation reconnect when they are sufficiently closely spaced.

To get an idea about how closely spaced the filaments should be in order to reconnect, we carried out several sets of experiments with varying inter-ring distance. Initial velocity of interaction (v_0) has been plotted as a function of initial inter-filament separation, Z_0 [Fig. 6.6 (a)]. It shows an attractive regime for $Z_0 < 1.1$ mm (negative

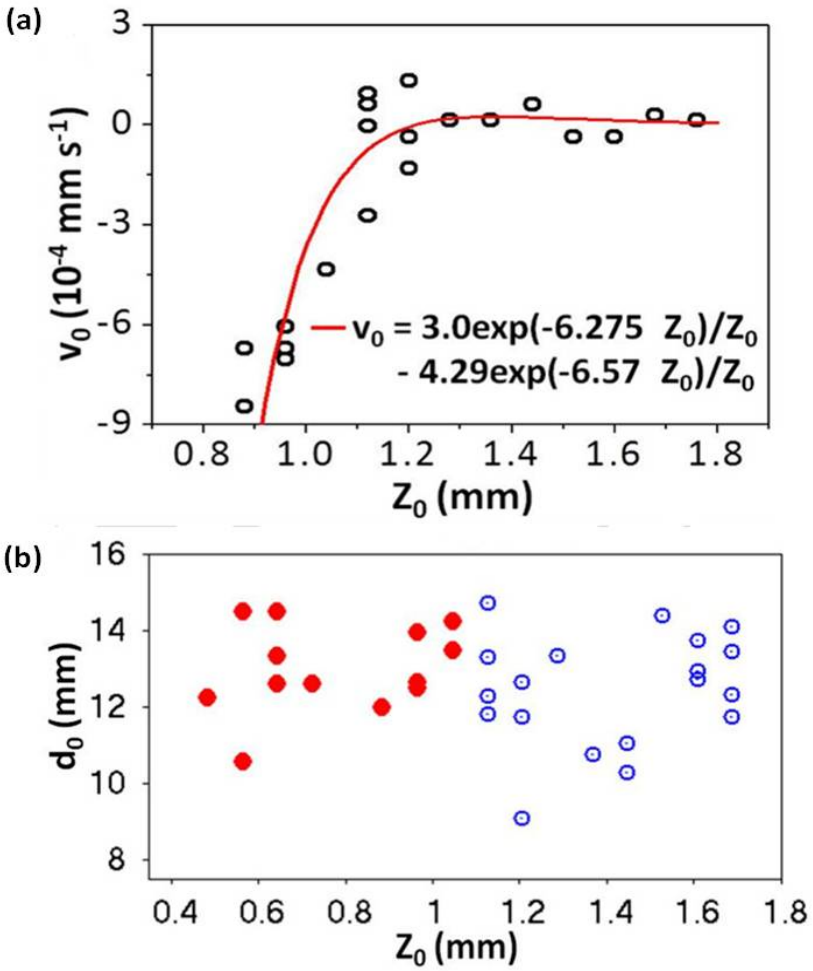

FIG. 6.6: (a) v_0 as a function of Z_0. The curve represents a fitting of the data as a difference of two Yukawa potentials. (b) Reconnection as a function of Z_0 and d_0. Reconnected filaments are marked as full (red) circles and non-reconnected ones as open (blue) circles.

v_0) and then a repulsive region beyond that (positive v_0), which reaches a maxima and then falls off. Beyond a certain distance, the scroll rings had no influence on each other. This could be fitted quite well as a difference of two Yukawa potentials, as has been predicted by earlier theoretical studies [5]. We also wanted to see if the size of the scroll rings played any role in the process. Figure 6.6 (b) shows a phase diagram of the reconnected versus non-reconnected filaments as a function of Z_0, and average of the initial ring diameters, d_0. The two filaments are initially more or less of similar dimensions (within 1 mm error). Hence average diameter of the two rings is a good measure of filament size. Our analysis shows that reconnection depends

only on the distance separating the filaments, and all filaments that were 1.04 mm apart or lesser, reconnected. This may be because, at this distance, the filaments lie within one core-length (1.09 mm) of each other [18]. The size of the rings, however did not have any marked effect on the phenomenon of reconnection.

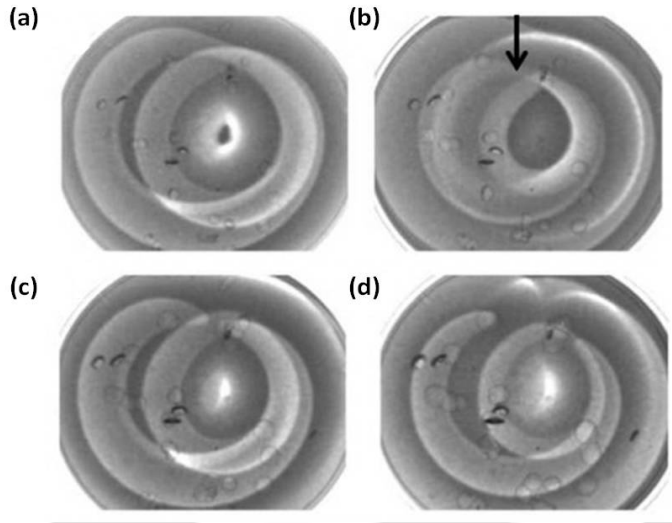

FIG. 6.7: Repulsion dynamics of vortex filaments with opposite sense of rotation. (a - d) Snapshots of two scroll waves placed one over the other at (a) 150 min, (b) 180 min, (c) 210 min, and (d) 240 min, after initiation. Each snapshot has an area of 2.5 cm x 2.2 cm.

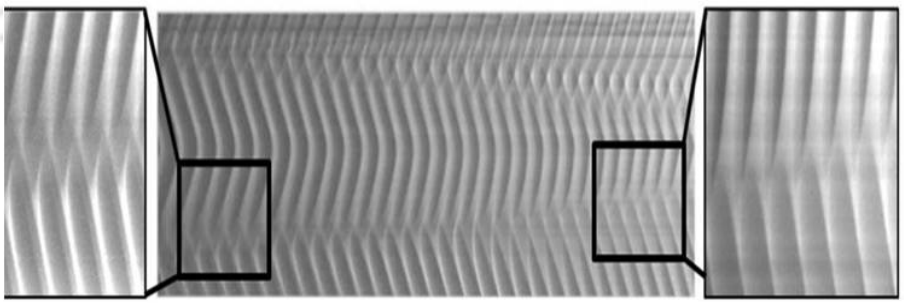

FIG. 6.8: Central panel: Time-space plot along the arrow shown in frame (b) of Fig. 6.7. It spans the duration from 140 min - 340 min of the reaction. Time advances from left to right. Left and right panels: magnified areas marked with boxes in the central panel.

When scroll rings with opposite sense of rotation are generated, we observe that at most times, when the scroll rings are appreciably large, one of the circular filaments

ruptures [Fig. 6.7 (c, d)]. We may hypothesize safely that they repel each other away, and when one of the filaments touches the system boundary (top or bottom petri-dish), it breaks. When the scroll rings are not so large, filament rupture is not seen, because the positive filament tension makes it disappear before it can touch the boundary. It is evident from the snapshots in Fig. 6.7 that amongst the two circular filaments in Fig. 6.7 (a), one clearly ruptures after a period of 90 min [Fig. 6.7 (d)]. The corresponding time-space plot [Fig. 6.8] also depicts the same phenomenon. The enlarged image shown in the left panel of Fig. 6.8 proves the presence of two filaments in that area at the early part of the experiment, while the right panel hints at a single filament at a later stage. This area corresponds to the tip of the arrow in Fig. 6.7 (b).

6.4 Numerical Simulations

To better understand the experimental results, we carried out simple numerical simulations of the two-variable Barkley model, which is frequently employed to model the dynamics of reaction-diffusion systems [19].

$$\frac{\partial u}{\partial t} = \frac{1}{\epsilon}\left\{u(1-u)\left(u-\frac{v+b}{a}\right)\right\}+D_u\nabla^2 u, \tag{6.1}$$

$$\frac{\partial v}{\partial t} = u-v+D_v\nabla^2 v \tag{6.2}$$

where, $D_u = 1.0$ and $D_v = 1.0$ are the translational diffusion coefficients of u and v respectively, $a = 0.84$, $b = 0.06$ and $\epsilon = 0.02$ are the system parameters. We use Euler's 9-point stencil method for integrating the equations in a finite system size of $350 \times 350 \times 250$ grid points and zero-flux boundary conditions. A time interval $\Delta t = 0.012$ and space step of $\Delta x = 0.35$ are employed. The filament of the scroll is identified at regions having $u = 0.5$ and $v = a/2 - b$.

Figure 6.9 shows crossover collision of the scroll wave filaments, leading to reconnection of the two individual scroll rings. Time-space plots [Fig. 6.9 (g,h)] depict the loss of two central filament sections along the horizontal arrow in Fig. 6.9 (a), and birth of two new filament sections along the vertical arrow. This bears ample proof of the

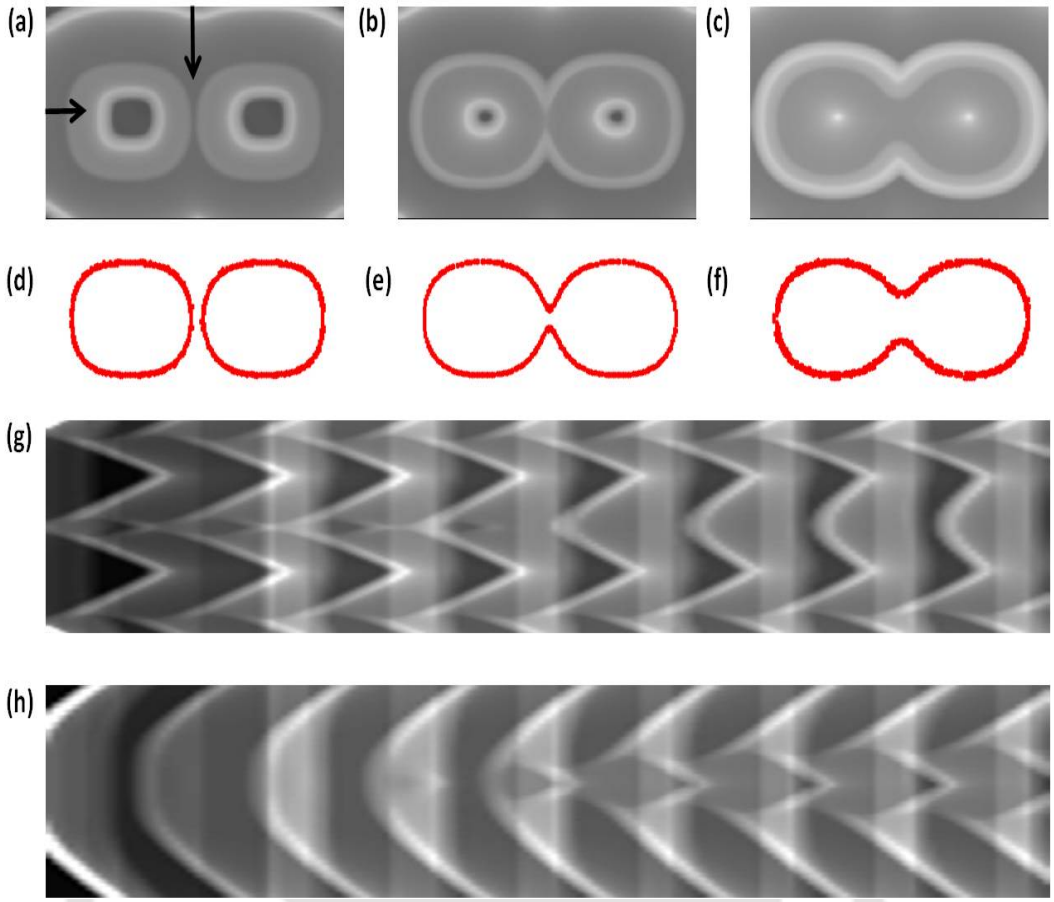

FIG. 6.9: Numerical simulation studies of scroll wave reconnection. (a - c) Two-dimensional snapshots of area 60 space units x 40 space units at (a) 9, (b) 19 and (c) 29 time units. (d - f) Filaments for the snapshots placed above. (g - h) Time-space plots generated along the arrows in frame (a), (g) along the horizontal direction and (h) along the vertical arrow.

crossover collision occurring at the point of nearest approach of the two filaments. These numerical results have absolute qualitative similarity with our experimental results in Fig. 6.3 - 6.5.

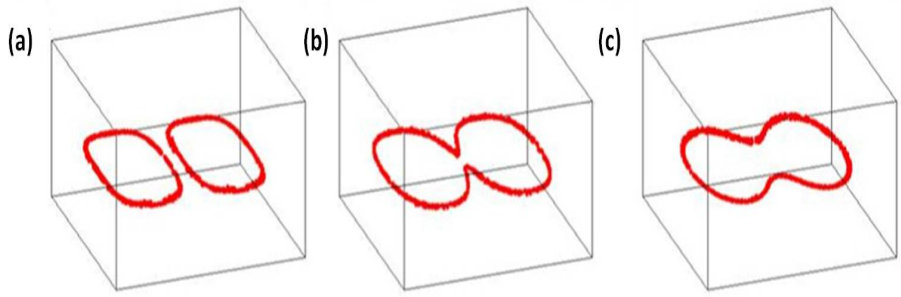

FIG. 6.10: (a - c) 3D Filament projection showing the reconnection of two filaments.

In Fig. 6.10, three dimensional projection of filament for scroll wave reconnection are shown. The filaments demonstrate that the scroll rings which were in the same plane at the beginning of the reaction, remains so. We also carried out numerical simulation by varying the diameter of the scroll ring (d_0) and the inter-filament separation (Z_0). We found that reconnection occurs when the inter-filament distance lies within one core length of each other and does not depend on diameter of the scroll (see figure in Appendix B).

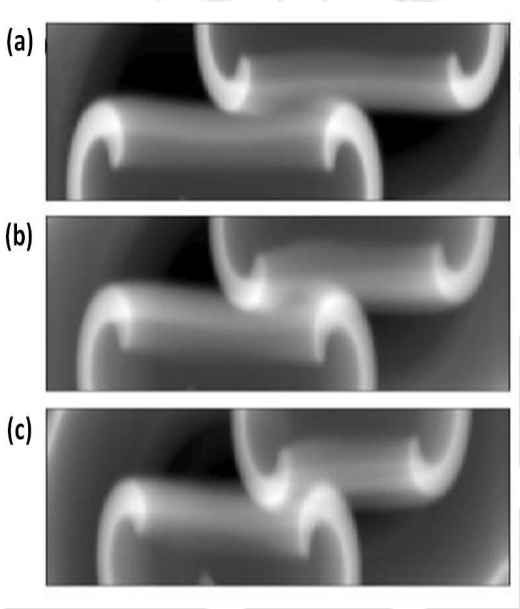

FIG. 6.11: Simulation studies of repulsion of scroll rings, having opposite sense of rotation. (a - c) Side-view of a pair of scroll rings placed one over the other at t = 45 (a), 130 (b), and 215 (c) time units. Snapshot areas are 350 space units x 100 space units.

Figure 6.11 - 6.13 tries to give us a three-dimensional overview of filament repulsion. The two scroll waves that were placed over each other, start repelling at the point of nearest approach [Fig 6.11 (c)]. Fig. 6.12 (c) shows the tilting of the filaments away from each other due to this mutual repulsion. If the system boundaries are close-by, as in the case of our experiments [Fig. 6.7], the filaments would touch the boundaries and rupture at those points. Towards this end, we also constricted our simulations along the z-direction (system size of $350 \times 350 \times 60$ grid points), and obtained similar results [Fig. 6.13 (a, b)]. Figure 6.10 (a) shows that the lower filament has tipped so much that it touches the boundary at the bottom and ruptures. Figure 6.13 (b) shows the projection of the filaments onto the xy-plane. This has close resemblance

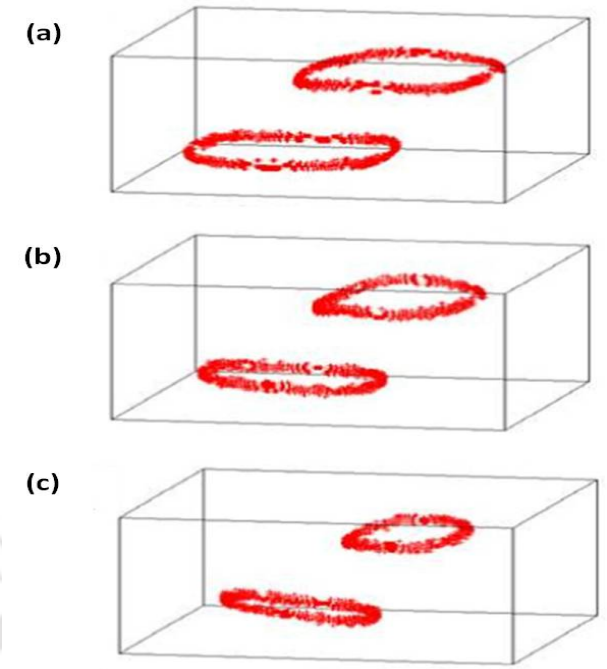

FIG. 6.12: Frames (a-c) depict the position of the filaments of the two scroll rings at the instances corresponding to the snapshots in Fig. 6.11.

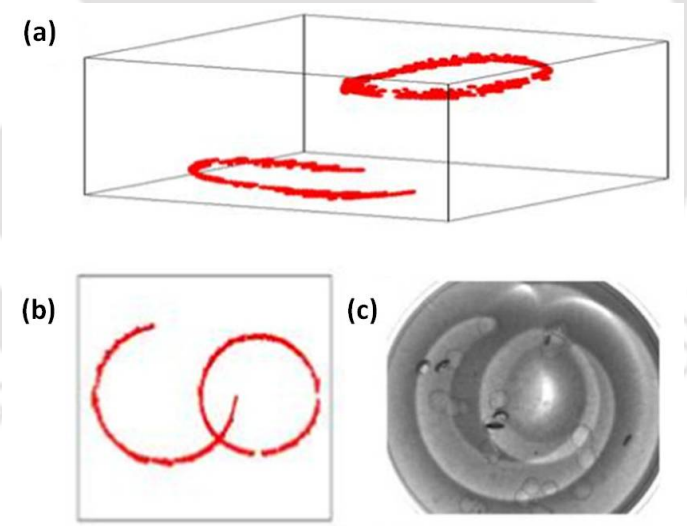

FIG. 6.13: Filaments computed in a restricted area of 350 space units x 350 space units x 60 space units. (b) Projection of the filaments shown in frame (a) on the x y-plane. (c) Result of scroll wave break up for filament repulsion in experiment similar to (b).

to our experimental results as seen in Fig. 6.7 (d) and Fig. 6.13 (c).

The local dynamics of the wave-fronts can be explained in view of the motion of the constituent spirals at the point of closest approach. Interaction of 2D spiral cores

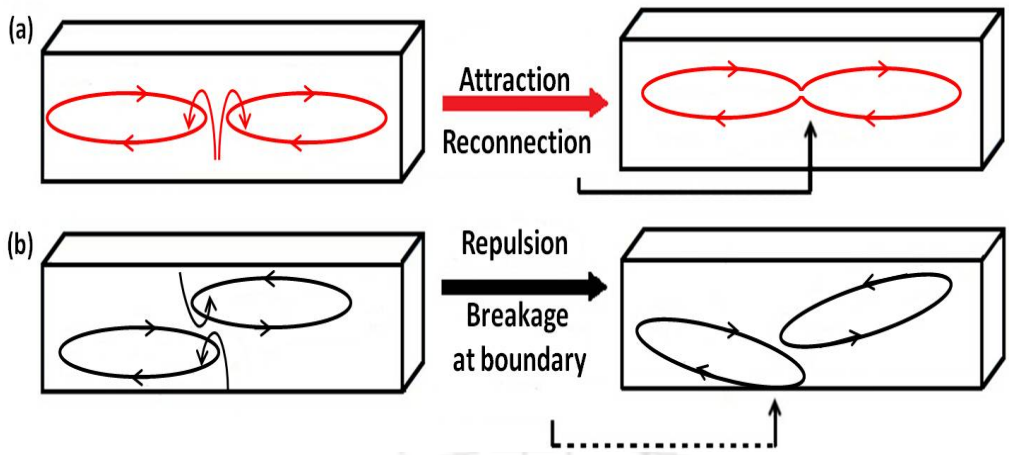

FIG. 6.14: Schematic representation of filament interaction. (a) Reconnection of vortex filaments having same sense of rotation. (b) Repulsion of filaments having an opposite sense of rotation, and possible rupture at the boundary. Small black arrows denote the motion of the constituent spirals around the points of nearest approach of the filaments.

are found in literature [20, 8]. It is known from an existing study of the FitzHugh-Nagumo model, that co-rotating spirals repel each other till they are far enough and become independent [20]. This happens with our filaments having opposite sense of rotation. As they shrink in size due to their positive filament tension, the constituent spirals of the two scroll rings that gain proximity are co-rotating [Fig. 6.14 (b)]. When they are very near, they repel, causing the filaments to tilt away from one another. Again, an earlier experimental study of a pair of spiral waves in 2D has shown that, a gradient can be used to move counter-rotating spirals towards each other. The separation between the spiral cores could be reduced to an extent that they annihilated [8]. In a similar fashion, we have seen that vortex filaments of scroll wave activity with the same sense of rotation can approach each other. At the point where the filaments are nearest, the constituent spirals are counter-rotating [Fig. 6.14 (a)]. This opposite sense of vorticity allows for them to mutually annihilate and paves the path for reconnection of the filaments. In this case, however, they are not forced to come close by any external gradient, but do so spontaneously. This is because of the interaction potential that acts amongst them and dictates reconnection or repulsion of the filaments depending on the distance that separates them [Fig. 6.6 (a)].

6.5 Conclusions

In conclusion, we have demonstrated the phenomenon of reconnection of scroll wave filaments for the first time in an experimental system. When two coplanar scroll rings with the same sense of rotation are brought close enough, the filaments undergo crossover collision and reconnect. It was also shown that the core-length is an upper bound to the inter-filament distance for reconnection to occur. However, when a scroll ring is placed over another, such that their nearest constituent spirals are co-rotating, they repel and break at touching the system boundaries. Both these phenomena will immensely effect the dynamics of scroll waves. Future work involving an extensive analysis of the mutual orientation and geometry of the filaments and scroll-ring lifetime could reveal further information. The present study illuminates important physics and paves the path for a better understanding of scroll wave interaction in other excitable medium, like the cardiac tissues.

Bibliography

[1] Y. Oshima, and N. Izutsu, Phys. Fluids **31**, 2401 (1988). Cross-linking of two vortex rings.

[2] I. Chuang, R. Durrer, N. Turok, and B. Yurke, Science **251**, 1336 (1991). Cosmology in the laboratory: Defect dynamics in liquid crystals.

[3] W. T. Ashurst, and D. I. Meiron, Phys. Rev. Lett. **58**, 1632 (1987). Numerical study of vortex reconnection.

[4] A. T. Winfree, and S. H. Strogatz, Physica D **13**, 221 (1984). Singular filaments organize chemical waves in three dimensions: IV. Wave taxonomy.

[5] M-A. Bray, and J. P. Wikswo, Phys. Rev. Lett. **90**, 238303 (2003). Interaction dynamics of a pair of vortex filament rings.

[6] B. Fiedler, and R. M. Mantel, Doc. Math. **5**, 695 (2000). Crossover collision of scroll wave filaments.

[7] M. Gabbay, E. Ott, and P. N. Guzdar, Phys. Rev. E **58**, 2576 (1998). Reconnection of vortex filaments in the complex Ginzburg-Landau equation.

[8] J. Schütze, O. Steinbock, and S. C. Müller, Nature **356**, 45 (1992). Forced vortex interaction and Aannihilation in an active medium.

[9] S. Dutta, and O. Steinbock, Phys. Rev. E **83**, 056213 (2011). Spiral defect drift in the wave fields of multiple excitation patterns.

[10] Z. A. Jiménez, and O. Steinbock, Phys. Rev. Lett. **109**, 098301 (2012). Stationary vortex loops Iinduced by filament interaction and local pinning in a chemical reaction-diffusion system.

[11] A. T. Winfree, Science **175**, 634 (1972). Spiral waves of chemical activity.

[12] M. Vinson, S. Mironov, S. Mulvey, and A. Pertsov, Nature **386**, 477 (1997). Control of spatial orientation and lifetime of scroll rings in excitable media.

[13] S. Dutta, and O. Steinbock, Phys. Rev. E **81**, 055202(R) (2010). Steady motion of hairpin-shaped vortex filaments in excitable systems.

[14] T. Amemiya, P. Kettunen, S. Kádár, T. Yamaguchi, and K. Showalter, Chaos **8**, 872 (1998). Formation and evolution of scroll waves in photosensitive excitable media.

[15] A. F. Taylor, B. R. Johnson, and S. K. Scott, Phys. Chem. Chem. Phys. **1**, 807 (1999). Analysis of reaction–diffusion waves in the ferroin-catalysed Belousov–Zhabotinsky reaction.

[16] T. Bánsági Jr., and O. Steinbock, Phys. Rev. Lett. **97**, 198301 (2006). Nucleation and collapse of scroll rings in excitable media.

[17] A. T. Winfree, and S. H. Strogatz, Physica D **9**, 333 (1983). Singular filaments organize chemical waves in three dimensions III Knotted waves.

[18] J. Koplik, and H. Levine, Phys. Rev. Lett. **71**, 1375 (1993). Vortex reconnection in superfluid helium.

[19] D. Barkley, M. Kness, and L. S. Tuckerman, Phys. Rev. A **42**, 2489 (1990). Spiral-wave dynamics in a simple model of excitable media: The transition from simple to compound rotation.

[20] E. A. Ermakova, A. M. Pertsov, and E. E. Shnol, Physica D **40**, 185 (1989). On the interaction of vortices in two-dimensional active media.

Chapter 7

Conclusion

This dissertation presents a detailed qualitative analysis of the dynamics of spiral and scroll waves. The initial work on spiral wave dynamics exhibits changes in excitability of the system which renders subsequent change in dynamics of spiral wave properties. The heart is a heterogeneous excitable medium in which spiral and scroll waves are present. Any change in the excitability may lead to changes in the dynamical behavior of the spiral or scroll wave. The frequency of these waves may either increase or decrease and this increment and decrement can be fatal to the heart. A scroll ring with a positive filament tension has a definite lifetime, i.e., it shrinks in size with time. The free vortex contracts and annihilates itself. Inert obstacles present within the BZ system can act as pinning sites for scroll vortex which can greatly alter annihilation time of scroll rings sometimes making it infinite. If this behavior develops in cardiac tissues, which is relevant due to its heterogeneous property, the lifetime of the scrolls will be infinitely increased. The scroll can no longer collapse and hence creates a lethal condition in the heart. We have shown that a temperature gradient can be successfully employed to induce unpinning of scroll waves from the inert beads in the BZ reaction. The unpinning process depends on the strength of the imposed thermal field. The unpinning efficiency is also affected by the orientation of the obstacles with respect to the direction of the thermal gradient. These studies may be extended to cardiac tissue research, since a thermal gradient is much milder compared to the strong electric shock, which is currently utilized in the present methods of cardioversion to cure cardiac arrhythmias. Understanding the behavior of the scroll waves under the influence of external fields and their varying orientation is very much essential, because

it is crucial to comprehend how these waves can be regulated in order to control and finally eliminate them completely. Our investigation with thermal and electric field gradients showed that the scroll vortex can be controlled with varying direction and magnitude of the external fields. The scroll vortex can also be guided in any direction in the presence of multiple fields. These studies can prove to be a major breakthrough in the control of the filament dynamics of scroll waves in excitable media. It provides newer insights of the nature of these waves. Again from our experimental results, we found that scroll ring in close vicinity to one another can interact with each other giving rise to different kinds of filament interaction. Two scroll rings placed side by side can undergo crossover collision resulting in the reconnection of the two filaments. This brings about the formation of a very large ring which increases the lifetime by 6-8 times of the original ring. Such a reconnection of scroll vortices in the heart will result in a large ring with longer lifetimes. On the other hand, our experiments have shown that two scroll rings placed one above the other can undergo repulsion leading to breakage of one of the filament due to collision with the boundary. In the cardiac tissue, such scroll wave breakage may lead to occurrence of ventricular fibrillation (VF), because the sole mechanism behind VF involves scroll wave breaking and turbulence. Thus, there is a need to understand these type of wave interaction in more detail.

Current defibrillation techniques employ strong electric shocks to remove unwanted waves so that heart rhythm can come back to normal. But such methods can cause burns in the tissues, thus creating unexcitable regimes which can cause further arrhythmias. So, physicians, biologists and basic scientists have been trying hard to understand and control these wave forms better. Based on the findings of our research, experiments may be designed to study if small pulses instead of sudden electric shock can control ventricular tachycardia and fibrillation. Such studies can be further extended to design targeted gadgets that will have less or no side effects, thus making them healthier and more reliable than the presently available medical technology.

Appendix A

Effect of temperature on scroll wave dynamics

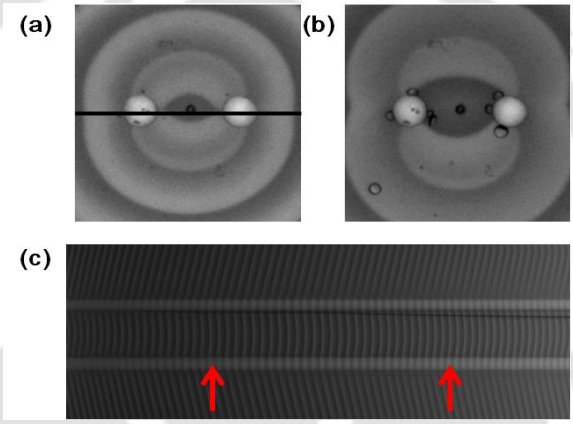

FIG. A.1: Snapshots (a) and (b) and time-space plot (c) along horizontal direction. Straight black lines on the snapshot show the stripe along which the corresponding time-space plot has been generated. The shining round-shaped objects are glass beads of 1 mm radius that act as our inert obstacles. The two arrows mark the position of the snapshots (a) and (b). The time-space plots (time going left to right) span a time interval of 300 min. Temperature, T = 22 °C.

Dynamics of a pinned scroll wave was studied at three different temperatures. Figure A.1, A.2 and A.3 shows the snapshots and time-space plots of three such experiments. The first result shown in Fig. A.1 was done at room temperature and the other two shown in Fig. A.2 and Fig. A.3 was performed at a temperature of T= 35 and 45 °C respectively. In our previous studies we have seen that the scroll wave pinned to an unexcitable obstacle gets unpinned in presence of thermal gradient. In these experiments we have studied the behavior of a scroll wave pinned to unexcitable

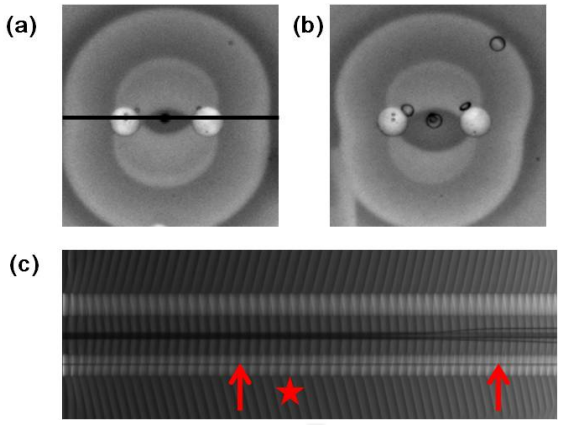

FIG. A.2: Snapshots (a) and (b) and time-space plot (c) along horizontal direction. Straight black lines on the snapshot show the stripe along which the corresponding time-space plot has been generated. The two arrows mark the position of the snapshots (a) and (b), one taken before the application of temperature and the other after before the end of the experiment. The star on the time-space plot marks the time at which the temperature has been applied on the system. The time-space plots (time going left to right) span a time interval of 240 min. Temperature, T = 35 °C.

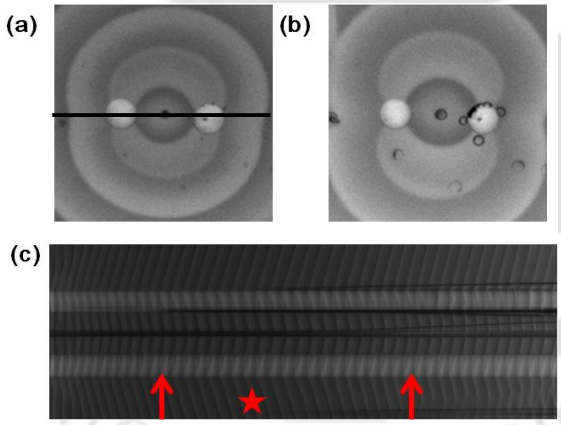

FIG. A.3: Snapshots (a) and (b) and time-space plot (c) along horizontal direction. Straight black lines on the snapshot show the stripe along which the corresponding time-space plot has been generated. The two arrows mark the position of the snapshots (a) and (b), one taken before the application of temperature and the other during the end of the experiment. The star on the time-space plot marks the time at which the temperature has been applied on the system. The time-space plots (time going left to right) span a time interval of 180 min. Temperature, T = 45 °C.

obstacles at low and high temperatures. The results show that the scroll wave shows no change in dynamics at these temperatures. The scroll remains pinned even any temperature. Unpinning of the scroll wave occurs only when temperature gradient is applied [Fig. 4.5 - Fig. 4.13].

Appendix B

Reconnection as a function of diameter and inter-filament separation in simulation

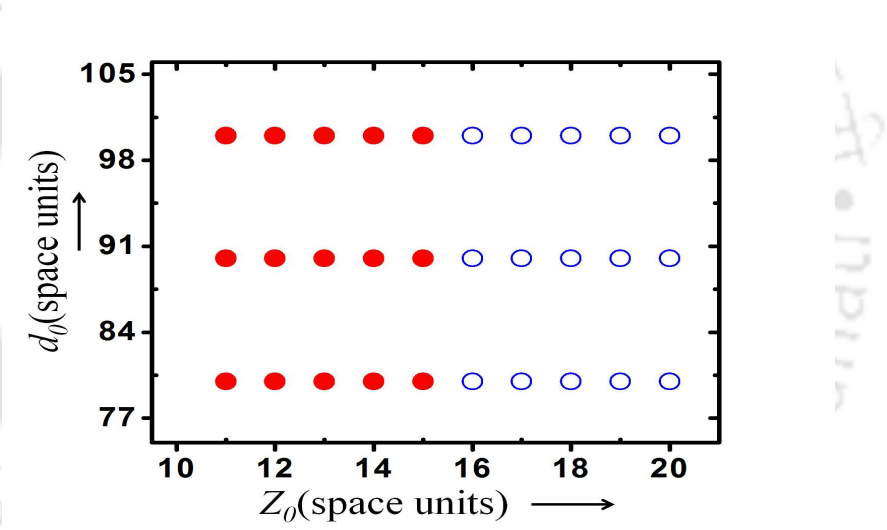

FIG. B.1: Simulation results of reconnection as a function of Z_0 and d_0. Reconnected filaments are marked as full (red) circles and non-reconnected ones as open (blue) circles.

Figure B.1 shows a phase diagram of the reconnected versus non-reconnected filaments as a function of inter-filament separation Z_0, and initial ring diameter, d_0. The two filaments are of same dimensions. Our analysis shows that reconnection depends only on the distance separating the filaments and does not depend on the diameter of the scroll which gives similar results as our previous experimental analysis [Fig. 6.6].

List of Publications

01. Nirmali Prabha Das, Dhriti Mahanta, and Sumana Dutta, Unpinning of scroll waves under the influence of a thermal gradient, Physical Review E **90**, 022916 (2014).

02. Nirmali Prabha Das, and Sumana Dutta, Interaction of scroll waves in an excitable medium: Reconnection and repulsion, Physical Review E **91**, 030901(R) (2015).

03. Nirmali Prabha Das, and Sumana Dutta, Control of three dimensional vortex by multiple external fields, *to be communicated*.

04. Nirmali Prabha Das, Dhriti Mahanta, and Sumana Dutta, A detailed study of spiral waves in concentration variant Belousov-Zhabotinsky reaction, *to be communicated*.

05. S. Dutta, N. P. Das and D. Mahanta, Dynamics and Control of Spiral and Scroll Waves, Book chapter, *submitted*.